New mechanistic insight into the gold-based propene epoxidation

Elena Parvulescu

ISBN: 978-90-393-5057-7
Drukkerij GVO drukkers & vormgevers B.V. | Ponsen & Looijen, Ede

New mechanistic insight into the gold-based propene epoxidation

Nieuw inzicht in het werkingsmechanisme van goud-gebaseerde propeen epoxidatiekatalysatoren

(met een samenvatting in het Nederlands)

Proefschrift

ter verkrijging van de graad van doctor aan de Universiteit Utrecht op gezag van de rector magnificus, prof. dr. J.C. Stoof, ingevolge het besluit van het college voor promoties in het openbaar te verdedigen op donderdag 7 mei 2009 des ochtends te 10.30 uur

door

Elena Parvulescu

geboren op 21 September 1980
te Oltenita, Romania

Promotor: Prof. dr. ir. B. M. Weckhuysen

Co-promotor: Dr. ir. T.A. Nijhuis

This thesis was accomplished with financial support from STW/NWO

To Andrei

Table of contents

Chapter 1

Introduction

1.1. The phenomenon of catalysis

Catalysis is crucial for the chemical industry. The number of catalysts applied in industry is very large and catalysts come in many different forms, from heterogeneous catalysts in the form of porous solids or homogeneous catalysts dissolved in the liquid reaction mixture to biological catalysts in the form of enzymes.

The word "catalysis" originates from Greek words *cata* & *lysis* meaning "a breaking down". Catalysis has been used from the time of Ancient Greece to signify the collapse of moral and ethical constrains. In the early part of 19th century, when the scientific study of chemistry was just beginning, it was observed that the occurrence of a number of chemical reactions was conditioned by the presence of trace amounts of substances that did not themselves take part in the reaction. A catalyst was first defined by J. J. Berzelius in 1836 as a compound, which increases the rate of a chemical reaction, but which is not consumed by the reaction. However, a catalyst increases the rate of the reaction and lowers the activation energy without changing the thermodynamics of the reaction and the equilibrium composition. A definition that is still valid today is due to Ostwald (1895): "a catalyst accelerates a chemical reaction without affecting the position of the equilibrium." Ostwald recognized catalysis as a ubiquitous phenomenon that was to be explained in terms of the laws of physical chemistry.

Catalysis is a cyclic process where the reactants are bound to one form of the catalyst, and the products are released from another leaving the catalyst unaltered such that it is available for the next reaction regenerating the initial state. In simple terms, a catalytic cycle can be described in Scheme 1.1. The cycle starts with the bonding of molecules A and B to the catalyst. A and B then react within this complex to give a product P, which is also bound to the catalyst. In the final step, P separates from the catalyst, thus leaving the reaction cycle in its original state.

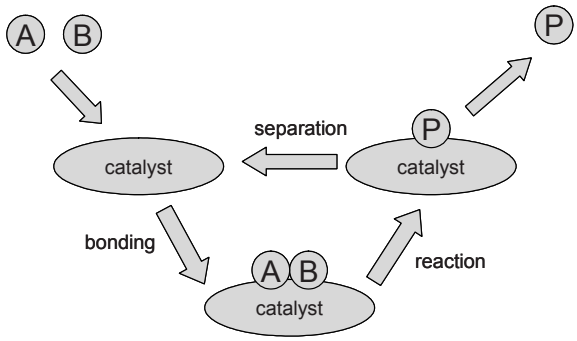

Scheme 1.1. Sequence of elementary steps in a catalytic cycle.

The intermediate catalyst complexes are in most cases highly reactive and difficult to detect. In theory, an ideal catalyst would not be consumed, but this usually is not the case in practice. Owing to competing reactions, the catalyst undergoes chemical changes, and its activity becomes lower (catalyst deactivation). Thus, catalysts must be regenerated or eventually replaced. The suitability of a catalyst for an industrial process depends mainly on the following three properties: activity, selectivity and stability. Today the efficient use of raw materials and energy is of major importance, and it is preferable to optimize existing processes than to develop new ones. For various reasons, the target quantities should be given the following order of priority: Selectivity > Stability > Activity.

1.2. Epoxidation of propene

Propene oxide (PO) is a highly reactive building block for the production of numerous commercial materials. It is produced at about six millions tons per year (2006) with demand still growing by ~ 5% annually [1,2]. The largest application of propene oxide is in the production of polyether polyols using about 60-70% of propene oxide demand. Polyether polyols are mainly used in the manufacture of polyurethane plastics. Propene oxide is also used in the production of propene glycol (20%), propene glycols ethers, polypropene glycol and propene carbonate [3]. Propene glycols are mainly used in the production of polyesters, whereas propene glycol ethers are primarily used as solvents.

Propene oxide is currently produced using two commercial processes: the chlorohydrin process (practiced by Dow, Asahi Glass and Tokuyama) and the hydroperoxide process (practiced in various forms by Lyondell, Shell, Sumitomo, Huntsman, Nihon Oxirane, SKC Chemical and Repsol). In what follows, we will discuss both processes in some detail.

1.2.1. The propene chlorohydrin process

The propene chlorohydrin process is in principle a two-stage: chlorohydrination and epoxidation. The main reactions involved are presented in Scheme 1.2. In a first step propene is reacted at 35 to 50º C and at pressures from 2 to 3 bar with an aqueous chlorine solution, in which HCl and HOCl are in equilibrium.

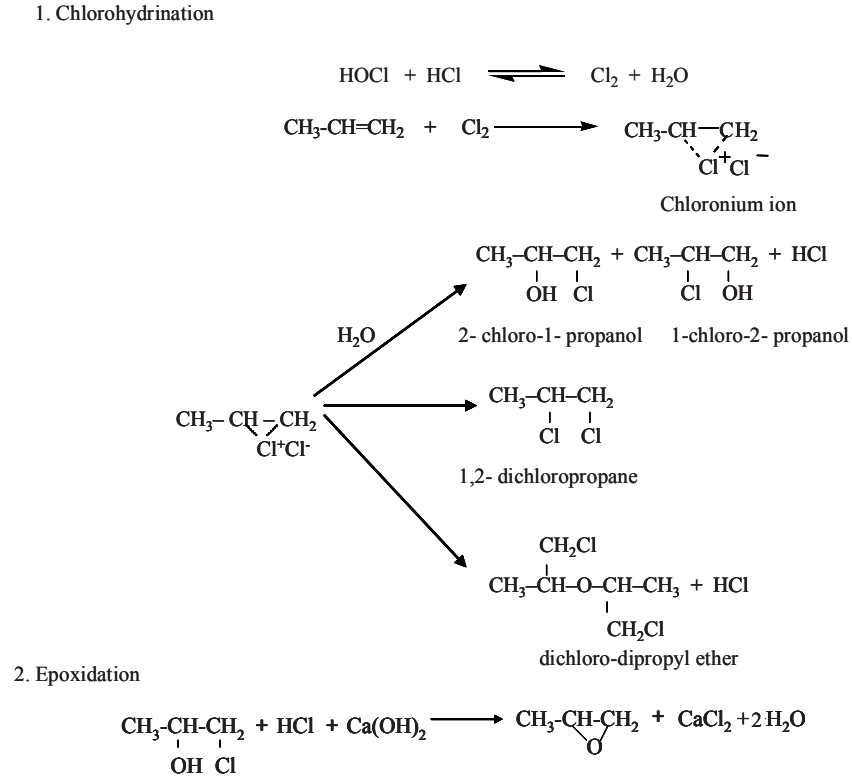

Scheme 1.2. The chlorohydrin process.

The resulting mixture of α- and β- chlorohydrin (ratio 9:1) will be dehydrochlorinated in the second step to propene oxide with a surplus of a base at 25º C. Propene oxide will then be rapidly removed out of the reaction mixture to avoid hydration by direct applying steam and then distillation. The selectivity is 87-90% based on C_3H_6.

The main by-products formed are 1,2- dichloropropane (from the gas-phase reaction of propene with chlorine) and smaller quantities of dichloropropanols (produced from allyl chloride, which is also formed in the gas phase from the reaction between propene and chlorine), as well as dichloroisopropyl ethers (from the reaction of the chloronium complex with propene chlorohydrin).

The relatively large amount of 1,2-dichloropropane (up to 10%) obtained as a second "product" from the separation section has very little usage and creates a disposal problem [4]. Alternatively, it is also possible to recycle the chlorinated propanes to propane or propene, which is a very effective way to improve the attractiveness of the process and reduce the environmental impact [5].

Each ton of propene oxide produced was formally accompanied by the production of a solution of 5% $CaCl_2$ usually 40 times larger than the amount of propene oxide produced. Reuse of $CaCl_2$ is not economically feasible, because of its low commercial value. Alternatively, sodium hydroxide can be used instead of calcium hydroxide. The advantage is that sodium chloride produced can then be used in the production of chlorine, which can be discharged easier or recycled in the first step of the process [3]. The process can remove the environmental problem to a large extent. The disposal of brine and chlorinated by-products are the main reason that no new chlorohydrin plants are built. Only the large-scale plants are expected to remain operational for a longer period because they are often integrated with chlorine production plants.

1.2.2. The hydroperoxide processes

The hydroperoxide processes involves epoxidation of propene with the hydroperoxide and conversion of the co-product alcohol to useful product. Commercially, three processes are used, namely the *tert*-butyl hydroperoxide process (PO-TBA) [6,7], the ethylbenzene hydroperoxide process (SMPO) [8,9,10] and the Sumitomo Chemical's cumene process [1].

The PO-TBA and SMPO processes were first developed by Halcon Corp. and Atlantic Richfield Oil Corp. (later ARCO). The coproducts of the first two processes that were mentioned above are *tert*-butanol, which is most often converted to methyl *tert*-butyl ether (MTBE) and 1-phenyl ethanol which is converted to styrene. These processes use isobutane and ethylbenzene respectively, to produce the hydroperoxide. With the ethylbenzene method, approximately 2.5 ton of styrene is coproduced for every ton of propene oxide, and with the isobutene method, 2.1 ton of isobutylene is co-produced for each ton of propene oxide. Typical producers using the SMPO process are Shell Chemicals Ltd., Lyondell Chemical Company, Repsol, SKC Chemical and Nihon Oxirane Co., Ltd. The PO-TBA producers are Lyondell and Huntsman International LLC.

The third process mentioned above, the Sumitomo Chemical's cumene process is using cumene for the production of propene oxide. Compared with the existing processes, this process has a high propene yield and can be called an environmentally friendly green process with almost no by-products. Other processes are using for example, acetaldehyde to acetic acid, 2-propanol to acetone, isopentane (via tert-pentyl alcohol) to isoprene and cyclohexene (via cyclohexanol) to cyclohexanone.

Each of these production methods will now be introduced.

1.2.2.1 The *tert*-butyl hydroperoxide process

In this process isobutane is oxidised to *tert*-butyl hydroperoxide (TBHP). TBHP is then mixed with a catalyst solution to react with propene (Scheme 1.3). The catalyst is typically an organometallic complex where the metal can be W, V or Mo. The selectivity to propene oxide is 95-98% based on TBHP and 97-98% based on propylene. The principal by-products are propene glycol, methyl formate and a propene dimer. Some of these by-products are difficult to be removed from the product propene oxide. Final purification of propene oxide is accomplished by a series of distillations.

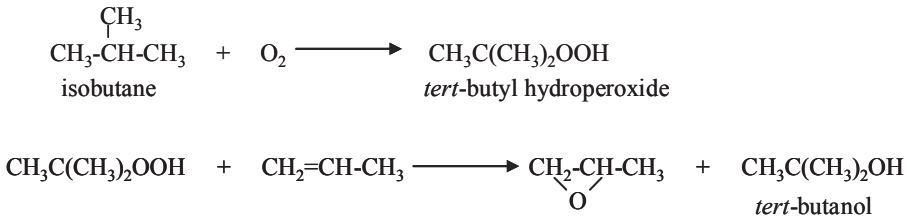

Scheme 1.3. The *tert*-butyl hydroperoxide process.

The *tert*-butanol (TBA) co-product is dehydrated to form isobutylene, which then reacts with methanol to form methyl *tert*-butyl ether (MTBE). Alternatively, the TBA is dehydrated to isobutene, which is further hydrogenated to isobutane for recycle in the propene oxide process [11]. This process become less attractive due to the fact that MTBE, which could be used as a gasoline additive, has declined in the United States in response to environmental and health concerns. It has been found to easily pollute large quantities of groundwater when gasoline with MTBE is spilled or leaked at gas stations.

1.2.2.2. The ethylbenzene hydroperoxide process

In this process, the steps are similar to the principle of PO-TBA process, ethylbenzene is oxidised with air to the hydroperoxide then the ethylbenzene hydroperoxide is reacting with propene, producing propene oxide and an alcohol (Scheme 1.4). The heart of this process is formed by the catalytic epoxidation of propene with ethylbenzene hydroperoxide (EBHP) using a silica-supported titanium catalyst. After epoxidation, propene oxide, excess propene, and propane are distilled overhead. The co-product 1-phenyl ethanol is dehydrated to styrene in a vapor-phase by passing the alcohol over a titania or alumina catalyst at 200-300º C.

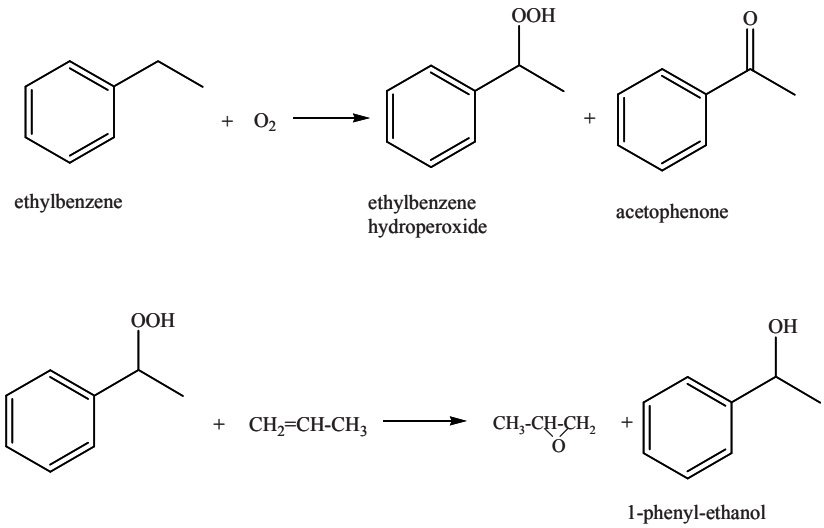

Scheme 1.4. The ethylbenzene hydroperoxide process.

The major disadvantage of the hydroperoxide processes (SMPO and PO-TBA) is the problem of the by-products, which are severely affected by market conditions. Therefore, it is difficult to say that these are always the optimal methods for producing propene oxide.

1.2.2.3. The Sumitomo Chemical's cumene process

Using cumene, Sumitomo Chemical has established a cumene propene oxide-only process as a new propene oxide production process [1,12]. This production method is fundamentally similar (Scheme 1.5) to the hydroperoxide processes and is made up of the following steps.

1. Oxidation process where cumene is oxidized in air to obtain cumene hydroperoxide;
2. Epoxidation process where propene oxide and α, α- dimethyl benzyl alcohol are obtained from cumene hydroperoxide and propene in the presence of an epoxidation catalyst;
3. Hydrogenation process where α, α- dimethyl benzyl alcohol is hydrogenated and cumene is obtained in the presence of a hydrogenation catalyst and hydrogen;
4. Cumene purification process where cumene obtained is purified and recycled to the oxidation process; and
5. Propene oxide purification process.

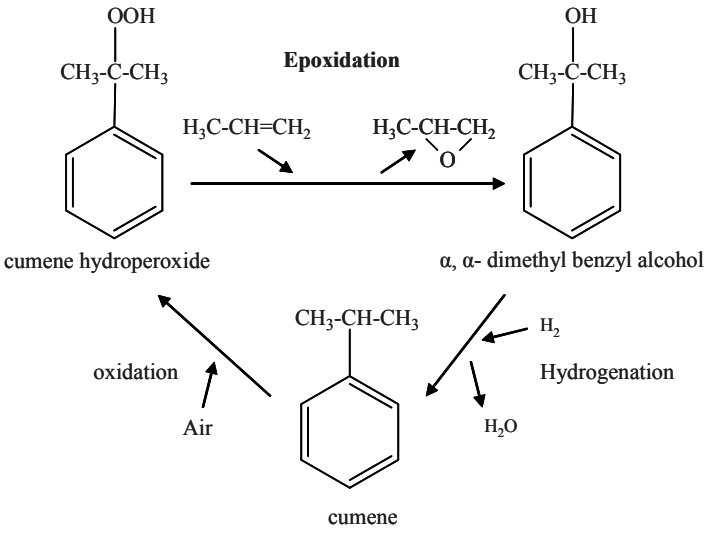

Scheme 1.5. The propene oxide cumene process.

The cumene oxidation rate is known to be approximately seven times faster than the ethylbenzene oxidation rate [13]. In addition, since cumene hydroperoxide is basically a stable peroxide, the hydroperoxide yields are higher than that for ethylbenzene and isobutene oxidation. The epoxidation process is a fixed bed process that uses a Ti-silicon oxide catalyst developed by Sumitomo Chemical. More specifically, the catalyst is a silicon oxide catalyst that contains Ti and has a mesoporous structure specially designed to exhibit a high level of activity for large molecules like cumene hydroperoxide. The main elements that have a crucial importance for the high activity of this catalyst are the presence of tetrahedral titanium in a highly dispersed state, its hydrophobic properties and the presence of mesoporous pores, which are effective for this reaction. The hydrogenation of α, α- dimethyl benzyl alcohol progress easily using various metal catalysts. The dimerization of α, α- dimethyl benzyl alcohol is not easily occurring and therefore the conversion to cumene can be done in an almost completely quantitative manner with this process.

The new process provides the flexibility to produce propene oxide as required by the market, without being restricted by the by-products demands.

1.2.3. The hydrogen peroxide process

In the Dow/BASF process, hydrogen peroxide is used to oxidize propene, producing PO and water. In this process titanium silicalite catalyst (TS-1) is used to produce propene oxide from propene and hydrogen peroxide. This process includes the in situ hydrogen peroxide production, propene reaction to propene oxide and product purification (Scheme 1.6). Hydrogen peroxide can

be obtained from the catalytic reaction of hydrogen and oxygen in alcohol or from the anthraquinone process. Hydrogen peroxide formation takes place in the liquid phase in the reactor and the reagents diffuse in the micropores of the TS-1 catalyst where the epoxidation reaction occurs.

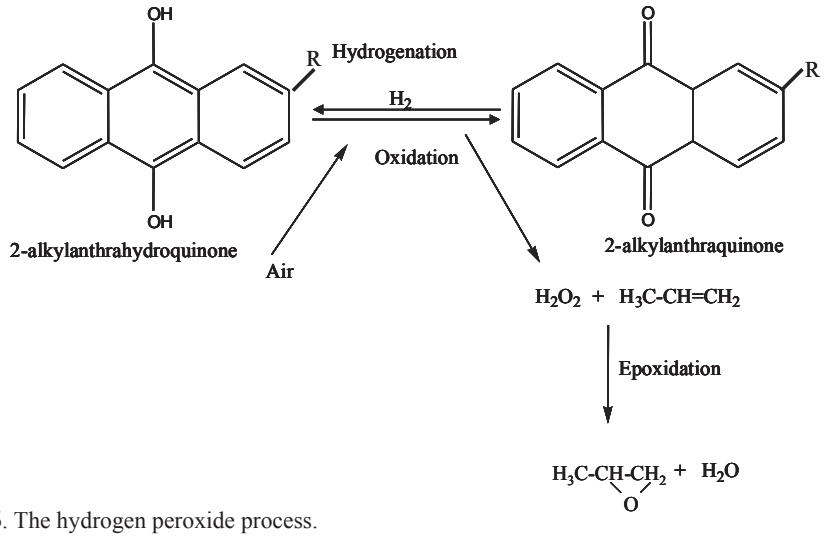

Scheme 1.6. The hydrogen peroxide process.

1.2.4. Other processes under investigation

An alternative process for H_2O_2 production involves the reduction of O_2 with H_2 over supported Pd catalysts. The combination of this chemistry with olefin epoxidation at sites provided by bifunctional solid catalysts has also been explored. Pd-Pt/TS-1 catalyst has been reported to produce propene oxide with 70% selectivity at a propene conversion of 34%. The reaction has been operated in semibatch in methanol-water solution at 42º C [14]. The mechanism proposed involves the synthesis of hydrogen peroxide at the metal sites of this bifunctional catalyst, followed by its consumption at the Ti sites that carry out the epoxidation. The principal side reaction was the hydrogenation of propene to propane due to the high activity of platinum group metals for olefin hydrogenation [14]. Early experiments have also shown that Cu/SiO_2 and $Ag/CaCO_3$ catalysts are capable of epoxidising propene, but with a conversion of ~ 1%, selectivity to propene oxide of 60%, and the propene oxide production decreasing with time [15]. While Ag catalysts work very well for epoxidising ethane, the main problem in the propene epoxidation reaction is that propene molecules contain reactive allylic hydrogens, which are sensitive to attack by nucleophilic oxygen species [16]. One class of materials, which attract the attention due to their possible application in the epoxidation process is represented by gold–type catalysts. These are typically characterized by nanoparticles of Au supported on TiO_2 [17,18] on other supports [19,20]. These materials are

carrying out the vapour-phase reaction of propene with a mixture of O_2 and H_2 to produce propene oxide.

1.3. Heterogeneous catalysis by gold

Catalysis by gold is a topic of much current interest because for a long time Au as a precious metal has been regarded as a poor catalyst material. There are several reasons that justify this interest. One explains that the catalytic activity of Au is directly related to the particle size in the nanometer length scale [21]. It can be observed in Figure 1.1 that the activity of an Au/TiO_2 catalyst for the oxidation of CO depends on the Au particle size. Catalysis by Au nanoparticles represents a bridge between homogeneous and heterogeneous catalysis since very small colloidal or supported gold nanoparticles have to be prepared [22]. Understanding the reason of this catalytic activity, optimizing and finding the reaction mechanism for gold-catalyzed reaction is a new research field in heterogeneous catalysis.

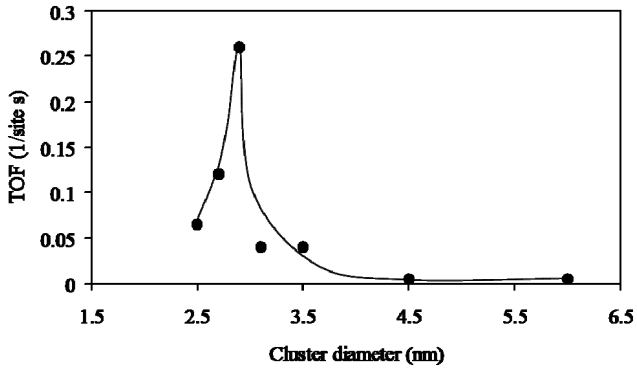

Figure 1.1. CO oxidation turnover frequencies (TOFs) at 27° C as a function of the average size of the Au clusters supported on a high surface area TiO_2 support. The Au/TiO_2 catalysts were prepared by the deposition-precipitation method. The average cluster diameters were measured by TEM. The solid line serves merely to guide the eye. Reproduced from Uphade et al. [20].

When Au is stabilized in the form of nanoparticles supported on metal oxide supports, it can have a surprisingly high catalytic activity in a number of reactions. However, early reports on the use of gold as a catalyst existed, but none of these showed to be superior to other catalysts [23,24]. The hydrogenation of olefins over supported Au catalysts reported in 1973 by the group of Bond changed the view regarding the catalytic activity of gold [25]. Haruta and Hutchings experimentally demonstrated that Au is an extraordinary catalyst for the low-temperature oxidation of CO and the hydrochlorination of ethyne to vinyl chloride [26-29]. For the first time these studies showed gold to be the best catalyst for these reactions, in strong contrast to previous reports on the poor activity of Au [23]. Another important example demonstrating the interesting properties of Au nanopaticles is their catalytic activity in direct synthesis of hydrogen peroxide. The group of Hutchings [30] showed gold to be active for the direct synthesis of hydrogen peroxide, which is one of the most challenging selectivity problems in oxidation chemistry. Since the discoveries of Hutchings and

Haruta, many more reactions have been found to be catalyzed by highly dispersed supported Au materials, including the water gas-shift reaction [31], the reduction of NO [32], the selective hydrogenation of acetylene and butadiene [25], the total oxidation of volatile organic compounds [33] and the selective oxidation of hydrocarbons [34]. Tuning to current work employing Au catalysts, the reaction that has attracted much attention is the oxidation of propene to propene oxide [17].

The fundamental question is therefore related with the properties of Au nanoparticles that make them catalytically active. There are many proposals, which associate the catalytic activity with the electronic nature of small Au particles. This electronic property can be significantly influenced by the nature of the support, especially the availability of defect sites [35,36,37]. The presence of Au atoms at the interface between Au particles and the oxide support has also been proposed as a model to explain the nature of active sites [35]. There are also a number of reports proposing that oxidized Au species (i.e. Au^{+}) on a support act as the active sites [38,39,40]. The support was also found to be crucial in the stabilization of different type of Au species. As the particle diameter decreases, the portion of gold atoms in contact with the support increases and the electronic nature of these atoms will be influenced by the support. Hence, the Au-support interaction determines the morphology of the Au particles and influences the number of low coordinated Au atoms. As a consequence, the activity of Au- catalysts is influenced by the method of preparation and activation of the catalyst [41,42,43].

A catalytic process that is using molecular oxygen as an oxidant is the most attractive for the epoxidation of propene because of its readily availability and low cost. However, the direct epoxidation of propene with O_2 does not produce sufficient selectivity [44] and considerable interest has arisen for the oxidation of propene with O_2/H_2 mixture. The copresence of H_2 can activate O_2 at relatively mild conditions with an energy input of less than 10 kJ mol^{-1}, while the energy required to activate O_2 for reaction by direct splitting it into its constituent atoms is 498 kJ mol^{-1}, which is larger than C-H bond energies. This leads to a possible alternative method of controlling the reactivity of oxygen species so as to produce valuable oxygenated organic compounds.

Approximatively ten years ago Haruta and co-workers [17] were the first to demonstrate that gold catalysts prepared by deposition-precipitation (DP) of Au on TiO_2 are capable to epoxidise propene very selectively using O_2 and H_2 over under mild conditions (> 90% selectivity to PO, 1 atm, 30-120º C) (Scheme 1.7). Despite this attractiveness, Au/Ti-based catalyst systems have a number of drawbacks, which need to be improved: the propene conversion levels remain low, often the catalyst stability is insufficient, and the hydrogen efficiency is low. The hydrogen efficiency (defined as the molar amount of propene oxide produced divided by the

amount of hydrogen consumed) is dominated by the water produced by the direct oxidation of hydrogen. Haruta and coworkers have estimated that the minimum requirements for a potential commercial process are a propene conversion of 10%, a propene oxide selectivity of 90% and a H_2 selectivity of 50% [45].

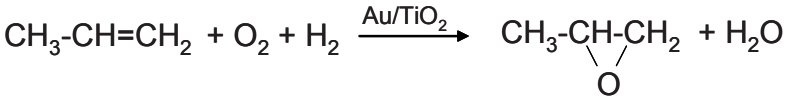

Scheme 1.7. Direct oxidation of propene using O_2 and H_2 over Au/TiO_2 catalyst.

According to Haruta et al. there are four important factors for the preparation of active Au catalysts in the direct epoxidation of propene. The first one is the method for Au deposition. In Figure 1.2 it can be observed that impregnation methods did not result into a selective oxidation process, but a complete oxidation to H_2O and CO_2. On the other hand, the deposition-precipitation method leads to epoxidation selectivities above 90% [46]. According to Haruta and Danté, using the deposition-precipitation method, Au particles of about 2-5 nm in size are deposited on the support in a hemispherical shape, which provides the longest distances around the perimeter interface of Au particles [47].

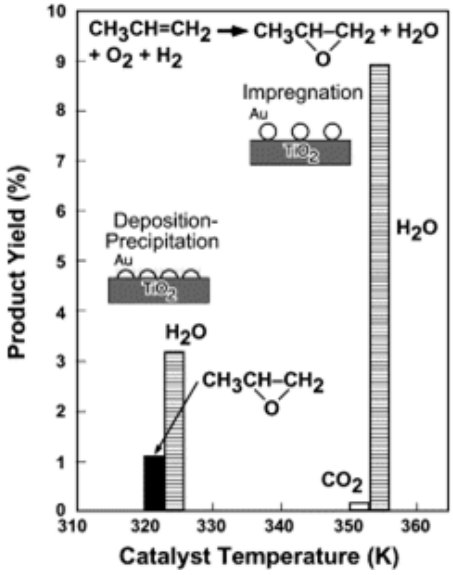

Figure 1.2. Epoxidation of propene over Au/TiO_2 catalyst prepared by different synthesis methods. Reproduced from Haruta and Danté [47].

The second one is the appropriate selection of the support materials. Depending on the nature of the support, not only the activity changes but also the productivity changes dramatically from PO to

other oxygenates or CO_2. Interestingly, the combination of Au with metal oxides, such as Al_2O_3, SiO_2, Fe_2O_3, Co_3O_4, ZnO and ZrO_2, does not selectively catalyze the partial oxidation of propene, and produced primarily H_2O and CO_2. Over Pd/TiO_2 and Pt/TiO_2, C_3H_6 is mostly transformed into C_3H_8 and only trace amounts of acetone are formed as an oxygenate [17]. Among single metal oxides, only TiO_2 in the form of anatase makes Au selective at temperatures below 100º C. But when Ti/SiO_2 support materials are used, Au is selective to the epoxidation up to 200º C, yielding improved conversions up to 5% at > 90% propene oxide selectivity [20,48-54]. The use of titanosilicate as either an amorphous or ordered support leads to the stabilization of propene oxide at higher temperature and an increase in propene oxide yield as the desorption of propene oxide is favored at higher reaction temperatures [18]. The third factor of influence is believed to be the shape and size of the Au particles. It has been proposed by the group of Haruta [17] that hemispherical Au particles of 2-5 nm in size are optimal for the epoxidation. Particles smaller than 2 nm catalyze the hydrogenation of propene to propane because of the different electronic properties of Au [17]. Particles that are too large have a relatively higher activity towards the combustion. Spherical Au particles are also less active than hemispherical particles because they have a relatively smaller gold-titania interface [18]. A picture of a typical Au/TiO_2 catalyst that can be used in the epoxidation of propene is shown in Figure 1.3.

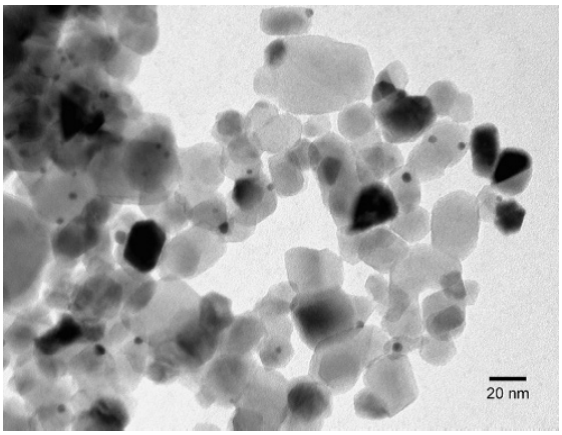

Figure 1.3. Transmission electron microscopy (TEM) picture of a typical Au/TiO_2 catalyst. The Au particles are the large (2-6 nm) round dark particles visible in the picture supported on the lighter-colored large (20-60 nm) titania particles. The larger dark particles are thicker titania particles. Reproduced from Nijhuis et al. [1].

The fourth factor of influence for the preparation of active epoxidation catalysts is the presence of additives. It has been claimed that many alkaline and alkaline earth salts act as good promoters and may play an important role in the selective epoxidation. Hydrogen consumption could be greatly suppressed when a promoter, such as CsCl, was physically mixed with Au catalysts. However, the optimum amount, the active sites and the mechanistic role of these promoters are not yet fully understood [48].

Catalyst instability is a problem for Au/TiO_2 materials. The activity of Au/TiO_2 catalysts is increasing with time on stream in the first 30 min [17,55] and can diminish by 50% in 2 h [19]. The sintering of Au can be largely solved by removing the chloride [56-58] since the catalysts are usually produced using gold chloride precursor and the residual chloride makes the catalyst very sensitive to sintering of the Au particles. The deactivation can be reversed by a high temperature cycle at 300º C in 10% O_2 in He, which indicates that catalyst deactivation has to do with adsorbed species and not with sintering of Au since this will be irreversible.

Cooperation between Au nanoparticles and the support in the catalytic cycle has been claimed frequently to rationalize the variations of catalytic activity of Au nanoparticles on different supports. For instance, for CO oxidation it is considered that amorphous, unstructured silica is an inadequate support. Both Au and Ti seem to be a necessity for a catalyst to epoxidise propene. For gold-titania catalysts, an improved stability and propene oxide yield can be obtained using a support that contains isolated tetrahedral Ti sites typically by using Ti-Si supports, such as TS-1, TS-2, Ti-MCM-41 and TI-MCM-48 [19,20,46-50,56,59-63].

1.3.1. Propene epoxidation over Au/TS-1 catalysts

Titanium Silicalite (TS-1) is a crystalline zeotype material in which tetrahedral $[TiO_4]$ and $[SiO_4]$ units are arranged in a MFI structure. The structure of TS-1 comprises a three-dimensional system of channels having molecular dimensions of 5.1-5.6 Å and which constitutes the micropores of the material. The heterogeneous Ti(IV) SiO_2 catalysts developed first by Clerici et al. can catalyze the liquid-phase epoxidation of propene with very high selectivities toward propene oxide (90-97%) using a dilute solution of H_2O_2 [64]. The active site was suggested to be tetrahedrally coordinated Ti with Lewis acid character capable of coordinating two nucleophile molecules. This inherent epoxidation activity makes TS-1 supported with nanoscale Au a promising candidate for the direct epoxidation of propene using H_2 and O_2. Futhermore, TS-1 is useful as a support to confine small Au clusters into the space of microcages [19]. Nijhuis et al. were able to produce propene oxide (95% selectivity) over a 1 wt% Au/TS-1 catalyst at a space velocity of 6,600 ml g_{cat}^{-1} h^{-1} (70-150º C) [19]. The propene conversion remains low (< 2%) with propene oxide formation rates ranging from 4-18 g_{PO} kg^{-1}_{cat} h^{-1}. They found that Au/TS-1 catalysts are more resistant to deactivation even after 2 h reaction time and produced slightly higher propene conversion comparable with the classical Au/TiO_2 catalyst. However, the H_2 efficiency was only 5-6% compared with 22-26% for the Au/TiO_2 catalysts. Nijhuis et al. performed a thermogravimetric analysis (TGA) on both Au/TiO_2 and Au/TS-1 catalyst and found two forms of carbon deposited on Au/TiO_2 [18]. The first coke type is benign, while the second one is leading to deactivation. Experiments on Au/TS-1 indicated only the deposition of benign carbon. In-situ FT-IR on Au/TiO_2

and $Au/TiO_2/SiO_2$ showed that bidentate propoxy species are formed on adjacent Ti sites active and selective in propene epoxidation and that occupation of these sites with propoxy groups is limited on the TiO_2/SiO_2 support due to the dispersion of Ti in the support [65]. Since no change in Au particle size between fresh and spent catalyst was observed from the TEM micrographs, these authors concluded that the cause of Au/TiO_2 deactivation is due to the accumulation of oligomerized products of propene oxide and carbonate derived intermediate on Ti sites that are in close proximity.

Time-dependent kinetic measurements showed that the stability of Au/TS-1 catalysts is dependent on the Au and Ti loading and that dilute Au and Ti systems produced more stable and active Au/TS-1 catalysts [59]. Haruta et al. have shown that low titanium and low Au loadings do produce very active catalysts when the rate is normalized to the Au content [66]. The group of Delgass reported that Au/TS-1 catalyst prepared with Si/Ti= 36 and a Au loading of 0.05 wt% produced 116 $g_{PO}\ g_{Au}^{-1}h^{-1}$ at 200º C, which is one of the highest rates reported for a TS-1 based catalyst with no evidence for deactivation during the 40 h of operation. The absence of visible Au particles in the TEM measurement implies high dispersion of the deposited gold and also indicates that significant activity is due to Au particles smaller than 1 nm [63]. The high specific activity per Au atom at very low loadings implies, at least for TS-1 supports, that the additional Au present at higher loadings is either less or completely inactive towards oxidant generation and that only a portion of Au deposited on the surface creates active Au-Ti epoxidation centers [59].

It is commonly believed that the Au particles have a critical effect on the activity and selectivity in the direct epoxidation of propene over Au/Ti catalysts. Haruta et al. suggested that Au/TiO_2 catalysts containing Au particles of 2-5 nm are responsible for the formation of propene oxide, while the one smaller than 2 nm form propane [17]. However, Delgass et al. suggested that Au particles smaller than 2 nm could contribute significantly to the epoxidation reaction [63]. They also performed Density Functional Theory (DFT) calculations and found that three atom Au clusters could form H_2O_2, suggesting that small Au clusters also could be active in propene oxide formation [67]. Barton and Podkolzin [68] have also shown with DFT calculations that the formation of H_2O_2 from H_2 and O_2 is dependent on the Au particle size. Thus smaller particles are proposed to be less reactive due to the instability of the OOH intermediate, whereas larger particles are less reactive due to the instability of adsorbed oxygen. The true nature of the active Au species and its interaction with Ti remain still a fundamental question.

It has been shown that the morphology of TS-1 particles plays also an important role in the epoxidation activity. Prismatic crystallites generally resulted in inferior catalysts as compared to materials with more globular or spheroidal particle morphologies. Superior performance from catalyst material made from poorly formed TS-1 crystallites implied that structural defects may play

a vital role in the activity of the Au/Ti system [69]. DFT calculations on non-defect (tetrapodal) and metal-vacancy defect (tripodal) Ti sites in TS-1 suggested that the H_2O_2 attack on Ti-defect sites is leading to Ti-OOH species (and water), while the H_2O_2 attack on Ti-nondefect sites is kinetically and thermodynamically less favourable (Schemes 1.8 and 1.9) [70]. Considering these studies Taylor et al. synthesised TS-1 supports that were grown around the carbon pearls [69]. This procedure increased the number of Ti-defect sites. Au/TS-1 catalysts prepared by this method with 0.33% Au were able to produce 132 $g_{PO}\,kg_{cat}^{-1}h^{-1}$ at 200º C. This implied that the modified synthesis procedure may have resulted in encapsulation of the octahedral Ti speciest and in improving the diffusion distances compared with the non-perfect TS-1 support.

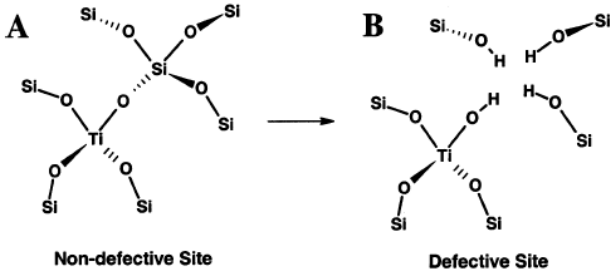

Scheme 1.8. Schematic view of a fully tetrahedrally bonded Ti ion substituted for a Si ion at one of the lattice positions of TS-1 (A) and the same Ti site located near a silicon vacancy terminated with hydrogen atoms forming a silanol nest (B). Reproduced from Wells et al. [70].

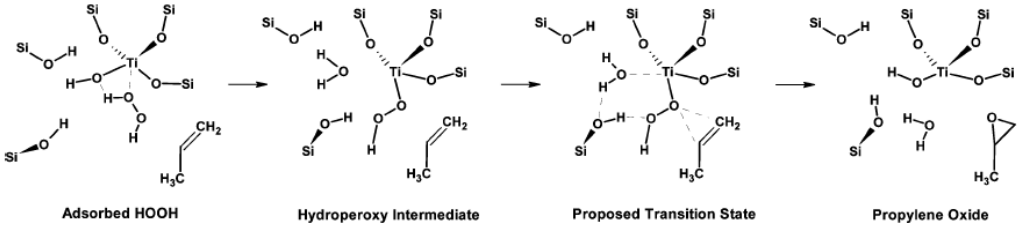

Scheme 1.9. Mechanism for HOOH/propene epoxidation on a defective Ti site in TS-1. Reproduced from Wells et al. [70].

1.3.2. Propene epoxidation over Au on Ti-containing mesoporous supports

The importance of the morphology of the supporting material is evidenced by the improved performance of Au dispersed on ordered and disordered mesoporous titanosilicates. Mesoporous Ti-containing materials are similar to microporous materials in that they offer highly dispersed Ti-centers and reasonably well-defined tetrahedral Ti sites incorporated in a siliceous framework. Moreover, the mesoporous system is able to incorporate Au species in the range of 2 nm and allows

for Au entities to access essentially the interior of the support surface area. The larger pores are also advantageous for the smooth diffusion of the reactant and rapid escape of the products formed [18]. Deposition of Au via deposition-precipitation onto the Ti-MCM-41 materials resulted in a particle-size distribution in which 70% of the Au particles were capable of fitting inside the pore system [71]. The Au/Ti-MCM-41 catalyst is more active and stable than the Au/TS-1 catalyst with similar Ti loading (Ti/Si≈ 0.028), which indicates that the introduction of an ordered pore system with a high surface area greatly enhances the catalytic activity, propene oxide selectivity and H_2 efficiency. In general, the reactivity of Au/Ti-MCM-41 materials can be influenced by the mode of Ti incorporation and the amount of Ti incorporated in the mesoporous structures. It has been shown that Au/Ti-MCM-41 materials with 4.5 mol% Ti prepared by the two-step Ti incorporation, hydrothermally during crystallization followed by post-synthesis grafting are more active for propene epoxidation reaction, than Au/Ti-MCM-41 catalysts prepared by the one-step Ti incorporation, hydrothermally or by post-synthesis grafting. The improved activity of Au/Ti-MCM-41 catalysts prepared by the two-step Ti incorporation was attributed to the greater number of accessible and well-dispersed Ti sites, which can utilize the in-situ generated hydroperoxy species for the epoxidation more efficiently [50]. With an increasing Ti content up to the framework incorporation limit of Ti/Si≈ 0.02, the amount of Au deposited during deposition-precipitation and the propene oxide production rate increases but the propene oxide selectivity and the H_2 efficiency decreases [50,53]. While MCM-41 materials are an improvement over microporous materials due to larger pore system, MCM-48 allows a greater access to the internal surface through its three dimensional channel system types. Au/Ti-MCM-48 are superior in comparison to Au/Ti-MCM-41 in their activity (53 $g_{PO}\,kg_{cat}^{-1}h^{-1}$ *vs* 47 $g_{PO}\,kg_{cat}^{-1}h^{-1}$), propene oxide selectivity (92% to 88%) and H_2 efficiency (10% to 7%). This is mainly attributed to the larger pore size and 3D mesoporosity of the support [20,72,73]. The group of Haruta reported that Au catalysts supported on three-dimensionally mesoporous wormhole titanosilicates exhibit propene oxide formation rates of 51.7-91.6 $g_{PO}\,h^{-1}Kg_{cat}^{-1}$ at 150º C. Despite significant deactivation, more than 80% of their activity can be recovered with a treatment in H_2 and O_2 at 250º C [74,75]. Addition of $Ba(NO_3)_2$ to the Au/Ti-based catalysts has also been shown to increase propene conversion probably due to the decreasing acidic character of the catalyst surface [74]. The introduction of trimethylamine in the feed stream as a gas-phase promoter has been shown to reduce water production as well to increase the hydrophobicity of the catalyst surface by bonding to Ti Lewis acid sites, aiding in propene oxide desorption, hence increasing the catalyst lifetime [76]. A more stable catalyst was prepared by deposition-precipitation of Au onto mesoporous Ti-TUD substrate. The maximum rate obtained with this catalyst was 53.7 $g_{PO}\,kg_{cat}^{-1}\,h^{-1}$ at 170º C using a 20/20/20/40 vol % mixture of $H_2/O_2/C_3H_6$/He [45].

Investigation of Au catalysts supported on different titania-silica materials indicated that conversion, selectivity and hydrogen efficiency results are depending on several parameters, like gold particle size, titanium coordination sphere, site isolation, hydrophobicity and pore size [17,53,61-63,74]. Also the presence of additives particularly amines are affecting the selectivity to propene oxide.

Silylation of Au/Ti-based catalysts is a method to replace the surface silanol groups with hydrophobic methylsilyl groups. By diminishing the strong interaction between surface silanol groups and propene oxide, it is possible to enhance the propene oxide desorption and to slow down the deactivation of the catalyst caused by the formation of the adsorbed propoxy intermediates [19]. Silylation of Au/Ti-MCM-48 with methoxytrimethylsiloxane before Au deposition prohibited it from getting deactivated faster and also helped to improve the propene oxide selectivity (95% *vs* 90%) and H_2 efficiency (12% *vs* 7.5%), but with a lower propene oxide rate (27 $g_{PO}Kg_{cat}^{-1}h^{-1}$ *vs* 43 $g_{PO}Kg_{cat}^{-1}h^{-1}$) caused by blocking of the active sites [20]. Another silylation procedure of Au/Ti-MCM-48 has been developed using N-methyl-N-(trimethylsilyl)trifluoroacetamide [74]. Deposition of Au via the deposition impregnation method could not be achieved due to the hydrophobic properties of the silylated Ti/MCM-48 support. A liquid grafting method was then applied using $(CH_3)_2Au(O_2C_5H_7)$ as the Au source. The catalytic activity of the resulted silylated Au/Ti-MCM-48 catalyst was low (2.1-15 $g_{PO}Kg_{cat}^{-1}h^{-1}$) and depended on the amount of N-methyl-N-(trimethylsilyl) trifluoroacetamide used in the preparation. The lower activity was a consequence of the low Au loading (~ 0.5 wt%) and of the use of the liquid grafting method that produced Au particles with different properties than the ones resulted from the deposition-precipitation method. The initial catalyst deactivation with time-on-stream was appreciably depressed for the silylated Au/Ti-MCM-48 catalyst but at longer times the deactivation rate appear comparable. The H_2 efficiency of this catalyst did not improve probably due to the different way of Au deposition that resulted in Au nanoparticles, which catalyze water formation in the absence of epoxidation activity [74]. Silylation of Au catalysts supported on disordered titanosilicates with methoxytrimethylsilane has been found to be very positive towards increasing the propene oxide production rate from 52-67 $g_{PO}Kg_{cat}^{-1}h^{-1}$ compared with an unsilylated material but having no significant effect on H_2 efficiency. Catalyst deactivation rate was also partially prevented. Highly dispersed Au nanoparticles supported on 3D mesoporous, silylated titanosilicates with large pores (< 7nm) in the presence of $Ba(NO_3)_2$ promoter have been found to be one of the most efficient catalysts for the epoxidation of propene with a PO rate of 92 $g_{PO}Kg_{cat}^{-1}h^{-1}$ at 150º C [75].

1.3.3. Mechanistic study of Au/Ti-based catalysts

Several reaction mechanisms have been proposed for the direct epoxidation of propene with O_2 and H_2 [57,58,67,70,81-83]. The catalytic mechanism requires the presence of both Au and Ti. Titania alone has no activity for the epoxidation of propene with H_2 and O_2. Au/SiO_2 does not produce significant quantities of propene oxide either. Nijhuis et al. [57,58] suggested that the reaction mechanism (Scheme 1.10) on Au/TiO_2 and $Au/Ti\text{-}SiO_2$ materials may involve the following steps: (1) propene reacts with titania to produce an adsorbed bidentate propoxy species, this reaction is catalyzed by the Au nanoparticles present on titania; (2) hydrogen and oxygen produce hydroperoxide species on Au; (3) the peroxide species aids in the desorption of the bidentate propoxy species from the catalyst, producing propene oxide and water and restoring the titania in its original state. The peroxide formation on Au from H_2 and O_2 has been confirmed in the literature both experimentally [29,77] and theoretically [67,68]. Furthermore, peroxide species are assumed to be the essential reaction intermediates in the propene epoxidation using H_2/O_2 over gold-titania catalysts [77]. Delgass et al. suggested the involvement of hydroperoxide species based on a D_2 kinetic isotope effect found for propene epoxidation reaction, but this species were not directly observed [78]. Using inelastic neutron scattering (INS), the group of Goodman reported the presence of hydroperoxide species on an Au/TiO_2 catalyst. However, the measurement conditions (-253º C) were far from reaction conditions [77]. Furthermore, no peroxide species could be spectroscopically observed by Nijhuis and co-workers [57]. Based on these observations the key role of hydrogen peroxide in the mechanism consists of aiding desorption of the bidentate propoxy species [79].

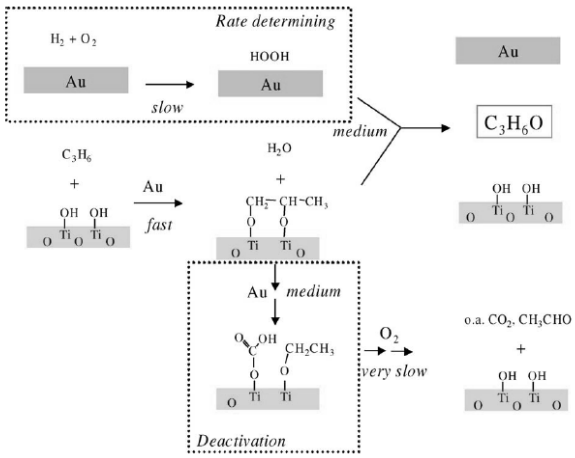

Scheme 1.10. Schematic representation of the model for the propene epoxidation over gold–titania catalysts and its related deactivation. Reproduced from Nijhuis et al. [58].

The question for the first step of this reaction mechanism is related with the source of oxygen that generates the bidentate species on the catalyst surface. In the FT-IR propene adsorption experiments, these species were formed without the presence of oxygen in the gas phase [79]. A kinetic reaction model based on the above model could be fitted to the experimental observations, yielding realistic values for the rate constants and activation energies [80].

Some theoretical work has been carried as well [67,70,81], and the kinetics of propene oxide synthesis over Au/TS-1 and Au-Ba/Ti-TUD have been investigated. The similarity in the power-rate law expressions for propene oxide synthesis on the Au/TS-1 [82] and Au-Ba/Ti-TUD [76] catalyst systems suggest that the steps occurring on both catalysts are similar. There seems to be an agreement that the important steps during propene oxide synthesis consist of the sequence shown in Scheme 1.11. The following steps can be distinguished (1) synthesis of hydrogen peroxide from hydrogen and oxygen on Au nanoparticles; (2) formation of Ti-hydroperoxo or peroxo species from hydrogen peroxide on tetrahedral Ti centers; (3) reaction of propene with the Ti-hydroperoxide species to form propene oxide and (4) decomposition of hydrogen peroxide to water.

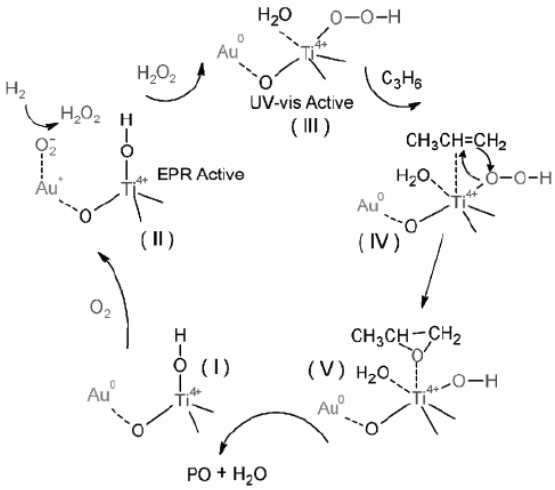

Scheme 1.11. Possible sequence of reaction steps for propene epoxidation with H_2 and O_2 over Au-supported titanosilicates. Reproduced from Bravo-Suárez et al. [83].

For this proposed mechanism Bravo-Suárez and co-workers [83] determined the dynamic change of the tetrahedral Ti^{4+} surface coverage using spectroscopic measurements (in-situ UV-Vis and X-ray Absorption Fine Structure or XAFS). The reaction rate appears to be determined by two irreversible steps: the production of hydrogen peroxide on a Au site and the epoxidation of propene by a hydroperoxide species on a Ti site. Despite these studies direct experimental evidence supporting this sequence of steps has been lacking. Chowdhury et al. reported the presence of Ti-

hydroperoxo species on a Au/(mesoporous) Ti-SiO_2 during in-situ UV-Vis measurements at propene oxide synthesis conditions, but did not confirm that it was a reactive species [84]. Bravo-Suárez and co-workers [83] determined the reaction rate based on the Ti coverage, and the value was close to the TOF for propene epoxidation, indicating that Ti-hydroperoxide is a true intermediate. From the in-situ FT-IR measurements, they also observed bands characteristic to bidentate propoxy species suggesting that they were no intermediates in this reaction.

1.3.4. Conclusions

Gold-catalysts have been attracting considerable interest. The development of efficient Au/Ti-based catalysts for the production of propene oxide has resulted in significant progress in the last decade. The activity of Au/Ti-based catalysts for the production of propene oxide was found to be influenced by numerous factors, such as preparation method, choice of the gold precursor, gold concentration, gold particle size, choice of support, amount, dispersion and coordination of Ti in the silica framework. After several studies into the use of microporous titanosilicate as highly dispersed Ti-supports for propene epoxidation, interest moved to mesoporous titanosilicates as these materials offer highly dispersed Ti centers and reasonably well-defined tetrahedral Ti sites incorporated in the mesoporous silica framework. Moreover, these materials allow incorporation of Au species inside their pores and facilitate the transport of reactants and products to and from the sites. It has been established that the activity of the Au/Ti-silica based catalysts follow the Ti loading as long as Ti remains isolated and tetrahedral. It has also been found that the highest Au efficiency is at the lowest loading and that excess Au is detrimental to stability. The literature strongly suggests that there must be small gold particles intimately connected with the Ti sites in the silica support and that the active sites may be the boundary between Au and Ti sites, i.e., the periphery of the metal particles. Precisely why Au particles in this small size range are so helpful to catalytic activity is not yet understood. In spite of major advances in catalyst development for propene oxide synthesis through the hydrogen-oxygen route, more effort has to be carried to understand the reaction mechanism.

1.4. Scope and outline of the PhD thesis

The goal of the research described in this PhD thesis is to study the catalytic mechanism of Au/Ti-based catalysts for the epoxidation of propene with H_2 and O_2. To achieve this goal, we have focused our work on the synthesis and characterization of new types of well-defined Au/Ti-based catalysts. Various preparation methods, such as hydrothermal and grafting methods for the incorporation of titanium, as well various deposition-precipitation methods for the gold deposition,

have been applied for the synthesis of well-defined Au/Ti-SBA-15 type materials. In-situ delta-mu XANES analysis and Steady State Isotopic Transient Kinetic Analysis have been used to provide new information on the propene epoxidation mechanism.

In **Chapter 2** the influence of the synthesis method on the final structure of Au/Ti-SBA-15 materials and their catalytic activity in the epoxidation of propene with H_2 and O_2 are studied. Two series of Au/Ti-SBA-15 materials differing in their Ti content were prepared by grafting or hydrothermal synthesis procedure. The choice of the preparation method of Ti-SBA-15 supports was found to be crucial for the deposition of Au. Moreover, we demonstrate that the catalytic activity of Au/Ti-SBA-15 materials can be linked to the amount of tetrahedral Ti sites, as well to the Au particle size.

In **Chapter 3** the impact of NH_4NO_3 treatment on the Au/Ti-SBA-15 materials is investigated in order to understand the enhanced activity in the direct epoxidation of propene with O_2 and H_2 compared with untreated Au/Ti-SBA-15. Various characterization techniques, such as XRD, N_2-sorption, UV-Vis DRS, ^{29}Si MAS NMR, FT-IR and TEM, have been applied to explain the relation between NH_4NO_3 treatment and catalyst activity. The characterization results indicated that the effect of the NH_4NO_3 pretreatment is related to the homogenous deposition of Au, thus increasing the number of active sites for the propene epoxidation reaction.

In the work described in **Chapter 4** in-situ XANES spectroscopy was used to investigate the adsorption of various hydrocarbons on Au. The hydrogen oxidation over Au/SiO_2 catalysts has been used as probe reaction in order to obtain more insights on the mechanism of Au/Ti-based catalysts for the propene epoxidation. Delta-mu analysis of the in-situ XANES spectra was applied to determine the adsorption mode of propene on Au. The work demonstrated that the adsorption of propene on Au nanoparticles can be a step in the epoxidation reaction mechanism.

In **Chapter 5**, Steady State Isotopic Transient Kinetic Analysis was used to investigate the reaction mechanism of Au/Ti-based catalysts. The aim of the study was to determine if support oxygen plays a role in the formation of propene oxide.

Chapter 6 comprises an extensive overview of theoretical, kinetic, and spectroscopic studies focusing on the mechanism of the propene epoxidation with O_2 and H_2 over Au/Ti-based catalysts. Our results are discussed together with the studies from the open literature in order to better understand the role of potential reaction intermediates and active sites in the propene epoxidation reaction. General conclusions are formulated and future perspectives are given.

References

1. T.A. Nijhuis, M. Makkee, J.A. Moulijn, B.M. Weckhuysen, Ind. Eng. Chem. Res., 45 (2006) 3447.

2. D.L. Trent, Encyclopedia of Chemical Technology, Wiley, New York, 2001.
3. D. Kalich, U. Wiechern, J. Linder, In Ullman's Encyclopedia of Industrial Chemistry, 5th Edition; Verlag Chemie: Weinheim, Germany, 1993; Vol. A22, p 239.
4. W.F. Richey, Chlorohydrins. In Kirk-Othmer: Encyclopedia of Chemical Technology, 4th Edition; Wiley: New York, 1994; Vol. 6, p 140.
5. M.D. Cisneros, M.T. Holbrook, L.N. Ito. U.S. Patent No. 5,476,984, 1995, (Dow Chemical Co).
6. J. Kollar, U.S. Patent No. 3,351,635, 1967, (Halcon Corporation).
7. E.T. Marquis, K.P. Keating, J.F. Knifton, W.A. Smith, J.R. Sanderson, J. Lustri, U.S. Patent No. 4,891,437, 1990, (Texaco Corporation).
8. M. Pell, E.I. Korchak, U.S. Patent No. 3,439,001, 1969, (Halcon Corporation).
9. W.S. Dubner, R.N. Cochran, U.S. Patent No. 5,210,354, 1993, (ARCO Corporation).
10. J.J. Van Der Sluis, U.S. Patent No. 6,504,038, 2003, (Shell Corporation).
11. http://www.dow.com/PublishedLiterature/dh_0036/0901b80380036c15.pdf?filepath=propyleneoxide/pdfs/noreg/117-01641.pdf&fromPage=GetDoc.
12. T. Seo, J. Tsuji, U.S. Patent No. 6,646,139, 2003, (Sumitomo Corporation).
13. Y. Kamiya, J. Fuel. Soc. Jpn. 1970, 603.
14. W. Laufer, W. F. Holderich, Appl. Catal. A: General, 213 (2001) 163.
15. J. Lu, J.J. Bravo-Suárez, A.Takahashi, M. Haruta, S.T. Oyama, J. Catal., 232 (2005) 85.
16. M.A. Barteau, R.J. Madix, J. Am. Chem. Soc., 105 (1983) 344.
17. T. Hayashi, K. Tanaka, M. Haruta, J. Catal., 178 (1998) 566.
18. A. K. Sinha, S. Seelan, S. Tsubota, M. Haruta, Top. Catal., 29 (2004) 95.
19. T.A. Nijhuis, B.J. Huizinga, M. Makkee, J.A. Moulijn, Ind. Eng. Chem. Res., 38 (1999) 884.
20. B.S. Uphade, T. Akita, T. Nakamura, M. Haruta, J. Catal., 209 (2002) 331.
21. G. R. Bamwenda, S. Tsubota, T. Nakamura, M. Haruta, Catal. Lett., 44 (1997) 83.
22. A. Corma, Catal. Rev. Sci. Eng., 46 (2004) 369.
23. G.C. Bond, Gold Bull., 5 (1972) 11.
24. A.S.K. Hashmi, Gold Bull., 37 (2004) 51.
25. G.C. Bond, P.A. Sermon, G. Webb, D.A. Buchanan, P.B. Wells, J. Chem. Soc. Chem. Commun., (1973) 444.
26. M. Haruta, Nature, 437 (2005) 1098.
27. G.J. Hutchings, Catal. Today, 100 (2005) 55.
28. M. Haruta, T. Kobayashi, H. Sano, N. Yamada, Chem. Lett., 16 (1987) 405.
29. G.J. Hutchings, J. Catal., 96 (1985) 292.
30. P. Landon, P.J. Collier, A.J. Papworth, C.J. Kiely, G.J. Hutchings, Chem. Commun., (2002) 2058.

31. D. Andreeva, V. Idakeiv, T. Tabakova, A. Andreev, R. Giovanoli, Appl. Catal. A: General, 134 (1996) 275.
32. A. Ueda, M. Haruta, Gold Bull., 32 (1999) 3.
33. B.E. Solsona, T. Garcia, C. Jones, S.H. Taylor, A.F. Carley, G.J. Hutchings, Appl. Catal. A: General, 312 (2006) 67.
34. M.D. Hughes, Y.-J. Xu, P. Jenkins, P. McMorn, P. Landon, D.I. Enache, A.F. Carley, G.A. Attard, G.J. Hutchings, F. King, E. Hugh Stitt, P. Johnston, K. Griffin, C.J. Kiely, Nature, 437 (2005) 1132.
35. G.C. Bond, D. T. Thompson, Gold Bull., 33 (200) 41.
36. M. Haruta, Gold Bull., 37 (2004) 27.
37. A.K. Sinha, S. Seelan, S. Tsubota, M. Haruta, Angew. Chem. Int. Ed, 116 (2004) 1572.
38. N.A. Hodge, C.J. Kiely, R. Whyman, M.R.H. Siddiqui, G.J. Hutchings, Q.A. Pankhurst, F.E. Wagner, R.R. Rajaram, S.E. Golunski, Catal. Today, 72 (2002) 133.
39. H.H. Kung, M.C. Kung, C.K. Costello, J. Catal., 216 (2003) 425.
40. J. Guzman, B.C. Gates, J. Am. Chem. Soc., 126 (2004) 2672.
41. A. Baiker, J.D. Grunwaldt, C.A. Mueller, L. Schmid, Chimia, 52 (1998) 517.
42. A. Wolf, F. Schuth, Appl. Catal. A: General, 226 (2002) 1.
43. C. Aprile, A. Abad, H. Garcia, A. Corma, J. Mater. Chem., 15 (2005) 4408.
44. S.T. Oyama, K. Murata, M. Haruta, Shokubai, 46 (2004) 13.
45. B. Choudhury, J.J. Brávo-Suarez, M. Danté, S. Tsubota, M. Haruta, Angew. Chem. Int. Ed. 45 (2006) 412.
46. M. Haruta, B.S. Uphade, S. Tsubota, A. Miyamoto, Res. Chem. Intermed., 24 (1998) 329.
47. M. Haruta, M. Daté, Appl. Catal. A: General, 222 (2001) 427.
48. B.S. Uphade, M. Okumura, S. Tsubota, M. Haruta, Appl. Catal. A: General, 190 (2000) 43.
49. B.S. Uphade, Y. Yamada, T. Akita, T. Nakamura, M. Haruta, Appl. Catal. A: General, 215 (2001) 137.
50. A.K. Sinha, S. Seelan, T. Akita, S. Tsubota, M. Haruta, Appl.Catal. A: General, 240 (2003) 243.
51. A.K. Sinha, T. Akita, S. Tsubota, M. Haruta, Stud. Surf. Sci. Catal., 142 (2002) 611.
52. A.K. Sinha, S. Seelan, S. Tsubota, M. Haruta, Stud. Surf. Sci. Catal., 143 (2002) 167.
53. A.K. Sinha, S. Seelan, T. Akita, S. Tsubota, M. Haruta, Catal. Lett., 85 (2003) 223.
54. M.P. Kapoor, A.K. Sinha, S. Seelan, S. Inagaki, S. Tsubota, H. Yoshida, M. Haruta, Chem. Commun., (2002) 2902.
55. T. Hayashi, K. Tanaka, M. Haruta, Am. Chem. Soc. Div. Petr. Chem., 41 (1996) 71.
56. A. Zwijnenburg, M. Makkee, J.A. Moulijn, Appl. Catal. A: General, 270 (2004) 49.
57. T.A. Nijhuis, T. Visser, B.M. Weckhuysen, J. Phys. Chem. B., 109 (2005) 19309.

58. T.A. Nijhuis, B.M. Weckhuysen, Catal. Today, 117 (2006) 84.
59. N. Yap, R.P. Andres, W.N. Delgass, J. Catal., 226 (2004) 156.
60. Y.A. Kalvachev, T. Hayashi, S. Tsubota, M. Haruta, J. Catal., 186 (1999) 228.
61. L. Cumaranatunge, W.N. Delgass, J. Catal., 232 (2005) 38.
62. E.E. Stangland, B. Taylor, R.P. Andres, W.N. Delgass, J. Phys. Chem. B, 109 (2005) 2321.
63. B. Taylor, J. Lauterbach, W.N. Delgass, Appl. Catal. A: General, 291 (2005) 188.
64. M.G. Clerici, G. Bellusi, U. Romano, J. Catal., 129 (1991) 159.
65. G. Mul, A. Swijnenburg, B. van der Linden, M. Makkee, J.A. Moulijn, J. Catal., 201 (2001) 128.
66. C. Qi, M. Okumura, T. Akita, M. Haruta, Appl. Catal. A: General, 263 (2004) 19.
67. D.H. Wells, W.N. Delgass, K.T. Thomson, J. Catal., 225 (2004) 69.
68. D.G. Barton, S.G. Podkolzin, J. Phys. Chem. B, 109 (2005) 2262.
69. B.Taylor, J. Lauterbach, W.N. Delgass, Catal. Today, 123 (2007) 50.
70. D.H. Wells, W.N. Delgass, K.T. Thomson, J. Am. Chem. Soc., 126 (2004) 2956.
71. Y.A. Kalvachev, T. Hayashy, S. Tsubota, M. Haruta, J. Catal., 186 (1999) 228.
72. B.S. Uphade, M. Okumura, N. Yamada, S. Tsubota, M. Haruta, Stud. Surf. Sci. Catal., 130 (2000) 833.
73. C. Qi, T. Akita, M. Okumura, K. Kuraoks, M. Haruta, Appl. Catal. A: General, 253 (2003) 75.
74. A.K. Sinha, S. Seelan, S. Tsubota, M. Haruta, Angew. Chem. Int. Ed., 43 (2004) 1546.
75. A.K. Sinha, S. Seelan, M. Okumura, T. Akita, S. Tsubota, M. Haruta, J. Phys. Chem. B, 109 (2005) 3956.
76. J.Q. Lu, X. Zhang, J.J. Bravo-Suarez, S. Tsubota, J. Gaudet, S.T. Oyama, Catal. Today, 123 (2007) 189.
77. C. Sivadinarayana, T.V. Choudhary, L.L. Daemen, J. Eckert, D.W. Goodman, J. Am. Chem. Soc., 126 (2004) 38.
78. E.E. Stangland, K.B. Stevens, R.P. Andres, W.N. Delgass, J. Catal., 1191 (2000) 332.
79. T.A. Nijhuis, T. Visser, B.M. Weckhuysen, Angew. Chem. Int. Ed., 44 (2005) 1115.
80. T.A. Nijhuis, T.Q. Gardner, B.M. Weckhuysen, J. Catal., 236 (2005) 153.
81. D.H. Wells. A.M. Joshi, W.N. Delgass, K.T. Thomson, J. Phys. Chem. B, 110 (2006) 14627.
82. B. Taylor, J. Lauterbach, G.E. Blau, W.N. Delgass, J. Catal., 242 (2006) 142.
83. J.J. Bravo-Suárez, K.K. Bando, J.Lu, M. Haruta, T. Fujitani, S.T. Oyama, J. Phys. Chem. C, 112 (2008) 1115.
84. B. Chowdhury, J.J. Bravo-Suárez, N. Mimura, J.Q. Lu, K.K. Bando, S. Tsubota, M. Haruta, J. Phys. Chem. B, 110 (2006) 22995.

Chapter 2

Propene epoxidation over Au/Ti-SBA-15 catalysts

Abstract

The synthesis of highly dispersed gold nanoparticles within the channels of mesoporous Ti-SBA-15 supports is presented, together with a thorough catalyst characterization and catalytic activity study for the selective epoxidation of propene to propene oxide. Two series of Ti-SBA-15 materials, differing in their Ti content were prepared by either a grafting or direct synthesis procedure. The resulting Au/Ti-SBA-15 catalyst materials were characterized by XRF, XRD, TEM, N_2-sorption, UV-Vis DRS, XANES and EXAFS, both at the Ti K-edge and Au L_{III}-edge. The catalytic performance of the Au/Ti-SBA-15 materials was evaluated in the direct epoxidation of propene making use of a mixture of H_2 and O_2. The reaction data indicate that Au-Ti-SBA-15 materials obtained by Ti grafting possess a higher catalytic activity than samples in which Ti-SBA-15 was obtained by the direct synthesis method. These differences in catalytic behavior are attributed to differences in the amount and dispersion of Ti within the mesoporous silica support, as well as to differences in the Au nanoparticle size. These data will be discussed in relation to results obtained for Au/TiO_2 catalysts.

2.1. Introduction

The surprising catalytic activity of gold, which was traditionally considered as a chemically inert element, in the direct epoxidation of propene with H_2 and O_2 attracted considerable academic and industrial interest [1]. Despite this attention, the mode of operation of these catalysts is still unclear and several reaction mechanisms have been proposed. In all cases, it was observed that both the presence of gold and titania are necessary to have reasonable propene epoxidation activity [2,3].

Although gold-on-titania (Au/TiO_2) catalysts are very selective (> 90%), these systems still need considerable improvements to be made attractive for application in a large scale industrial process. The low activity (1-2%) and related PO yield, hydrogen efficiency (30%) and catalyst stability are the main problems to be tackled [4,5]. Several factors have been investigated to improve these points.

An active part of the catalyst was found to be the support oxide. Various Ti-based metal oxides with distinct crystalline structures and porosities have been used for supporting Au nanoparticles [5-16]. The production of propene oxide was found to be influenced by the crystalline nature of the supports, the anatase form of titanium dioxide resulted in PO formation; in contrast the rutile structure and amorphous TiO_2 caused complete oxidation to CO_2 [6]. Nonporous silica has been used to support Ti and Au. However, an ideal activity has not been achieved. A high temperature is required to create the tight Ti-O-Si bonding, which is necessary for PO selectivity besides supported Au nanoparticles [17].

Titanium silicalite-1 (TS-1) is an excellent propene epoxidation catalyst when hydrogen peroxide is used as oxidant. When Au nanoparticles are supported on TS-1 the catalytic materials are active in the direct propene epoxidation, however, at low temperature these materials are less active than Au/TiO_2 catalysts and a higher reaction temperature is needed to reach a conversion identical to that of Au/TiO_2. On the other hand, the main advantage of Au nanoparticles on a TS-1 support is their ability to resist deactivation and to achieve a higher selectivity at higher reaction temperature [18]. The difference in activity between TS-1 and TiO_2-based catalysts can be explained by the presence of isolated Ti sites, whereas the lower reactivity of Si-OH sites that neighbor the active site leads to improved catalyst durability. Ti has also been incorporated in catalyst materials with high surface areas, such as mesoporous MCM-41 and MCM-48 supports, using different preparation techniques, including the hydrothermal synthesis and sol-gel procedures [5,10,11-13]. It was found that the increase in epoxide yield is dependent of the method and amount of Ti incorporated in the mesoporous silica.

Along with the well-dispersed tetrahedral coordinated Ti sites in a silica matrix, the size of the Au nanoparticles is also important for an active catalyst. Ion exchange [18], deposition-precipitation [17,19,20] and impregnation [21] are a few of the synthesis methods that have been used to create well-dispersed Au nanoparticles on Ti-based support oxides. The most frequently used method to obtain suitable nano-sized Au particles is the deposition- precipitation process.

Haruta et al. [22] claims that the catalyst requirements for the epoxidation of propene involves isolated Ti sites combined with Au nanoparticles with sizes between 2-4 nm, support oxides with mesopores higher than 5 nm for the effective dispersion of Au nanoparticles inside the pores, and good support hydrophobicity for better propene oxide desorption. Considering the

possible types of support oxides that could meet these requirements mesoporous modified Ti-SBA-15 is a suitable option. The main advantages of SBA-15 compared with MCM-41 materials are the higher hydrothermal stability, thicker walls and large pore size [23,24]. Ti-SBA-15 has been synthesized using different procedures and it was used for the selective oxidation of variety of organic compounds in liquid phase with hydrogen peroxide as oxidant [25-27].

In this **Chapter**, we present the synthesis of Au/Ti-SBA-15 materials using two different preparation routes that is Ti was incorporated in the SBA-15 structure by either a direct hydrothermal synthesis or a grafting procedure. In the second step, Au was introduced in the Ti-SBA-15 material by the deposition-precipitation method. The influence of the preparation method on the final catalyst structure and its catalytic activity in the epoxidation of propene with hydrogen and oxygen has been investigated in detail.

2.2. Experimental

2.2.1. Catalyst preparation

For the preparation of Ti-SBA-15 supports the following chemicals have been used: tetraethylorthosilicate (TEOS, Aldrich, 98%), triblock copolymer, poly(ethylene glycol)-poly(propylene glycol)-poly(ethylene glycol) (PEG-PPG-PEG) (Aldrich), isopropanol (Aldrich, > 99.5%), titanium isopropoxide (Across, 98%), Titanium (IV) oxyacetylacetonate monohydrate (Aldrich, p.a.) and $HAuCl_4$-$4H_2O$ (Aldrich, 30%). Ti was incorporated into the mesoporous SBA-15 material by two routes: direct synthesis and grafting. The catalyst supports prepared by hydrothermal Ti incorporation are designated as Ti-H-n, whereas those prepared by Ti grafting are designated as Ti-G-n with n the Si/Ti molar ratio. Preparation of mesoporous silica SBA-15 was carried out according to Zhao et al. [23,24]. In the synthesis procedure, amphiphilic triblock copolymer, poly(ethylene glycol)-poly(propylene glycol)-poly(ethylene glycol) was first dissolved in aqueous acidic solution containing deionized water and hydrochloric acid (Merck, 37%) under continuous stirring. The mixture was heated at 40º C for 12 h before TEOS was slowly added under vigorous magnetic stirring. The gel with a molar composition of 1.00 SiO_2/0.013 PEG-PPG-PEG/13.49 HCl/152.96 H_2O was stirred for another 10 h and then transferred into a Teflon-lined steel autoclave and kept at 100º C under static conditions for 24 h. The resulting solid was filtered, washed with de-ionized water, dried in open air and calcined in static air at 550º C for 6 h with a heating rate of 2º C/min to decompose the triblock copolymer.

Titanium-grafted SBA-15 samples with different Si/Ti molar ratios (10, 20, 40 and 80) were prepared by dry impregnation using titanium isopropoxide as a titanium source [28]. Titanium was loaded into the SBA-15 support oxide under a dry N_2 atmosphere in a glovebox at room temperature. Then 2 g of SBA-15 was impregnated with 6 mL solution of titanium isopropoxide in

dry isopropanol. The solvent was removed from impregnated materials under flowing nitrogen at room temperature for 48 h. The Ti-SBA-15 samples were calcined at 400º C for 4 h. In addition, a series of Ti-SBA-15 materials with Si/Ti molar ratios between 10-80 were synthesized hydrothermally [29]. TEOS and Titanium (IV) oxyacetylacetonate monohydrate have been used as silicon and titanium sources, respectively. The triblock copolymer (PEG-PPG-PEG) was used as the structure-directing agent, whereas concentrated HCl was used to adjust the pH. The synthesis was carried out similarly as for pure SBA-15, but with the difference that the Ti source was added after the introduction of TEOS. The titanium (IV) oxyacetylacetonate was predissolved in a solution of isopropanol. The resulting samples were washed with deionized water and dried overnight at 60º C. Once dry, the resulted white powder was calcined at 550º C for 6 h.

1% Au catalysts were prepared via a deposition-precipitation method [8], in which the gold precursor, $HAuCl_4$ was precipitated on the supports by increasing the pH to 9.5. A solution of chloroauric acid in water was slowly added to a stirred suspension of 2 g Ti-SBA-15 support in water. The pH of the solution was kept at 9.3 with aqueous ammonia (Merck, 25%) diluted with deionized water and the solution was aged for 30 min at the room temperature. The catalyst was washed repeatedly with distilled water, dried in air overnight at 60º C and calcined at 400º C for 4 h.

2.2.2. Catalyst characterization

The degree of crystallinity and morphology of the obtained Au/Ti-SBA-15 materials were characterized using transmission electron microscopy (TEM) and X-ray diffraction (XRD). The latter was performed using a Bruker-AXS D8 Advance powder X-ray diffractometer, equipped with an automatic divergence slit, Våntec-1 detector and a cobalt $K\alpha_{1,2}$ (λ= 1.79026 Å) source. TEM images were obtained using a FEI Tecnai 20F transmission electron microscope operated at 200 KeV, with a Schottky Field Emission gun and a twin objective lens. The magnification range was 25kx-700kx, the point-to-point resolution was 0.27 nm and lattice image resolution was 0.14 nm. The specific surface area and pore volume were determined by N_2 sorption measurements with a Micromeritics ASAP 2400 instrument. Surface areas were calculated by using the BET model with micropores and macropores described by the Horvath-Kawazoe and BJH models, respectively. UV-Vis DRS measurements were carried out at room temperature on a Varian Cary 500 instrument in the range of 200-2200 nm. This set-up was equipped with a diffuse reflectance accessory, which was set to collect diffuse reflected light only. The scan was made with an averaging time of 1 s, data interval of 1 nm and a scan rate of 60 nm/min. A baseline correction was performed using a white Halon standard. Ti K-edge and Au L_{III}-edge XAFS measurements were carried out on station BM26A at the ESRF (Grenoble, France) operating at 6 GeV with a typical current of 150 to 250 mA. The station was equipped with a Si(111) double crystal monochromator, followed by two

vertically focusing Pt- and Si-coated mirrors for harmonic rejection. X-ray absorption spectra were recorded using ion chambers for measuring incident and transmitted beam intensities and a nine-element monolithic germanium detector for fluorescence measurements. The maximum in the first derivative plot for the Ti (4966.4 eV) and Au (11918.7 eV) foil data was used respectively to calibrate the monochromator position. In a typical experiment, about 100 mg of sample was pressed to form self-supporting wafers before being mounted in a specialised cell for recording XAFS data. The samples were then dehydrated at 300º C. Measurements were performed at room temperature in normal step scanning mode, multiple scans were obtained to improve the signal to noise ratio. For the Ti K-edge measurements a step size of 0.2 eV/point over an energy range of 4964-4990 eV was used in order to obtain detailed information on the pre-edge feature at ca. 4969.2 eV. This peak was then profiled using a Lorentzian function in order to extract information on its position and intensity, which was then used to obtain indirect information on the proportion of tetrahedral Ti^{4+} species in the samples. The XAFS data were processed using the suite of programs available at Daresbury laboratory, namely EXCALIB (for converting the raw data to energy *vs* absorption coefficient), EXBROOK (for normalization of XANES data at 20 eV above the absorption edge and background subtraction to extract EXAFS) and EXCURV98 (to perform a least squares fitting analysis of the data to extract more detailed local structural details) [30]. An amplitude reduction factor (S_o^2) value of 0.83, obtained from fitting the FCC structured Au foil with a fixed coordination number(s) up to the 4th shell, was also used in the analysis. Multiple scattering contributions were considered when fitting the higher shells, but were only observed to be significant for simulating amplitude related information when fitting the 4th shell and were thus ignored when obtaining coordination numbers for the 2nd and 3rd shells.

2.2.3. Catalyst testing

A flow reactor was used to determine the catalytic performance of the different catalysts prepared. Typically the experiments were carried out with 0.4 g of catalyst material and a flow of 50 Nml/min. The gas mixture consisted of 10% O_2, 10% H_2, and 10% C_3H_6 in He. The analysis of the gas leaving the reactor was carried out using an Interscience Compact GC system, equipped with a Molsieve 5A and a Porabond Q column, each with a thermal conductivity detector (TCD). The Porabond Q column was used to separate hydrocarbons (propene and propane), oxygenates (i.e., propene oxide, acetaldehyde, acetone, acrolein, methanol, ethanol, 2-propanol and propanal) and CO_2 and H_2O, respectively, whereas the Molsieve 5A was used to separate H_2, O_2, N_2, methane and CO, respectively. Gas samples were analyzed every 3 min. The experiments were carried out in cycles of 5 h at reaction temperature with the reactant mixture, followed by a regeneration cycle. In regeneration, 10% oxygen in helium was used. The catalyst was heated at 300º C and was kept for 1

h, after which it was cooled to the next reaction temperature in the cycle. The performance was typically investigated at 10-15 different temperatures (including duplicates) to determine the deactivation pattern for each catalyst. The propene conversion, propene oxide selectivity, and H_2 efficiency were defined as follows:

Propene conversion = mol of (oxygenates + CO_2/3)/mol of propene in feed

Propene oxide selectivity = mol of PO/mol of (oxygenates + CO_2/3)

H_2 efficiency = mol of propene oxide/moles of H_2O

During the catalytic tests, UV-Vis DRS measurements were performed in-situ at 250-1100 nm using an Avantes Avaspec-2048-4 spectrometer.

2.3. Results and discussion

2.3.1. X-ray fluorescence spectroscopy

Elemental analysis of the calcined powders reveals the actual amounts of titanium incorporated into the SBA-15 framework (Table 2.1). All of the Au/Ti-SBA-15 samples prepared by grafted method exhibit a final Si/Ti molar ratio close to the target loading. XRF results for the direct synthesized Au/Ti-SBA-15 materials show low titanium contents in the final products, compared to grafted samples. UV-Vis analysis of the filtrate (not shown) of the hydrothermally synthesized materials demonstrates that most of the titanium was not incorporated in the SBA-15 structure and washed out. The gold loading for all the catalysts was always close to the target loading and the amount of chloride was below the detection limit.

2.3.2. X-ray diffraction

XRD patterns of the synthesized materials are typical for SBA-15 [24].

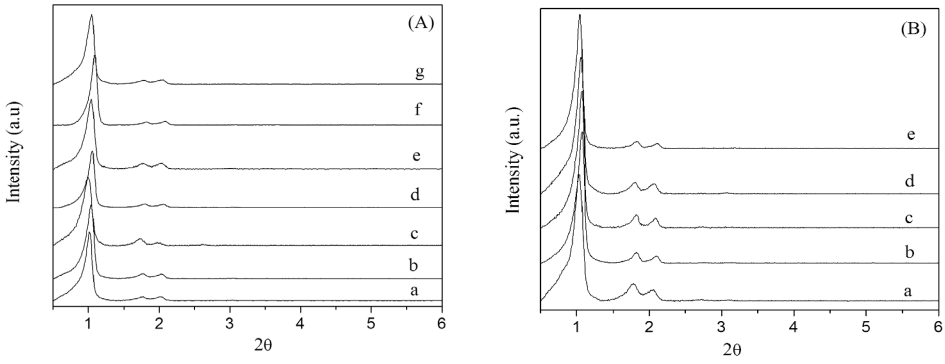

Figure 2.1. XRD patterns of : (A) (a) pure silica SBA-15, (b) Ti-G-80, (c) Ti-G-40, (d) Ti-H-40, (e) Ti-G-20, (f) Ti-H-20 and (g) Ti-G-10; (B) (a) Au/Ti-H-80, (b) Au/Ti-H-40, (c) Au/Ti-H-20, (d) Au/Ti-G-20 and (e) Au/Ti-G-10.

Figure 2.1 A illustrate the presence of peaks at 2θ angle of 1.01º, 1.74º and 2.01º corresponding to the (100), (110) and (200) Bragg reflections confirming the hexagonal symmetry (P6mm) of the SBA-15 materials prepared [23,24]. A well-resolved peak at 1.02º and two other peaks at 1.75º and 2.05º can be seen for the Ti-SBA-15 (Figure 2.1 A) and Au/Ti-SBA-15 samples (Figure 2.1 B). The incorporation of Ti and Au did not significantly change the hexagonal ordering of the SBA-15 framework. No peak for Au metal at 38.19º can be observed in the XRD patterns. The absence of this reflection indicates that the Au particle sizes are too small.

2.3.3. UV-Vis diffuse reflectance spectroscopy

Diffuse reflectance spectroscopy in the UV-Vis region is a sensitive method for the characterization of the coordination environment of Ti in SBA-15. The UV-Vis DRS spectra of the Ti-H-n and Ti-G-n samples, TS-1 (tetrahedral reference) and TiO_2 anatase phase are given in Figures. 2.2 A and 2.2 B.

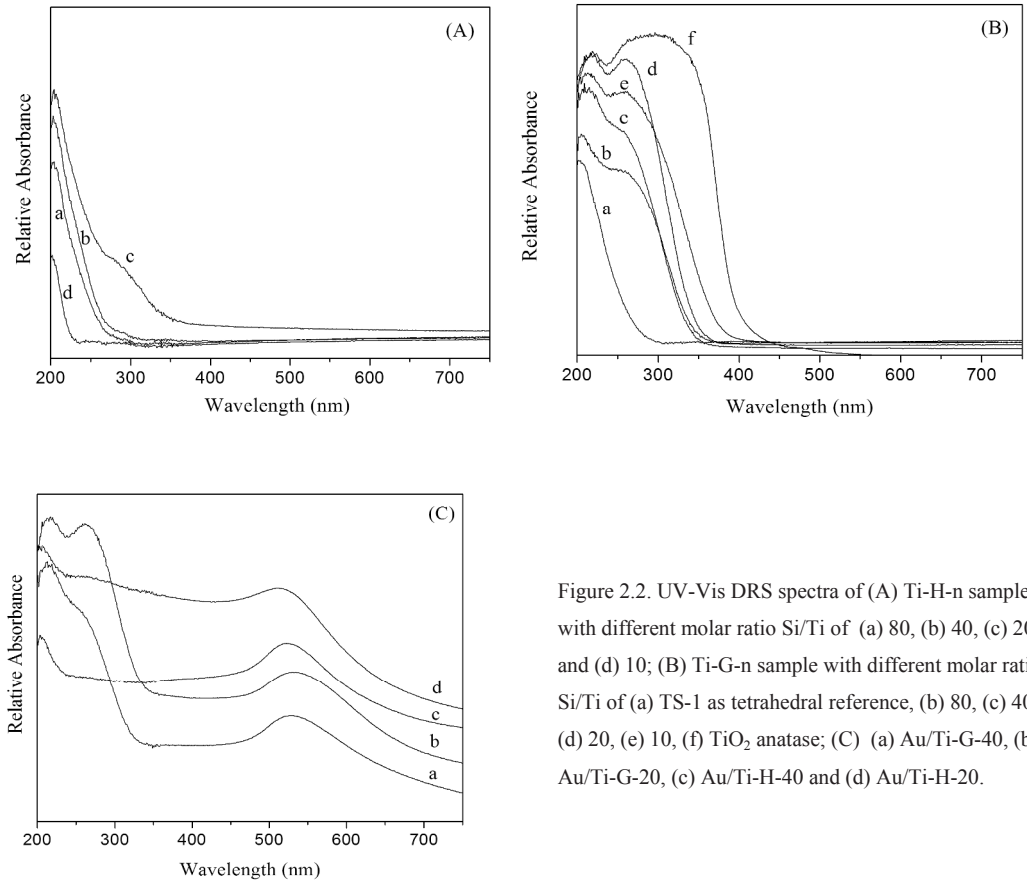

Figure 2.2. UV-Vis DRS spectra of (A) Ti-H-n sample with different molar ratio Si/Ti of (a) 80, (b) 40, (c) 20 and (d) 10; (B) Ti-G-n sample with different molar ratio Si/Ti of (a) TS-1 as tetrahedral reference, (b) 80, (c) 40, (d) 20, (e) 10, (f) TiO_2 anatase; (C) (a) Au/Ti-G-40, (b) Au/Ti-G-20, (c) Au/Ti-H-40 and (d) Au/Ti-H-20.

The catalyst samples prepared by the direct synthesis method (Figure 2.2 A) with different Si/Ti molar ratio show an intense absorption band at 208 nm, assigned to the ligand-to-metal charge transfer (LMCT) from oxygen to Ti of an isolated tetrahedral Ti species [31]. For the sample with a Si/Ti ratio of 20 along with this band a shoulder with a maximum around 257 nm can be seen, possibly due to the presence of Ti atoms in five-fold and six-fold coordination. These are probably generated on hydration by one or two water molecules of a tetrahedral titanium ion in the first coordination sphere [32]. The hydrophilic surface and high surface area of SBA-15 material yield a high water adsorption capacity leading to a hydration of surface Ti ions. Figure 2.2 B displays the UV-Vis DRS spectra obtained for the Ti-SBA-15 samples prepared by the grafting method. All these samples have a UV band at around 208-218 nm. This can be related to the tetrahedral Ti sites or to a distorted tetrahedral environment, which is a direct consequence of the amorphous nature of the walls of the mesoporous material [32]. With decreasing the Si/Ti molar ratio from 80 to 10, the UV-Vis DRS bands become broader in the high wavelength region, indicating that the Ti atoms were no longer completely isolated in the SBA-15 structure. A shoulder at around 330 nm would be expected in the UV-Vis DRS spectrum if the catalyst samples contained some bulk titanium oxide [31].

After Au deposition-precipitation in the Ti-SBA-15 support materials prepared by the two methods of Ti incorporation and consecutive calcination in air at 400º C, it was observed that all materials attained a pink color typical of the presence of Au nanoparticles. These materials have a characteristic absorption band in the visible region of the electromagnetic spectrum at around 520–550 nm (Figure 2.2 C). This absorption band is due to surface plasmon vibrations, which are dependent on the gold particle size and the used support oxide [33].

2.3.4. N_2 sorption measurements

Isotherms of the nitrogen adsorption–desorption experiments of the calcined materials and the related pore size distribution curves are shown in Figures 2.3 A and 2.3 B. The BET surface area, micropore volume, BJH mesopore volume [34], and pore sizes of these materials are given in Table 2.1. The isotherms for SBA-15 silica and Ti-SBA-15 sample presented in Figure 2.3 A exhibit a H1 hysteresis loop of type IV according to the IUPAC classification and are typical of materials with cylindrical mesopores [35]. All isotherms show a sharp inflection in the adsorption branch at a relative pressure of about 0.72. This is characteristic of capillary condensation within uniform pores. A good match between the points of inflection of the adsorption branch of each isotherm suggests that all samples have similar pores (Figure 2.3 A).

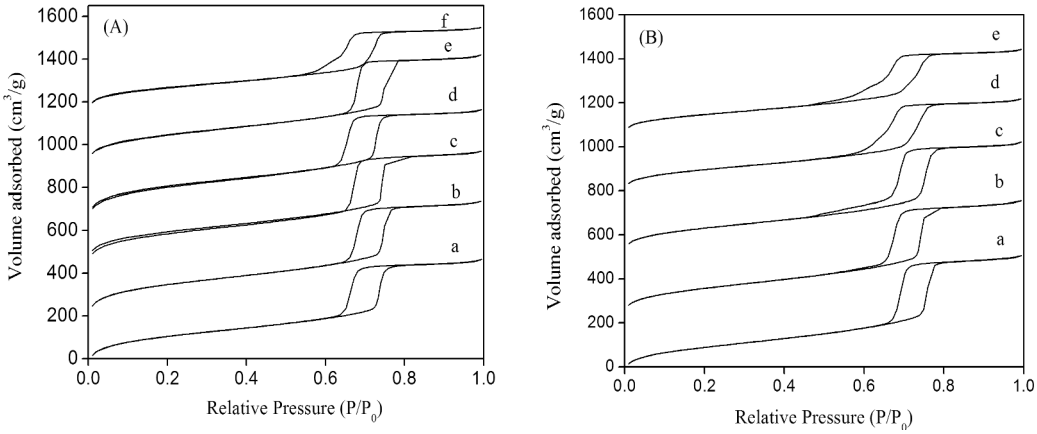

Figure 2.3. Nitrogen adsorption-desorption isotherms for (A) (a) SBA-15, Ti-H-n sample with molar ratio Si/Ti of (b) 80, (c) 20, (d) 10 and Ti-G-n sample with molar ratio Si/Ti of (e) 80 and (f) 10. (B) Au/Ti-H-n of (a) 80, (b) 40 and Au/Ti-G-n of (c) 80, (d) 20 and (e) 10.

The pore size distribution curves shown in Figure 2.4 A present an average pore size of about 62 Å for the Ti-H-n samples, whereas in the case of the Ti-G-n samples, partial pore blocking results from increasing titanium content (Figure 2.4 A). The introduction of Au nanoparticles in the SBA-15 support materials resulted in a much broader hysteresis loop, as illustrated in Figure 2.3 B.

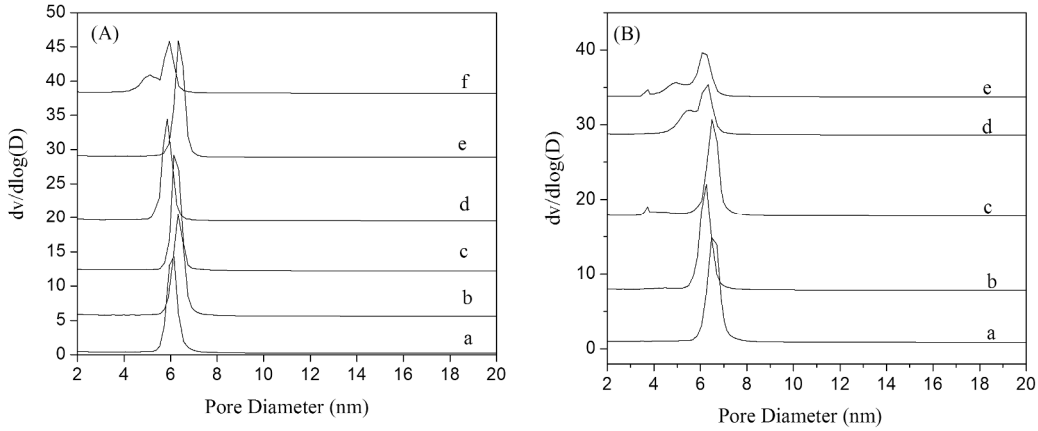

Figure 2.4. Pore size distribution of (A) (a) SBA-15, (b) Ti-H-80, (c) Ti-H-20, (d) Ti-H-10, (e) Ti-G-80 and (f) Ti-G-10. (B) (a) Au/Ti-H-80, (b) Au/Ti-H-40, (c) Au/Ti-G-80, (d) Au/Ti-G-20 and (e) Au/Ti-G-10.

The presence of the Au nanoparticles caused a shift in the desorption branch to lower pressures, whereas the adsorption branch was only affected slightly. This adsorption-desorption behavior has been shown to be consistent with a structure comprising open and closed/blocked

cylindrical mesopores [36,37]. The additional features in Figure 2.4 B at 5-5.5 nm can be ascribed to partial pore blocking of the pores of the Ti-SBA-15 materials by Au nanoparticles. This blockage increases significantly with increasing titanium loading, as shown in Figure 2.4 B for sample Au/Ti-G-10.

Table 2.1. Summary of the characterization results of the different SBA-15, Ti-SBA-15 and Au/Ti-SBA-15 samples prepared (na = not applicable).

Sample	Si/Ti (initial gel)	Si/Ti (final product)	Au (wt%) (final product)	BET surface area (m^2/g)	Micropore volume (cm^3/g)	Pore volume BJH(cm^3/g)	Pore size BJH (nm)
SBA-15	na	na	-	580	0.1	0.9	6.1
Ti-G-80	80	85.3	-	572	0.08	0.91	6.3
Ti-G-20	20	21.4	-	513	0.004	0.8	6.4
Ti-G-10	10	14.5	-	447	0.08	0.71	5.9
Au/Ti-G-80	80	88.2	~1	499	0.05	0.87	6.5
Au/Ti-G-20	20	23.2	~1	439	0.05	0.74	6.3
Au/Ti-G-10	10	16.1	~1	407	0.04	0.68	6.1
Ti-H-80	80	2033	-	631	0.1	0.98	6.3
Ti-H-40	40	1233	-	633	0.1	0.9	6.1
Ti-H-20	20	599	-	568	0.1	0.93	6
Ti-H-10	10	4824	-	608	0.11	0.93	5.9
Au/Ti-H-80	80	2330	~1	531	0.04	0.9	6.5
Au/Ti-H-40	40	1256	~1	545	0.03	0.9	6.2
Au/Ti-H-20	20	712	~1	526	0.04	0.9	6.2
Au/Ti-H-10	10	5354	~1	470	0.03	0.78	6

2.3.5. Transmission electron microscopy

Figure 2.5 shows some TEM micrographs of the samples under investigation. More specifically, Figure 2.5 a presents a TEM micrograph of the SBA-15 starting material, showing a uniform hexagonal structure, consistent with the corresponding XRD data. The TEM micrographs of the Ti-modified SBA-15 samples, illustrated in Figures 2.5 b and 2.5 c, show no significant changes in spacing between the SBA-15 channels, suggesting that the inclusion of Ti in the SBA synthesis mix or the grafting process does not adversely affect the structural integrity of the SBA-15 structure. After deposition of Au (Figures 2.5 d and 2.5 e), the Au particles are smaller on average in the hydrothermally prepared sample (Figure 2.5 d) than in the corresponding grafted sample (Figure 2.5 e). The other interesting point is that the Au particles seem to extend along the lengths of the mesopore channels. However, it appears that some of the Au particles are larger than the mesopore channels, which may suggest that (a) the Au particles expand across the mesoporous wall

or (b) some Au nanoparticles seems to be formed on the outer surface of the support. To elaborate further on this point, Figure 2.6 shows the size distribution of the gold nanoparticles observed for both the Au/Ti-G-20 and Au/Ti-H-20 samples.

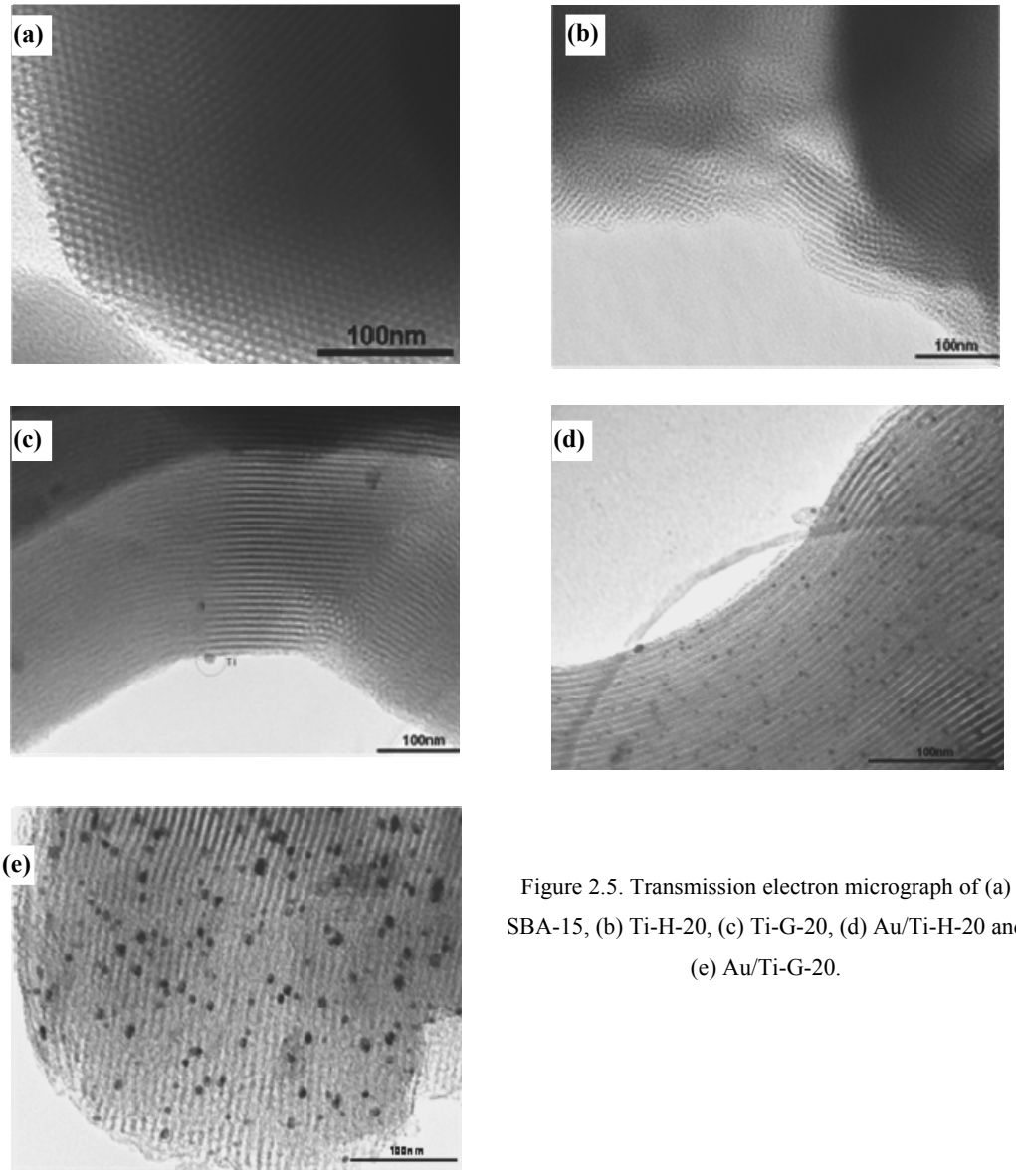

Figure 2.5. Transmission electron micrograph of (a) SBA-15, (b) Ti-H-20, (c) Ti-G-20, (d) Au/Ti-H-20 and (e) Au/Ti-G-20.

The particle size distribution was determined by measuring a number of TEM pictures out of which over 400 particles were measured. From the metal particle size distributions, it can be concluded that for the hydrothermally prepared samples, the Au nanoparticles are smaller on

average (4.45 nm) than those formed in the grafted samples (6.58 nm). The N_2-sorption and XRD measurements show that apart from the presence of titanium, the support oxides are almost identical. Considering that the supports were prepared identically, this difference must be caused by a difference in interaction between the metal and the support oxide. It is also seen that smaller gold particles are formed for silica-supported Au catalysts compared with identically prepared titania-supported Au catalysts [38]. Because the catalysts did not exhibit significant sintering of gold during the reaction and regeneration, it must be concluded that the different gold particle size originates from the preparation procedure, in which nucleation and particle growth must be different when titanium is present in the SBA-15 material.

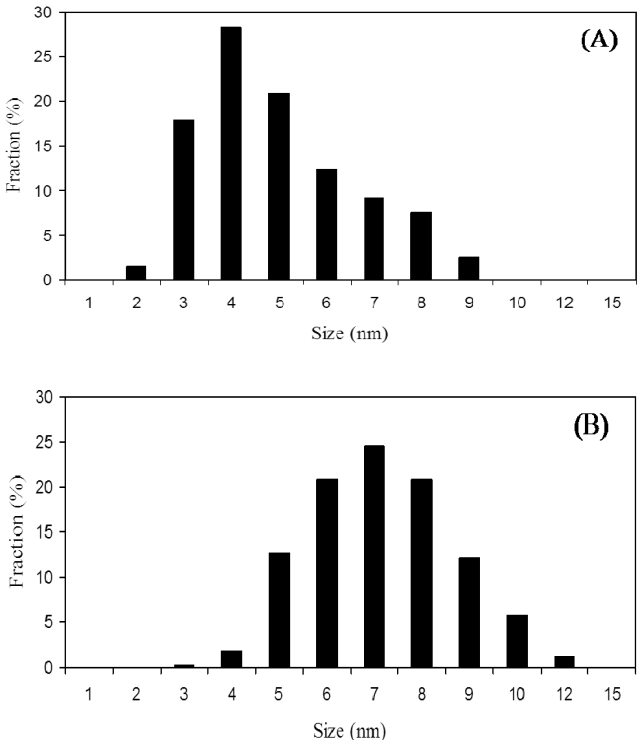

Figure 2.6. Size distribution plot of supported Au nanoparticles in (a) Au/Ti-H-20 and (b) Au/Ti-G-20.

2.3.6. Ti K-edge X-ray absorption spectroscopy

To determine the local coordination chemistry of Ti^{4+} in the different catalyst materials, X-ray absorption spectroscopy measurements were performed at the Ti K-edge. The near-edge region in the XANES spectra provides valuable information on the environmental geometry of the absorbing atom (i.e., Ti). Indeed, for Ti^{4+}, the position and intensity of the pre-edge peak due to a 1s–3d transition is related to its coordination environment. The feature above the Ti K-edge is attributed to a 1s-4p transition and a decrease in the pre-edge intensity correlates with an increase of

the feature corresponding to the 1s-4p transition. This may provide evidence of increased formation of pentagonal, distorted octahedral, and octahedral coordinated Ti centers [39-41]. When Ti^{4+} is tetrahedrally substituted or grafted into/onto a silica matrix, the position of the peak using a Si (111) monochromator appears to remain consistently around 4969.2 eV (Figure 2.7), but its intensity can vary. For example, Thomas and Sankar [39] showed that whereas numerous samples, including $Ti(OSiPh_3)_4$ and $C_6H_{11}Si_7O_{11}Ti$-O-X (where X= $SiPh_3$) have been shown crystallographically to contain tetrahedral Ti^{4+} species, the XANES peak at 4969.2 eV has an intensity of 0.85 and 0.61, respectively. Perhaps more significantly for our work, grafted Ti samples on mesoporous MCM-41 type structures give a pre-edge intensity (for a calcined/ dehydrated sample) close to 0.65 [40,42].

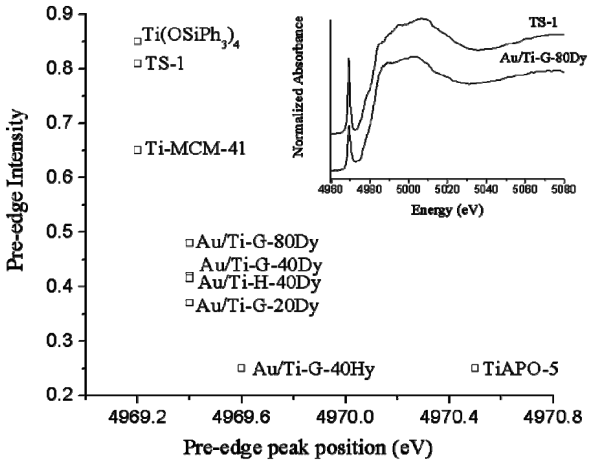

Figure 2.7. Variation of the pre-edge peak intensity for several titanium-containing Au/Ti-SBA-15 catalysts, as well as some reference compounds (TS-1, TiAPO-5, Ti-MCM-41 and Ti $(OSiPh_3)_4$).

Dy-dehydrated,

Hy- hydrated.

Figure 2.7 plots the 1s–3d peak intensity versus the pre-edge energy position for some of our samples in relation to three standard materials, including a reference compound containing framework substituted tetrahedral Ti^{4+} (TS-1), the predominantly octahedral Ti^{4+}-containing reference sample TiAPO-5, and the Ti-MCM-41 sample reported previously [40,42,43]. For dehydrated samples, the position of the 1s-3d peak was found to be shifted in energy by 0.2 to 4969.4 eV relative to the tetrahedral containing Ti^{4+} standards and to have lower intensities. From these observations, it is possible to conclude that the coordination of Ti^{4+} within these samples is likely to be higher than 4, suggesting that a mixture of both tetrahedral and higher coordinated (5 and 6) titanium species are present. However, the relative amounts of each of these species appear to vary, because the intensity decreases with increasing titanium loading.

2.3.7. Au L_{III}-edge X-ray absorption spectroscopy

Figure 2.8 shows the Fourier transforms (FTs) for the Au/Ti-SBA-15 materials with the corresponding data determined from the least squares fitting process shown in Table 2.2. An

evaluation of Figure 2.8 shows that the FT magnitudes of the samples increase with increasing titanium oxide loading. In addition, the general profiles of the Au/Ti-G-n samples appear similar to one another but different than the Au/Ti-H-n sample. Most notably, for the Au/Ti-H-20 sample, the largest peak at ca. 2.85 Å due to Au-Au scattering appeared much broader than in the Au/Ti-G-n samples, suggesting a rather broad particle size distribution in this sample.

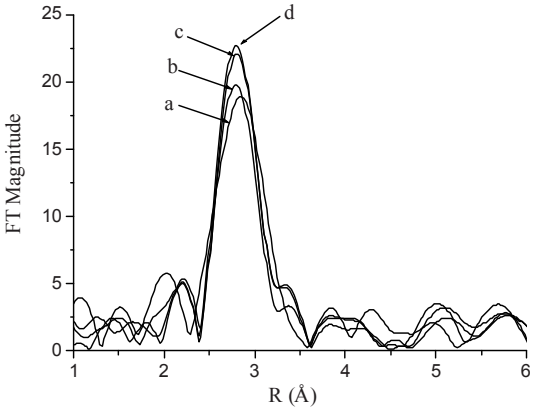

Figure 2.8. Comparison of the Fourier-transformed EXAFS data of (a) Au/Ti-H-20, (b) Au/Ti-G-80, (c) Au/Ti-G-40 and (d) Au/Ti-G-20.

Closer inspection of the data obtained after analysis confirms the relationship between the average Au-Au coordination number and the titanium loadings of the Au/Ti-SBA-15 materials. In particular, a N_1 value of 7.8 (± 0.78) was obtained for the lowest titanium-loaded sample Au/Ti-H-20, whereas a N_1 value of 9.7 (± 0.97) was obtained for the Au/Ti-G-20 material containing the most titanium. Because it is well known that for small particles (ca. < 50 Å), the relationship between the particle diameter and coordination number is a strong and nonlinear function, it would appear that the lower titanium loaded sample, Au/Ti-H-20, has the smallest gold particles. Further proof for these observations can be obtained by comparing the first shell near-neighbor distances where a 0.7% contraction of the average N_1 Au-Au distance was observed in the Au/Ti-H-20 relative to that of the Au foil [44]. An estimation of the particle size from the N_1 coordination numbers suggests that the particle size ranges from 14 to 30 Å, which is typically some ~ 30 Å lower than the average size determined from TEM. Because EXAFS is a more "volume-sensitive" technique, it is possible that these systems are more polydisperse than suggested by TEM because the EXAFS shows a greater sensitivity toward species that cannot be seen by TEM [45]. We also note that the estimation is based on the assumption that the particles are essentially spherical/ cubooctahedral, although it has also been shown that the N_1 values for different shapes with similar sizes do not differ significantly [46-48]. However, it has been previously suggested that the ratio between the third and first coordination numbers can be used to obtain geometric information on the particles [48]. Interestingly, we see very similar values for this ratio between the Au/Ti-G samples (~ 1.3) (Table 2.2), which was previously proposed to be indicative of distorted cubic or slab-like

structures in which two of the dimensions that describe particle size, are similar, whereas the third dimension is significantly different. For the Au/Ti-H-20 and Au/Ti-G-80 samples, a lower ratio (ca. 0.8) was obtained, possibly reflecting a more extreme elongation but more likely due to the particles being smaller. Indeed, despite the sensitivity of the XAFS method toward smaller species, there does appear to be some correlation with the TEM images, in which many of the Au particles appear to be elongated along the length of the channels.

Table 2.2. EXAFS fit parameters for different Au-Ti-SBA-15 samples compared with Au foil and Au/TiO_2 reference materials (with k^3 weighting: Δk = 4.3–17.0 $Å^{-1}$ and Δr = 0–6.0 Å; na = not applicable).

Sample and coordination shells	Au-Au distance (Å)	Coordination number	Debye-Waller ($2\sigma^2$)*	E_f (eV)	EXAFS Particle size estimate (Å)	TEM Particle size estimate (Å)	N_3/N_1 ratio	R(%)*
Au foil								27.5
N_1	2.86	12	0.016	-6.2	Na	-	2	
N_2	4.06	6	0.023					
N_3	4.99	24	0.027					
Au/Ti-G-80								31.6
N_1	2.84	7.9	0.016	-7.9	15	45	0.87	
N_2	4.06	3.4	0.023					
N_3	4.99	6.9	0.027					
Au/Ti-G-40								29.7
N_1	2.85	9.6	0.016	-7.3	28	60	1.33	
N_2	4.06	4.1	0.023					
N_3	4.97	12.2	0.027					
Au-Ti-G-20								32.2
N_1	2.85	9.7	0.016	-6.7	28	66	1.29	
N_2	4.05	4.1	0.023					
N_3	4.97	11.9	0.027					
Au/Ti-H-20								30.3
N_1	2.84	7.8	0.016	-8.5	14	42	0.79	
N_2	4.03	3.4	0.023					
N_3	4.94	6.3	0.027					
Au/TiO_2								35.9
N_1	2.84	8.1	0.016	-8.1	15	40	1.3	
N_2	4.07	3.38	0.023					
N_3	4.97	10.64	0.027					

*Note – Due to correlation problems the Debye-Waller factors reported for the samples were extracted from fitting the foil data and were not refined.

2.3.8. Catalytic performance

The catalytic performance of the different Au/Ti-SBA-15 catalyst materials was tested for the direct epoxidation of propene. Conversion, selectivity, and hydrogen efficiency at different reaction temperatures for the grafted and hydrothermally prepared catalysts with Si/Ti molar ratios are summarized in Table 2.3. Major differences can be seen among the catalysts prepared using different preparation methods. The principal products of the grafted catalysts are propene oxide,

acetaldehyde, acrolein, CO_2, H_2O and propane. The hydrothermally synthesized catalyst materials have a low activity in propene epoxidation, with propane the principal product obtained besides propene oxide. Figure 2.9 presents the conversions and selectivities versus temperature for the Au/Ti-H-40 and Au/Ti-G-40 samples. It can be seen that the catalytic conversion increases with increasing reaction temperature, whereas the selectivity decreases at higher temperatures. Interestingely, Au/Ti-G-40 has a greateer activity than Au/Ti-H-40.

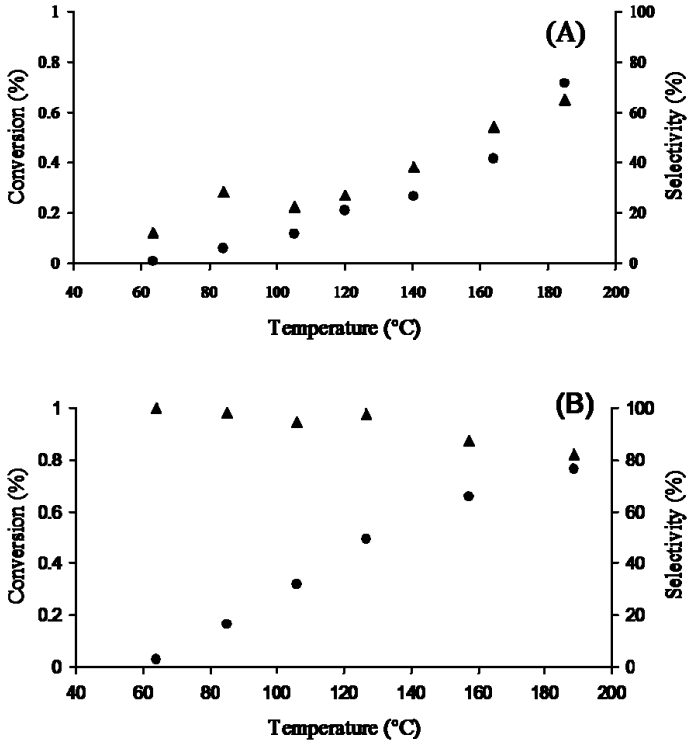

Figure 2.9. Catalytic performance of (a) Au/Ti-H-40 and (b) Au/Ti-G-40 (conversion (●) and selectivity (▲) (Pressure 1 bar, GHSV ($m^3/m^3/h$), 1765 h^{-1}).

Because the reaction rate in Figure 2.9 did not increase with temperature as fast as expected, we verified if the measurements were not performed in a mass-transfer limited regime. Calculation of the Carberry number and Weisz criterion [49] resulted in values of 10^{-6} and 10^{-9}, respectively. Based on these values, we can conclude that the reaction is not internally or externally mass transfer limited. The nonexponential increase in the reaction rate can be explained by an insufficiently short lifetime of one of the reaction intermediates on the catalytic surface in the complex kinetic network [38]. Most likely, this is related to the decomposition of the hydroperoxide intermediate, which is

assumed to be the essential reactive intermediare, because the water production rate does increase exponentially with temperature.

Table 2.3. Overview of the catalytic performances of the Au/Ti-SBA-15 catalyst samples under study (Conversions and selectivity values reported are average values taken from 30-270 min within one the epoxidation cycle). Pressure 1 bar, GHSV ($m^3/m^3/h$), 1765 h^{-1} for Au/Ti-SBA-15 catalysts and 5000 h^{-1} for Au/TiO_2 catalyst.

Catalyst	Temperature (° C)											
	50			80			120			150		
	Conv(%) C_3H_6	PO sel (%)	H_2 Eff (%)	Conv(%) C_3H_6	PO sel (%)	H_2 Eff (%)	Conv(%) C_3H_6	PO sel (%)	H_2 Eff (%)	Conv(%) C_3H_6	PO sel (%)	H_2 Eff (%)
Au/Ti-H-20	0	0	0	0.25	24	0.27	0.41	19.2	0.15	0.54	52	0.32
Au/Ti-H-40	0	0	0	0.06	28.6	0.22	0.21	27	0.1	0.39	54	0.25
Au/Ti-G-20	0	0	0	0.1	87.5	6.5	0.4	83.5	8.8	0.55	64.7	4.2
Au/Ti-G-40	0.02	100	8.12	0.16	98.3	9.1	0.48	96.5	9.23	0.65	88	4.5
Au/Ti-G-80	0.04	100	5.39	0.3	95.2	6.65	0.7	91.41	5.6	1.1	83.7	4
Au/TiO_2	0.26	99.2	12.02	0.11	89.19	3.72	0.19	29.9	0.32	2.32	0.47	0.01

2.3.9. Catalyst stability

The catalyst materials were tested in successive 5 h cycles including an intermediate regeneration procedure. Figure 2.10 shows the catalytic performance of the Au/Ti-G-40 catalyst. Small losses in catalytic activity can be seen within a cycle, whereas the activity can be almost completely restored during regeneration at 300º C in O_2/He.

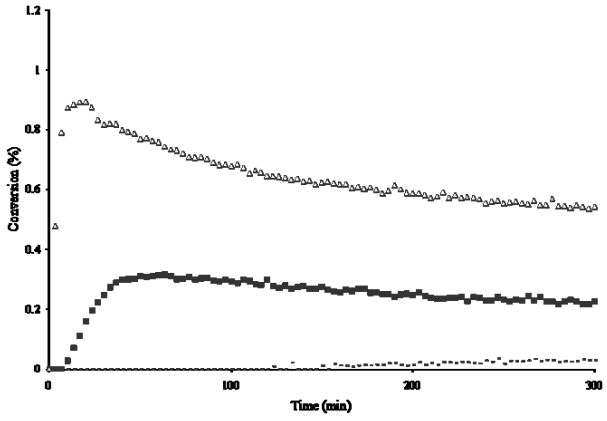

Figure 2.10. Catalytic performance of Au/Ti-G-40 catalyst. Conversion at 50º C (-), 100º C (■), 150º C (Δ). Pressure 1bar, GHSV ($m^3/m^3/h$), 1765 h^{-1}.

Compared with the Au/TiO_2 catalysts reported by Nijhuis et al. [38], Au/Ti-SBA-15 catalysts are more stable during the propene epoxidation reaction. We argue that the stability of Au/Ti-SBA-15 catalysts is related to the presence of isolated Ti in the SBA-15 framework.

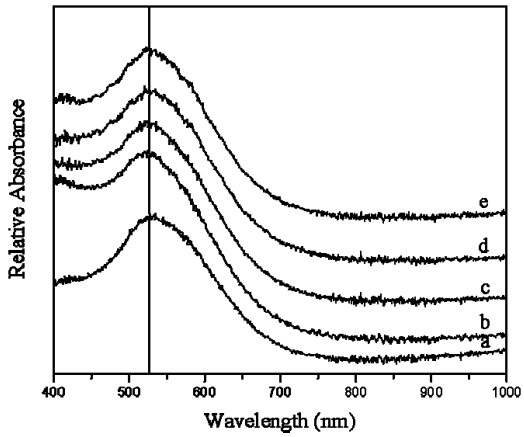

Figure 2.11. In-situ UV-Vis DRS spectra of Au/Ti-G-40 catalyst. (a) fresh catalyst; epoxidation reaction at: (b) 80° C, (c) 100° C, (d) 150° C, (e) 200° C. Note that after each reaction, a regeneration procedure has been made.

During the epoxidation reaction, the catalyst was also monitored by in-situ UV-Vis DRS measurements. The similarity of the UV-Vis DRS spectra in Figure 2.11 indicates that no detectable changes in the nature of the Au particles were seen during these experiments.

Finally, Figure 2.12 shows a TEM micrograph of Au/Ti-G-40 catalyst after 14 activity-regeneration cycles. No sintering of supported Au nanoparticles can be observed, ensuring the stability of the catalyst materials during catalytic operation.

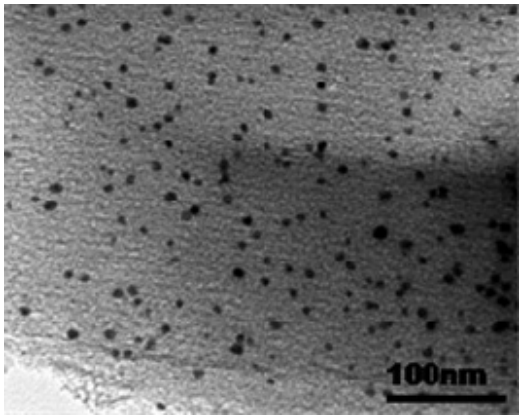

Figure 2.12. TEM picture of a spent Au/Ti-G-40 catalyst.

2.3.10. Relating catalyst preparation and structure to propene epoxidation activity

The characterization results of the Au/Ti-SBA-15 samples prepared via hydrothermal synthesis show a small amount of titanium incorporated in these samples compared with the ones

prepared via the grafting method. Moreover, the supported Au nanoparticles are smaller in the hydrothermally synthesized catalysts than in the grafted Au/Ti-SBA-15 catalysts. Characterization of these catalysts by UV-Vis DRS and XANES showed that the Au/Ti-G-n catalysts contain a higher absolute amount of isolated tetrahedral titanium than the Au/Ti-H-n samples. Given the fact that Ti-SBA-15 support materials prepared by grafting method are containing more tetrahedral Ti sites than the supports prepared by hydrothermal synthesis, the higher activity of Au/Ti-G-n catalysts can be attributed to a higher amount of tetrahedral Ti sites perhaps localized close to the gold particles and to a greater accessibility of the reactants towards these sites. In the hydrothermal prepared catalysts, titanium sites are probably less accessible towards reactants due to their incorporation in the thick walls of SBA-15, where in the grafted samples, Ti sites are probably present at the surface of the SBA-15 pores. Besides the fact that the catalytic activity was found to be influenced by the amount of tetrahedral Ti present in the sample, another factor that was found to influence the activity is the Au particle size. It was determined from TEM and XAFS that Au/Ti-G-n samples are containing larger Au particles than the Au/Ti-H-n samples, moreover from the catalytic measurements it was found that grafted catalysts are more active than the hydrothermal prepared ones. Along this line, Haruta and coworkers have suggested that Au/TiO_2 catalysts can be selective towards propene oxide or propane depending on the Au particle size [7]. Considering that Au and Ti are the active sites in propene epoxidation, the increase in the propene yield for Au/Ti-G-n catalysts can be linked to the greater amount of isolated titanium sites in a tetrahedral environment, as well to the Au particle size which appear in this case to be more active towards epoxidation. The influence of the Ti loading and Au particle size on the catalytic activity of Au/Ti-SBA-15 materials can also be observed in the series of the grafted samples. Thus, the catalytic activity of Au/Ti-G-n samples was increasing with decreasing Ti loading and Au particle size. The Au/Ti-G-80 catalyst, which has the highest absolute amount of tetrahedral Ti, has the highest catalytic activity probably due to the fact that isolated Ti sites are favoring the desorption of propene oxide [38]. Interestingly from the grafted series, the Au/Ti-G-40 sample is the most selective catalyst towards propene oxide synthesis. These results demonstrate again the influence of the amount of tetrahedral Ti and the Au particle size on the activity. Therefore, the amount of tetrahedral Ti sites, the acidity of the support oxide, the accessibility of Ti species and the Au particle size are all playing an important role in the catalytic performance of Au/Ti-SBA-15 catalysts.

2.4. Conclusions

Au/Ti-SBA-15 catalysts were prepared with Ti incorporated through hydrothermal synthesis or grafting. XRD confirmed the integrity of the hexagonal structure of the SBA-15 material after Ti

(resp. Au) incorporation. XRF showed that the hydrothermal method used to incorporate Ti into the SBA-15 structure resulted in materials with very low Ti amounts, whereas the theoretical amount of Ti in the grafted prepared Ti-SBA-15 materials equalled that in the final materials. N_2 sorption showed that the Ti-SBA-15 materials preserved their mesoporous structure, although higher Ti loadings can lead to a decreased order of the SBA-15 framework. The latter was more evident when Au nanoparticles were loaded into the Ti-SBA-15 materials. A bimodal pore size distribution was observed with increasing titanium content. UV–Vis DRS and XAFS measurements confirmed that the amount of tetrahedral Ti increased with increasing Si/Ti molar ratio. TEM and Au L_{III}-edge XAFS analysis showed that the Au particle size was dependent on the amount of titanium present. Au nanoparticles were larger in the grafted samples than in the hydrothermally prepared sample. The TEM images also showed that for the Ti-grafted materials, Au nanoparticles were present at higher density on the outer surface compared with the hydrothermally synthesized materials. Au/Ti-SBA-15 catalysts prepared by Ti grafting were active and stable in propene epoxidation, whereas Au/Ti-SBA-15 materials prepared via the direct synthesis method showed very low catalytic activity. This catalytic behaviour is related to the differences in the amount of dispersed Ti in the SBA-15 structure, as well to differences in the Au nanoparticle size distribution.

References

1. SciFinder search for publications with keywords "gold" and ("propene" or "propylene") and ("oxidation" or "epoxidation") d.d. 14.11.08 resulting in 289 relevant citation hits.
2. E.E. Stangland, K.B. Stavens, R.P. Andres, W.N. Delgass, J. Catal., 191 (2000) 332.
3. C. Sivadinarayana, T.V. Choudhary, L.L. Daemen, J. Eckert, D.W. Goodman, J. Am. Chem. Soc., 126 (2004) 38.
4. C. Qi, M. Okumura, T. Akita, M. Haruta, Appl. Catal. A: General, 263 (2004) 19.
5. A. Zwijnenburg, M. Makkee, J.A. Moulijn, Appl. Catal. A: General, 270 (2004) 49.
6. M. Haruta, B.S. Uphade, S. Tsubota, A. Miyamoto, Res. Chem. Intermed., 24 (1998) 329.
7. Y.A. Kalvachev, T. Hayashi, S. Tsubota, M. Haruta, J. Catal., 186 (1999) 228.
8. T.A. Nijhuis, B.J. Huizinga, M. Makkee, J.A. Moulijn, Ind. Eng. Chem. Res., 38 (1999) 884.
9. B.S. Uphade, M. Okumura, N. Yamada, S. Tsubota, M. Haruta, Stud. Surf. Sci. Catal., 130 (2000) 833.
10. B.S. Uphade, Y. Yamada, T. Akita, T. Nakamura, M. Haruta, Appl. Catal. A: General, 215 (2001) 137.
11. B.S. Uphade, T. Akita, T. Nakamura, M. Haruta, J. Catal., 209 (2002) 331.

12. A.K. Sinha, S. Seelan, T. Akita, S. Tsubota, M. Haruta, Appl. Catal. A: General, 240 (2003) 243.
13. C. Qi, T. Akita, M. Okumura, K. Kuraoka, M. Haruta, Appl. Catal. A: General, 253 (2003) 75.
14. N. Yap, R.P. Andres, W.N. Delgass, J. Catal., 226 (2004) 156.
15. E.E. Stangland, B. Taylor, R.P. Andres, W.N. Delgass, J. Phys. Chem. B, 109 (2005) 2321.
16. A.K. Sinha, S. Seelan, S. Tsubota, M. Haruta, Angew. Chem. Int. Ed., 43 (2004) 1546.
17. C. Qi, T. Akita, M. Okumura, M. Haruta, Appl. Catal. A: General, 218 (2001) 81.
18. S. Ivanova, C. Petit, V. Pitchon, Appl. Catal. A: General, 267 (2004) 191.
19. M. Haruta, S. Tsubota, T. Kobayashi, H. Kageyama, M.J. Genet, B.J. Delmon, J. Catal., 144 (1993) 175.
20. S. Tsubota, D.A.H. Cunningham, Y. Bando, M. Haruta, Stud. Surf. Sci. Catal., 91 (1995) 227.
21. W. Li, C. Massimiliano, F. Schüth, J. Catal., 237 (2006) 190.
22. A.K. Sinha, S. Seelan, S. Tsubota, M. Haruta, Top. Catal., 29 (2004) 95.
23. D. Zhao, J. Feng, Q. Huo, N. Melosh, G.H. Fredrickson, B.F. Chmelka, G.D. Stucky, Science, 279 (1998) 548.
24. D. Zhao, J. Feng, Q. Huo, N. Melosh, B.F. Chmelka, G.D. Stucky, J. Am. Chem. Soc., 120 (1998) 6024.
25. Y. Chen, Y. Huang, J. Xiu, X. Han, X. Bao, Appl. Catal. A: General, 273 (2004) 185.
26. P. Wu, T. Tatsumi, Chem. Mater., 14 (2002) 1657.
27. Z. Luan, E.M. Maes, P.A.W. van der Heide, D. Zhao, R.S. Czernuszewics, L. Kevan, Chem. Mater., 11 (1999) 3680.
28. X. Gao, S.R. Bare, J.L.G. Fierro, M.A. Banares, I.E. Wachs, J. Phys. Chem. B, 102 (1998) 5653.
29. V. Parvulescu, C. Anastasescu, C. Constantin, B.L. Su, Catal. Today, 78 (2003) 477.
30. N. Binsted, J.W. Campbell, S.J. Gurman, P.C. Stephenson, EXAFS Analysis Programs, Daresbury Laboratory, Warrington, 1991.
31. D. Trong On, S. Nguyen, V. Hulea, E. Dumitriu, S. Kaliaguine, Micropor. Mesopor. Mater., 57 (2003) 169.
32. M.S. Morey, S. O'Brien, S. Schwarz, G.D. Stucky, Chem. Mater., 12 (2000) 898.
33. M.C. Daniel, D. Astruc, Chem. Rev., 104 (2004) 239.
34. E.B. Barrett, L.G. Joyner, P.P. Halenda, J. Am. Chem. Soc., 73 (1951) 373.
35. K.S.W. Sing, D.H. Everett, R.A.W. Haul, L. Moscow, R.A. Pierotti, J. Rouquerol, T. Siemieniewska, Pure Appl. Chem., 57 (1985) 603.
36. P.I. Ravikovitch, A.V. Neimark, Langmuir, 18 (2002) 9830.

37. P. Van Der Voort, P.I. Ravikovitch, K.P. De Jong, M. Benjelloun, E.A. Van Bavel, H. Janssen, A.V. Neimark, B.M. Weckhuysen, E.F. Vansant, J. Phys. Chem. B, 106 (2002) 5873.
38. (a) T.A. Nijhuis, T. Visser, B.M. Weckhuysen, J. Phys. Chem. B, 109 (2005) 19309; (b) T.A. Nijhuis, B.M. Weckhuysen, Chem. Commun., (2005) 6002; (c) T.A. Nijhuis, T.Q. Gardner, B.M. Weckhuysen, J. Catal., 236 (2005) 153; (d) T.A. Nijhuis, T. Visser, B.M. Weckhuysen, Angew. Chem. Int. Ed., 44 (2005) 1115.
39. F. Farges, G. Brown, J. Rehr, J. Geochim. Cosmochim. Acta, 60 (1996) 3023.
40. J.M. Thomas, G. Sankar, Acc. Chem. Res., 34 (2001) 571.
41. D. Gleeson, G. Sankar, C.R.A. Catlow, J.M. Thomas, G. Spanó, S. Bordiga, A. Zecchina, C. Lamberti, Phys. Chem. Chem. Phys., 2 (2002) 4812.
42. A. Hagen, K. Schueler, F. Roessner, Microp. Mesopor. Mater., 51 (2002) 23.
43. F. Farges, G.E. Brown, J. Rehr, Phys. Rev. B, 56 (1997) 1809.
44. J.T. Miller, A.J. Kropf, Y. Zha, J.R. Regalbuto, L. Delannoy, C. Louis, E. Bus, J.A. van Bokhoven, J. Catal., 240 (2006) 222.
45. S. Calvin, S.X. Luo, C. Caragianis-Broadbridge, J.K. McGuinness, E. Anderson, A. Lehman, K.H. Wee, S.A. Morrison, L.K. Kurihara, Appl. Phys. Lett., 87 (2005) No. 233102.
46. A.I. Frenkel, C.W. Hills, R.G. Nuzzo, J. Phys. Chem. B, 105 (2001) 12689.
47. A. Carlsson, A. Puig-Molina, T.V.W. Janssens, J. Phys. Chem. B, 110 (2006) 5286.
48. A. Jentys, Phys. Chem. Chem. Phys., 1 (1999) 4059.
49. R.A van Santen, P.W.N.M. van Leeuwen, J.A. Moulijn, B.A. Averill, Catalysis: An Integrated Approach 1999, Elsevier, Amsterdam.

Chapter 3

Understanding the effect of post-synthesis ammonium treatment on the catalytic activity of Au/Ti-SBA-15 catalysts for the oxidation of propene

Abstract

The influence of a post-synthesis ammonium treatment of Au/Ti-SBA-15 catalyst materials was investigated in order to explain the impact on the catalytic activity for the direct epoxidation of propene using hydrogen and oxygen. The propene oxide formation rate of a calcined Au/Ti-SBA-15 catalyst prepared by this method increased from 4.3 mg $_{PO}$ $h^{-1}g_{cat}^{-1}$ to 37.2 mg $_{PO}$ $h^{-1}g_{cat}^{-1}$ at 200º C compared with a catalyst prepared in an identical manner without this treatment. The catalysts were characterized by XRD, N_2-sorption, UV-Vis DRS, ^{29}Si MAS NMR, FT-IR spectroscopy and TEM in order to understand the relation between ammonia treatment and catalyst activity. ^{29}Si MAS NMR measurements proved that the ammonium nitrate solution caused hydrolysis of ≡Si-O-Si≡ or ≡Ti-O-Si≡ bonds, resulting in a Ti-SBA-15 surface with a higher amount of surface hydroxyl groups, FT-IR measurements indicated the presence of amine species that favor the homogeneous deposition of Au nanoparticles. This was confirmed by TEM measurements, which show higher metal dispersion for NH_4NO_3 treated Au/Ti-SBA-15 materials.

3.1. Introduction

The size and distribution of Au nanoparticles are very important for their activity and selectivity in propene epoxidation with H_2 and O_2 [1-5]. The synthesis route, like the way of

reducing the Au, the pH of the solution, the source of Au and the physical-chemical properties of the support, are greatly influencing the size and distribution of the Au nanoparticles. Yap et al. [6] have shown that only a portion of gold deposited on the TS-1 surface create active Au/Ti epoxidation centers. Thus, it is very important to maximize the number of deposited Au nanoparticles on the support and eventually their proximity to the Ti species [1,2,6]. This can be influenced both by the method of Au deposition as well by modification of the support properties. Indeed, each support has a specific capacity for Au capture during deposition–precipitation. Taylor et al. found that a TS-1 support with high Ti loading was capturing almost 5 times more Au than TS-1 support with low Ti loading [1]. To maximize the adsorption capacity, it is very important to choose the proper type of the support or to perform further pretreatments to obtain narrow well-dispersed Au nanoparticles. Delgass et al. [2] showed that a NH_4NO_3 treatment of TS-1 can enhance the gold capture during the deposition–precipitation procedure.

In this **Chapter**, we discuss the influence of a post-synthesis ammonium treatment of Ti-SBA-15 support on the morphology of Au nanoparticles and their catalytic performance in the epoxidation of propene. By making use of a variety of characterization methods it has been possible to put forward plausible explanations for the observed differences in catalytic performances.

3.2. Experimental

3.2.1. Catalyst preparation

Pure mesoporous silica SBA-15 material was hydrothermally synthesized according to the procedure described by Zhao et al. [7]. The reagents used were poly(ethylene glycol)-block-poly(propylene glycol)-block-poly(ethylene glycol) (PEG-PPG-PEG) (average molecular weight 5800, Aldrich), TEOS (Aldrich, 98%), HCl (Merck, 37%), and distilled water. The gel solution was prepared by dispersing 8 g of PEG-PPG-PEG in 60 g of distilled water, followed by 15 min of vigorous stirring at 40º C. The resultant solution was mixed with 48 g HCl and 190 g H_2O and stirred for another 17 h. Finally, 21.2 g TEOS solution was added dropwise in the gel mixture at 40º C with stirring for 9 h before being placed in a Teflon autoclave at 100º C for 12 h. After the completion of the synthesis, the product was filtered, washed with distilled water, and air-dried overnight at 60º C. The solid was calcined at 550º C for 6 h.

The Ti-SBA-15 grafted support designated as Ti-G and with a Si/Ti molar ratio of 40 was synthesized using titanium isopropoxide (Across, 98%) as titanium source [8]. Titanium grafting was performed inside a glove box in a nitrogen environment. Titanium (IV) isopropoxide was dispersed in 2 g of dry isopropyl alcohol (99.7%, Merck) and mixed with 1 g of SBA-15 at ambient temperature. The solid was dried at ambient temperature under flowing nitrogen. Finally, the

titanium-grafted material was calcined at 400º C for 4 h. The post-synthesis ammonium treatment was carried out using a NH_4NO_3 (1 M) solution [2]. Ammonium-treated Ti-SBA-15 supports were prepared by suspending 1 g of calcined Ti-SBA-15 material in 60 g of NH_4NO_3 solution. The solution was heated at 80º C under continuous stirring from 6 h to 30 h. The product obtained was washed with 80 ml of deionized water and dried at 60º C overnight. The resulting samples were labeled Ti-N-n, with n representing the ammonium treatment time. The ammonium-treated Ti-SBA-15 supports were not calcined before Au deposition. A post-synthesis water treatment was also carried out, following the same procedure as for the ammonium treatment to determine to what extent the NH_4NO_3 treatment would be the cause of changes in activity in comparison to other treatments. The water-treated Ti-SBA-15 support is labeled as Ti-H-30h. Au catalysts, designated as Au/Ti-N-n and Au/Ti-H-30h, were prepared by the deposition-precipitation method [2] using aqueous $HAuCl_4$ with the amount of Au dissolved corresponding to a 1 wt% loading on the support and Na_2CO_3 (1 M) as precipitant. In this method, $HAuCl_4$ solution was dissolved in 50 ml of deionised water, followed by the dispersion of 1 g of Ti-SBA-15 support in this solution. The solution mixture was stirred for 15 min before the pH was adjusted to 9 with 1 M Na_2CO_3. The mixture was stirred at room temperature for 4 h, with the pH maintained at 9. The catalysts were washed with distilled water, dried in air overnight at 60º C, and calcined at 400º C for 4 h. To understand the effect of the ammonium treatment, an Au/Ti-G catalyst was prepared as reference. Futhermore, AuN-Ti-n catalyst was synthesized by changing the order of Au and Ti incorporation. In this preparation procedure, calcined SBA-15 material was treated with ammonium before Au deposition, after which titanium grafting was performed on the calcined 1% AuN material.

3.2.2. Catalyst characterization

The degree of crystallinity and morphology of the Au/Ti-SBA-15 materials was characterized using transmission electron microscopy (TEM) and X-ray diffraction (XRD). The latter was performed using a Bruker-AXS D8 Advance powder X-ray diffractometer, equipped with an automatic divergence slit, a Våntec-1 detector, and a cobalt Kα1,2 (λ= 1.79026 Å) source. TEM images were acquired in bright-field mode using a Tecnai F20 electron microscope (FEI Company). The microscope, operated at 200 keV, was equipped with a field emission gun, a twin objective lens, and a 1k×1k Gatan Slow Scan CCD camera. TEM sample preparation proceeded as follows. A small portion of dry powder (~ 15 mg) was placed in a 16-mm mold/die commonly used for pelletization. The powder was then pressed to approximately 12 tons (460 MPa), after which the pressure was immediately released. The resulting pellet was ground up in a mortar and a small portion of the very fine powder was dispersed in ethanol by ultrasonication for 30 s. Finally, a few droplets of the suspension were placed on a Quantifoil R2/1 lacey carbon support film and dried

under a lamp. The additional step of compressing the SBA-15 powder before conventional TEM sample preparation was found to be advantageous for imaging of the examined material. As shown in earlier work, imaging of small metal (oxide) particles in the pores of SBA-15 can be carried out by electron tomography [9-11]. However, for conventional TEM, imaging of small metal (oxide) particles through large or thick SBA-15 structures is difficult. In this case, very thin support structures are advantageous. During pressing of the material, the SBA-15 particles, roughly 2000 × 500 × 500 nm in size, fracture leaving much smaller and thinner pieces intact. Very small Au particles (nm) are found in the pores of these thin pieces. Parts of the SBA-15 structure collapsed, resulting in disordered amorphous silica. Comparison of pressed and unpressed material ensured that pressing did not affect the gold particle. The particle size distribution was estimated by measuring the diameter of more than 100 particles in each sample using a Analysis software. The corresponding volume and surface area weighted distributions were calculated directly from the particle diameters, assuming a spherical particle shape. The specific surface area and pore volume were determined by N_2 sorption measurements using a Micromeritics ASAP 2400 instrument. Surface areas were calculated using the BET model, with micropores and macropores described by the Horvath–Kawazoe and BJH models, respectively. UV-Vis diffuse reflectance spectroscopy (DRS) measurements were carried out at room temperature on a Varian Cary 500 instrument in the range of 200–2200 nm. This set-up was equipped with a diffuse reflectance accessory, which was set to collect diffuse reflected light only. A baseline correction was performed using a white Halon standard. ^{29}Si MAS NMR measurements were carried out with a Bruker Avance 500 WB spectrometer at a spinning rate of 10 kHz using $\pi/4$ pulses of 2.2 μs and a repetition delay of 30 s. FT-IR spectra were recorded on a Perkin-Elmer Spectrum One instrument on self-supported catalyst wafers placed in an IR transmission cell equipped with CaF_2 windows. For each sample, an IR spectrum was recorded before and after drying in helium at 300º C.

3.2.3. Catalyst testing

A flow reactor was used to evaluate the catalytic performance of the different catalysts prepared. The experiments were carried out typically with 0.4 g of catalyst material and a flow of 50 N ml min^{-1}. The gas mixture consisted of 10% O_2, 10% H_2, and 10% C_3H_6 in He. The analysis of the gas leaving the reactor was carried out using an Interscience Compact GC system, equipped with a Molsieve 5A and a Porabond Q column, each with a thermal conductivity detector (TCD). Gas samples were analyzed every 3 min. The experiments were carried out in cycles: 5 h at reaction temperature with the reactant mixture, followed by a regeneration cycle. For the regeneration step, 10% O_2 in He was used, and the catalyst was heated at 300º C and maintained at that temperature for 1 h, then cooled to the next reaction temperature in the cycle. The performance was typically

tested at 10-15 different temperatures (including duplicates to determine for each catalyst the deactivation pattern).

3.3. Results

Figure 3.1 shows the catalytic activities of two different Au/Ti-SBA-15 samples in the propene epoxidation reaction with O_2 and H_2.

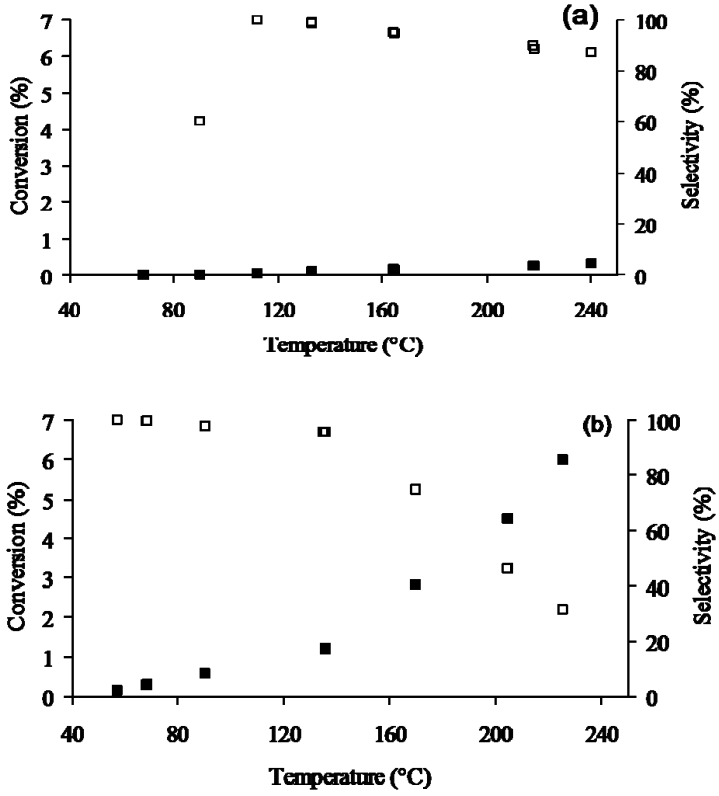

Figure 3.1. Catalytic performance of (a) Au-Ti-G and (b) Au/Ti-N-30h catalysts (conversion (■) and selectivity (□), pressure of 1 bar and GHSV ($m^3/m^3/h$) of 1765 h^{-1}).

The untreated Au/Ti-G catalyst showed relatively low activity under the reaction conditions applied. This activity is typical for unmodified Au/TS-1 catalysts under these conditions. But the Au/Ti-N-30h catalyst with Au supported on a NH_4NO_3-pretreated Ti-SBA-15 support showed substantial activity for propene oxide formation. NH_4NO_3 treatment clearly exerted a pronounced effect on the catalytic performance of the Au/Ti-N-30h catalyst. As the reaction temperature was increased, the selectivity to propene oxide decreased, corresponding to an increase in the total

amount of oxidation products. The conversion, selectivity, hydrogen efficiency and product distribution of the different Au/Ti-SBA-15 catalysts studied are summarized in Table 3.1. All catalysts exhibited higher conversion levels with increasing reaction temperature, but at the expense of the selectivity towards propene oxide due to an increase in the total oxidation to CO_2. The water-treated Au/Ti-H-30h catalyst was inactive in propene epoxidation reaction with propane as the main product.

Table 3.1. Overview of the catalytic performances of the Au/Ti-SBA-15 catalyst materials under investigation (C%- conversion, S%- selectivity), Pressure of 1 bar and GHSV ($m^3/m^3/h$) of 1765 h^{-1}.

Catalyst	Temperature (^{0}C)	C (%) C_3H_6	Selectivity (%)					H_2 eff (%)
			S% PO	S% CO_2	S% Propanol	S% Propane	S% Other oxigenates	
Au/Ti-N-6h	90	0.4	99.4	0	0.6	0	0	4.6
	135	0.8	97.7	0	1.1	0	1.2	3.3
	170	1.6	89.4	7.6	1.5	0	1.5	2.7
	200	2.7	65	31.9	1.9	0	1.2	1.5
Au/Ti-N-15h	90	0.5	97.5	0	1.8	0	0.7	3.8
	135	0.9	92.8	0	1.7	3.6	1.9	2.8
	170	1.9	83	11.1	2.4	0.7	2.8	2.3
	200	3.2	58.5	38.9	0	0	2.6	1.4
Au/Ti-N-30h	90	0.7	98	0	1.3	0	0.7	5.5
	135	1.4	95.8	1	1.3	0	1.9	3.6
	170	2.8	74.6	21.2	1.7	0	2.5	2.2
	200	4.6	46.4	50.3	2	0	1.3	1.4
AuN-Ti-15h	90	0.4	98.7	0	1.3	0	0	12.4
	135	0.7	96.5	0	3.5	0	0	8.5
	170	0.8	89	0.1	10.9	0	0	4.5
	200	1.9	39.8	33.6	26.6	0	0	0.9
Au-Ti-G	90	0	0	0	0	0	0	0
	135	0.08	98.9	0	0	0	1.1	14.1
	170	0.13	95.2	0	2.8	0	2	11.8
	200	0.2	90.1	0	5.1	0	4.8	4.5

Another important finding is that the catalytic activity of the Au/Ti-N-n materials was enhanced when the NH_4NO_3 treatment of Ti/SBA-15 support was increased from 6 h to 30 h. Figure 3.2 shows the yields of propene oxide over different Au/Ti-SBA-15 catalysts as a function of time on stream. The propene oxide yields were lower for the Au-Ti-G and AuN-Ti-15h catalysts than for the Au/Ti-N-30 catalyst. Small losses in the activity of Au/Ti-SBA-15 catalysts at 200º C during 5 h time on stream were observed, although the catalytic activity could be restored almost completely after an activation procedure at 300º C. Comparing the activities of the Au/Ti-SBA-15

catalysts for which the order of Au and Ti incorporation differed shows that the Au/Ti-N-15h (Ti first deposited) material had higher catalytic activity than the AuN-Ti-15h material. Propene oxide production was measured after 3–5 h of steady-state activity at 200º C.

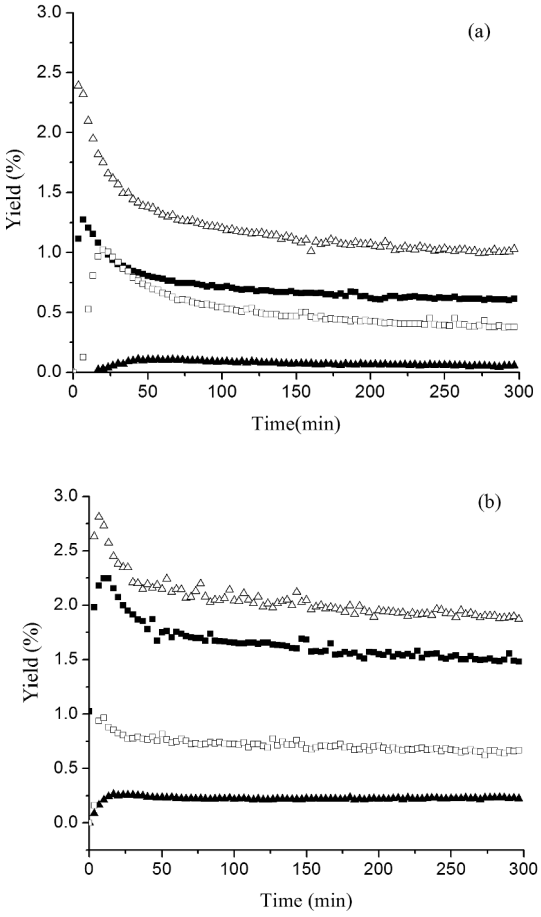

Figure 3.2. Catalytic performance of Au-based catalyst materials tested at two different temperatures (a) 130º C and (b) 200º C. The catalyst materials are : (▲) Au-Ti-G, (□) AuN-Ti-15h, (■) Au/Ti-N-6h and (Δ) Au/Ti-N-30h. 0.4 g catalyst, 50 Nml/min gas fed rate (10% H_2, O_2, propene) and total pressure 1100 mbar.

The Au-Ti-G catalyst had a rate of 4.3 $mg_{PO}\ h^{-1}\ g^{-1}_{cat}$, whereas the NH_4NO_3 treated Au/Ti-N-30h catalyst had a rate of 37.2 $mg_{PO}\ h^{-1}\ g^{-1}_{cat}$. Delgass et al. [2] reported the increased catalytic activity of NH_4NO_3-treated catalyst materials for Au/TS-1 materials. This research group explained the observed differences in catalytic performances in terms of an increasing active site density. However, the reason for the increased number of active sites due to NH_4NO_3 treatment remaind unclear. Delgass et al. suggested that the formation of an Au-amine complex near Ti sites could be responsible for boosting the catalytic activity of NH_4NO_3-treated Au/TS-1 catalysts [2]. To gain more insight into this beneficial effect, we thoroughly characterized the different Au/Ti-SBA-15 catalyst materials under investigation

3.3.1. X- ray diffraction

The powder XRD patterns of the calcined samples are shown in Figures 3.3 and 3.4. In the small-angle region of the XRD patterns (Figure 3.3), all samples exhibit three well-resolved diffraction peaks that can be indexed to the (100), (110), and (200) reflections of the p6mm hexagonal space group, which matches the SBA-15 structure [7].

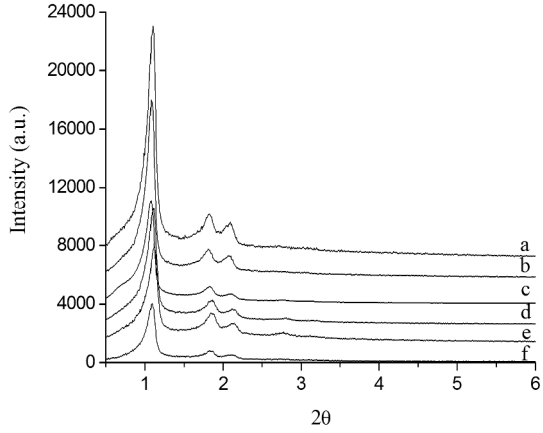

Figure 3.3. Small angle XRD patterns of: (a) SBA-15, (b) Ti-G, (c) AuN-Ti-15h, (d) Au/Ti-N-6h, (e) Au/Ti-N-15h and (f) Au/Ti-N-30h.

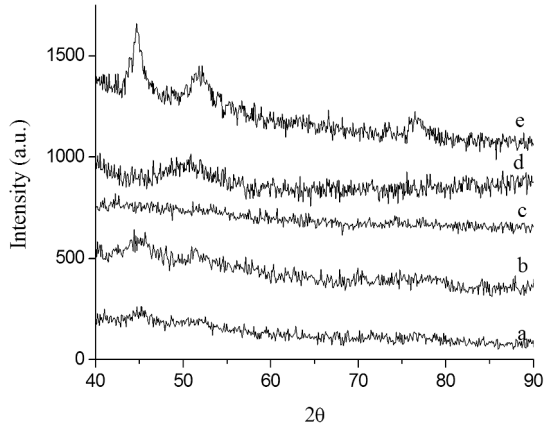

Figure 3.4. Wide angle XRD patterns of : (a) Au/Ti-N-6h, (b) Au/Ti-N-15h, (c) Au/Ti-N-30h, (d) Au-Ti-G and (e) AuN-Ti-15h.

After incorporation of Ti, the SBA-15 structure was preserved, as shown by the presence of intense reflection peaks of the Ti-SBA-15 sample. But the intensities of these peaks decreased in the case of the ammonium-treated Au/Ti-SBA-15 samples and this tendency is even more pronounced for increasing ammonium treatment time. The XRD results may indicate that the incorporation of Au and the increase in ammonium treatment time from 6 h to 30 h decreased the long-range order of the SBA-15 structure. XRD data from the high-angle region of the Au/Ti-SBA-15 samples are shown in Figure 3.4.

The absence of the Au peaks for the NH_4NO_3-treated Au/Ti-SBA-15 samples indicates that Au nanoparticles were highly dispersed through the silica matrix and that the average particles size was too small to be detected by XRD. Interestingly, in the AuN-Ti-15h sample, broad reflections of Au were seen, due to the formation of larger Au nanoparticles.

3.3.2. N_2 sorption measurements

Nitrogen adsorption–desorption isotherms of all synthesized samples are displayed in Figure 3.5. The calcined samples exhibit type IV isotherms with H1-type hysteresis, typical of mesoporous materials with one-dimensional cylindrical channels [12]. The sharp inflection between the relative pressure P/Po 0.66 and 0.8 observed in the isotherm of SBA-15 correspond to the capillary condensation within uniform mesopores. The sharpening of this step reflects the uniform pore size distribution in the material.

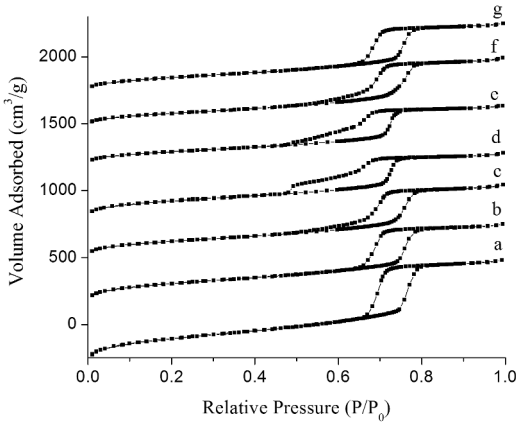

Figure 3.5. N_2 adsorption-desorption isotherms of : (a) SBA-15, (b) Ti-G, (c) Ti-N-30h calcined, (d) Ti-H-30h, (e) Au/Ti-H-30h, (f) Au/Ti-N-30h and (g) Au-Ti-G.

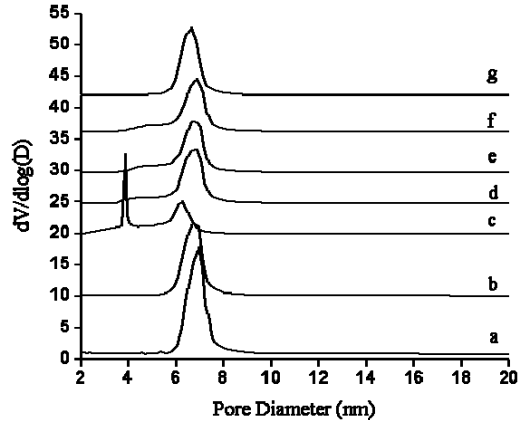

Figure 3.6. Pore size distributions derived from desorption branches of N_2-sorption isotherms of : (a) SBA-15, (b) Ti-G, (c) Ti-H-30h, (d) Ti-N-30h calcined, (e) Au/Ti-N-6h, (f) Au/Ti-N-30h and (g) Au-Ti-G.

The introduction of Ti induced a decrease in the BET surface area of the SBA-15 material from 970 $m^2 g^{-1}$ to 740 $m^2 g^{-1}$ and a decrease in the pore volume from 1.3 $m^3 g^{-1}$ to 1 $m^3 g^{-1}$ (Table 3.2). The BET surface area and pore volume of Ti-SBA-15 were also modified after the 6 h ammonium treatment and changed slightly when this treatment was prolonged to 30 h. The decreased specific surface area of the ammonium-treated Ti-SBA-15 supports is likely caused by the modification of the Ti-SBA-15 structure.

Figure 3.6 shows the BJH pore size distribution of the samples. The Ti-SBA-15 supports exhibited a bimodal structure after the water and ammonium treatment, both of which can cause hydrolysis of the ≡Si–O–Si≡ or ≡Ti–O–Si≡ bonds, which may be associated with the formation of smaller pores in the structure. The introduction of Au inside the SBA-15 channels also induced a decrease in the pore volume and BET surface area of the Ti-SBA-15 material, indicating that some pore blocking occurred during Au incorporation [13,14]. Interestingly, the decrease in the pore volume was more pronounced in the AuN-Ti-15h sample than in the Au/Ti-N-15h sample. This suggests that the order of Au and Ti incorporation has also an influence on the textural properties of the resulting material. This is likely due to the presence of larger Au nanoparticles in the SBA-15 channels, as was observed in the XRD spectrum (Figure 3.2).

Table 3.2. Summary of the characterization results of the different SBA-15, Ti-SBA-15 and Au/Ti SBA-15 samples

Catalyst	Si/Ti final molar ratio	Au loading (wt%) final product	BET surface area (m^2/g)	Micropore vol (cm^3/g)	t-Plot area (m^2/g)	Pore volume BJH (cm^3/g)	Pore size BJH desorption (nm)
SBA-15	-	-	970	0.07	810	1.3	6.9
Ti-G	43.0	-	740	0.05	615	1	6.8
Ti-N-6h (calcined)	43.5	-	640	0.04	550	0.92	4.6 ; 6.9
Ti-N-30h (calcined)	49.4	-	615	0.03	525	0.9	4.6 ; 6.9
Ti-H-30h	48.3	-	648	0.06	512	0.86	3.8 ; 6.3
Au/Ti-H-30h	-	0.05	483	0.01	447	0.74	3.8 ; 6.3
Au/Ti-N-6h	-	1	480	0.007	460	0.83	4.6 ; 6.9
Au/Ti-N-15h	-	1	510	0.009	475	0.87	4.6 ; 6.9
Au/Ti-N-30h	-	1	490	0.007	460	0.83	4.6 ; 6.9
Au-Ti-G	-	0.1	510	0.006	490	0.83	6.6
AuN-Ti-15h	-	1	430	0.009	440	0.82	6.8

3.3.3. UV-Vis diffuse reflectance spectroscopy

UV-Vis DRS can distinguish framework and extra-framework titanium species in a silica matrix [15,16]. Representative UV-Vis DRS spectra of the samples are shown in Figure 3.7. In all spectra of the Ti-containing SBA-15 samples, an intense band centered at ca. 220 nm can be observed, along with a shoulder at 260-270 nm. The band at 220 nm is due to the charge-transfer process of isolated framework titanium in tetrahedral coordination [15]. The shoulder at 270 nm has been attributed to the presence of Ti in five-fold and six-fold coordination, generated through the hydration of tetrahedrally coordinated sites [17]. Note that the intensity of this shoulder is much lower for the as-synthesized Ti-N-n supports than for the calcined Ti-N-n supports. These results suggest that the Ti environment for as-synthesized ammonium-treated Ti-SBA-15 supports differed from those measured after calcination. Moreover, the intensity of the shoulder at 270 nm decreased after NH_4NO_3 treatment, as seen by comparing the Ti-G support with the calcined Ti-N-6h support (Figure 3.7, spectra a and e). The UV-Vis DRS spectra cannot be used to estimate the quantity of Ti in the sample, but the variation in the intensity may reflect changes in the amount and type of species of Ti in Ti-SBA-15 after the ammonium treatment.

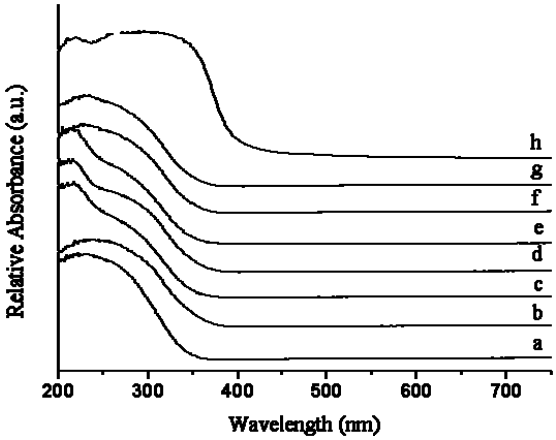

Fig. 3.7. UV-Vis DRS spectra of Ti-SBA-15 supports: (a) Ti-G, (b) Ti-H-30h (c) Ti-N-6h, (d) Ti-N-15h, (e) Ti-N-30h, (f) Ti-N-6h calcined, (g) Ti-N-30h calcined and (h) TiO_2 anatase.

These results confirm that during NH_4NO_3 treatment, some extra-framework titanium was removed from the surface of SBA-15, in good agreement with the ICP-AES results. Note that the DRS spectrum of the water-treated Ti-H-30h sample (Figure 3.7 b) is similar to that of the Ti-G support (Figure 3.7 a). The absence of a band at 330-340 nm indicates that no bulk titania was formed during synthesis [17]. The presence of a UV-Vis absorption band at around 520 nm originates from the plasmon resonance of nanosized metallic gold particles present in the Au/Ti-SBA-15 samples (Figure 3.8) [18]. The intensity of this band was greater for the AuN-Ti-15h

sample than for the Au/Ti-N-n samples, confirming the presence of smaller Au particles in the Au/Ti-N-n samples, as also demonstrated in the XRD pattern analysis.

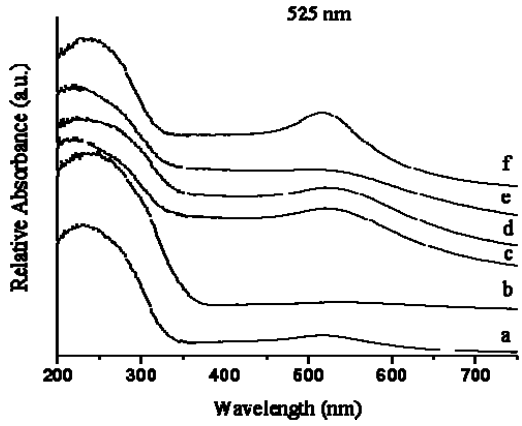

Figure 3.8. UV-Vis DRS spectra of Au/Ti-SBA-15 samples of : (a) Au-Ti-G, (b) Au/Ti-H-30h, (c) Au/Ti-N-6h, (d) Au/Ti-N-15h, (e) Au/Ti-N-30h and (f) AuN-Ti-15h.

3.3.4. ^{29}Si Magic Angle Spinning Nuclear Magnetic Resonance Spectroscopy

^{29}Si MAS NMR spectroscopy can provide information about the nature and amount of silanol groups present in the Ti-SBA-15 mesostructure [19.20]. The ^{29}Si MAS NMR spectra for the calcined SBA-15, Ti-SBA-15, Au/Ti-SBA-15 and as-synthesized Ti-N-n supports are shown in Figure 3.10. For the calcined SBA-15 and Ti-SBA-15 materials (Figure 3.10, spectra a and b), the ^{29}Si MAS NMR spectra have an intense peak at about −107 ppm, associated with silicon linked via siloxane bridges to four other silicon atoms, $(\equiv SiO)_4Si$, designated as Q^4. The two downfield resonance peaks at −97 and −89 ppm are attributed to silicon in single silanols, $(\equiv SiO)_3SiOH$, designated as Q^3, and geminal silanols, $(\equiv SiO)_2Si(OH)_2$, designated as Q^2 [21], respectively. The schematic representation of Q^2, Q^3 and Q^4 species is shown in Figure 3.9.

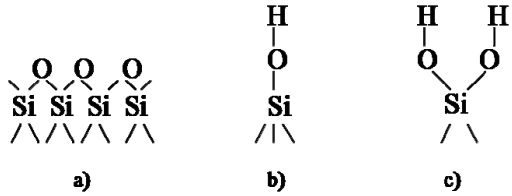

Figure 3.9. Schematic representation of: a) Surface siloxanes Q^4, b) Isolated silanols Q^3 and c) Geminal silanols Q^2.

The ^{29}Si MAS NMR spectra of Ti-SBA-15 before (Figure 3.10 b) and after treatment with NH_4NO_3 (Figure 3.10, spectra c, d, and e) are considerably different. A significant increase in signal intensity of the peaks at −97 and −89 ppm occurred after the NH_4NO_3 treatment (Figure 3.10, spectra c, d, and e). However, the duration of this treatment did not seem to be reflected in comparable spectra after 6, 15 or 30 h of treatment time. ^{29}Si MAS NMR spectra of Ti-SBA-15 supports before and after water treatment are shown in Figure 3.11. Again, an increase in the intensity of Q^2 and Q^3 species can be observed caused in this case by the water treatment (Figure 3.11 b). This is very similar to the effect of the NH_4NO_3 treatment. The increased intensity of Q^2 and Q^3 species on pretreatment of Ti-SBA-15 with 1 M solution of NH_4NO_3 or with water can be associated with the partial hydrolysis of some of ≡Si–O– Si≡ or ≡Ti–O–Si≡ bonds.

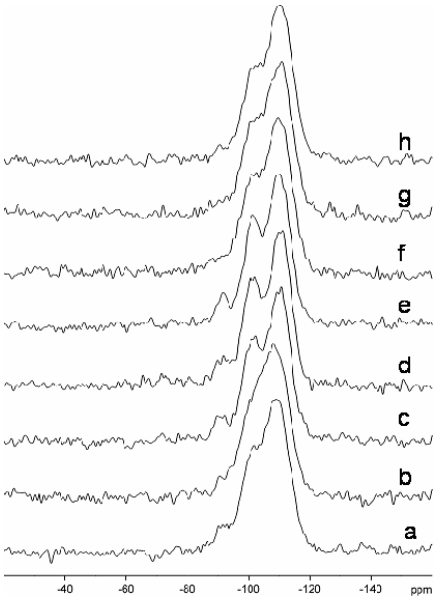

Figure 3.10. ^{29}Si MAS NMR spectra of: a) SBA-15 calcined, (b) Ti-G calcined, (c) Ti-N-6h as synthesized, (d) Ti-N-15h as synthesized, (e) Ti-N-30h as synthesized, (f) Au/Ti-N-30h calcined, (g) Au-Ti-G calcined and (h) AuN-Ti-15h calcined.

This is shown in Scheme 3.1, resulting in an increased density of surface hydroxyl groups. The possibility that these two resonance peaks also may contain contributions from Si(3Si, 1Ti) sites and from Si(2Si, 1Ti, 1H) sites cannot be excluded, however. ^{29}Si MAS NMR spectra of the Au/Ti-SBA-15 samples (Figure 3.10, spectra f, g, and h) after gold deposition and calcination again exhibited reduced intensity of the Q^2 and Q^3 signals, which can be assigned to a decrease in surface hydroxyl groups due to condensation during the calcination procedure.

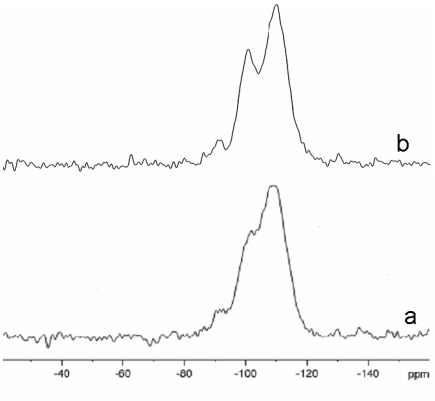

Fig. 3.11. ^{29}Si MAS NMR spectra of: (a) Ti-G calcined and (b) Ti-H-30 as synthesized.

3.3.5. FT-IR spectroscopy

Figure 3.12 shows the FT-IR spectra of Ti-G (a), Ti-N-30h (b), and Au/Ti-N-30h (c) before the thermal treatment. A narrow band at 3750 cm^{-1} and a broad absorption band in the 3700–3300 cm^{-1} range can be seen for all samples. The band at 3750 cm^{-1} is assigned to the stretching vibration of isolated silanol or geminal silanol groups located at the surface of the inner walls of the SBA-15 channels [21]. The band in the 1700-1600 cm^{-1} region can be attributed to the water deformation vibration. The presence of NH_4NO_3 after post-synthesis treatment of the Ti-N-30h sample (Figure 3.12 b) is confirmed by the presence of two broad absorption bands at 1500-1250 cm^{-1} and 3600-3300 cm^{-1}, which can be assigned to the NH_4^+ bending and stretching vibrations.

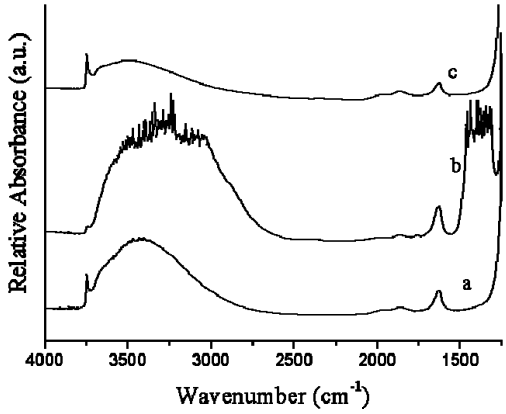

Figure 3.12. FT-IR spectra of: (a) Ti-G, (b) Ti-N-30h and (c) Au/Ti-N-30h recorded at room temperature.

After the thermal treatment at 300º C in He (Figure 3.13 b) decomposition of NH_4NO_3 occurred, and the spectra of all samples became similar. The band at 3750 cm^{-1} became sharper and

more intense, whereas the bands at 3700-3300 cm^{-1} and 1700-1600 cm^{-1} decreased in intensity during thermal treatment because of water and NH_4NO_3 removal.

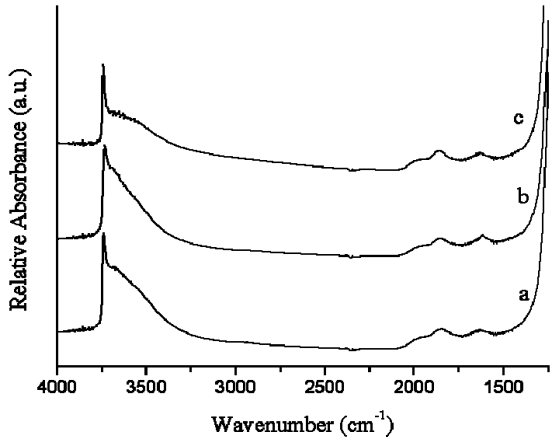

Figure 3.13. FT-IR spectra of: (a) Ti-G, (b) Ti-N-30h and (c) Au/Ti-N-30h recorded after thermal treatment at 300º C.

3.3.6. Transmission electron microscopy

To gain more insight into the effect of the post-synthesis NH_4NO_3 treatment and water treatment, the Au/Ti-SBA-15 materials were analyzed by TEM. Figure 3.14 presents TEM micrographs of Au/Ti-SBA-15 samples with (Au/Ti-N-30h) and without (Au-Ti-G) NH_4NO_3 treatment of the support before the Au deposition. The corresponding number-, surface-, and volume-weighted particle size distributions [22] are given in Figure 3.15. The TEM image of the Au-Ti-G material (Figure 3.14 a) shows that very few Au particles were deposited on the support, which is in good agreement with the ICP-AES results.

Furthermore, the Au particles were not well dispersed in the channels of Ti-SBA-15. Some of them, mainly large particles, seemed to be formed on the outer surface of the SBA-15 support. The Au particles in this sample had an average particle diameter of 5 nm (number-weighted), 11 nm (surface-weighted) and 15 nm (volume-weighted). In the case of water treated Au/Ti-H-30 sample, it was difficult to determine the exact location of the Au nanoparticles from the TEM micrographs (not shown). However, presumably because of the very low gold loading deposited on the water-treated Ti-SBA-15 supports. The TEM image of the Au/Ti-N-30h sample (Figure 3.14 b) clearly shows the presence of only small gold nanoparticles. In addition, particles with a mean diameter of 2-3 nm (number weighted), 4 nm (surface weighted) and 5 nm (volume weighted) were dispersed homogeneously within the Ti/SBA-15 mesopores.

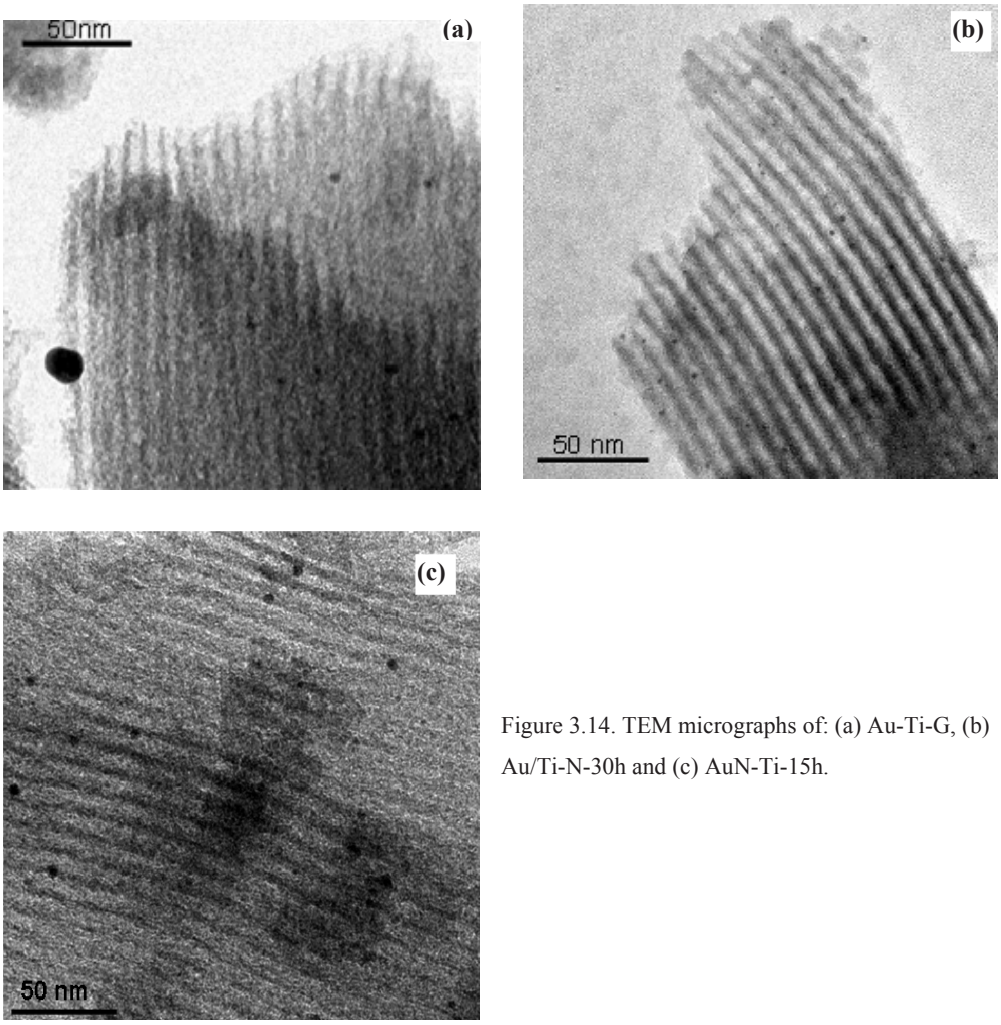

Figure 3.14. TEM micrographs of: (a) Au-Ti-G, (b) Au/Ti-N-30h and (c) AuN-Ti-15h.

The need for titanium in the SBA-15 structure to ensure good Au dispersion/adsorption is clearly demonstrated by the TEM micrograph of the AuN-Ti-15h sample (Figure 3.14 c), for which Au was first deposited on an NH_4NO_3 pretreated SBA-15 and Ti was then grafted. In this case, larger Au nanoparticles were formed, comparable with those in the Au/Ti-N-30h sample in which the Ti-SBA-15 support was pretreated before Au deposition. The average diameter of Au nanoparticles for AuN-Ti-15 material was around 6 nm for number-weighted, 8 nm for surface-weighted, and 9 nm for volume-weighted analyses. These finding clearly indicate that the post-synthesis NH_4NO_3 treatment of the Ti-SBA-15 support lead to smaller, more uniform Au nanoparticles inside the SBA-15 channels.

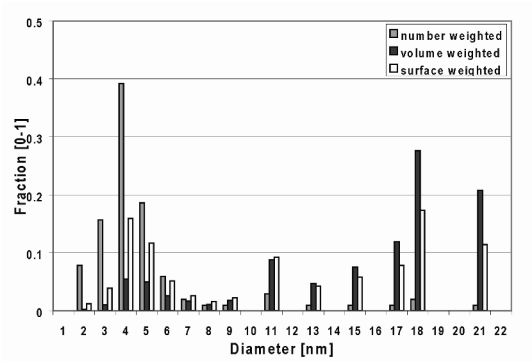

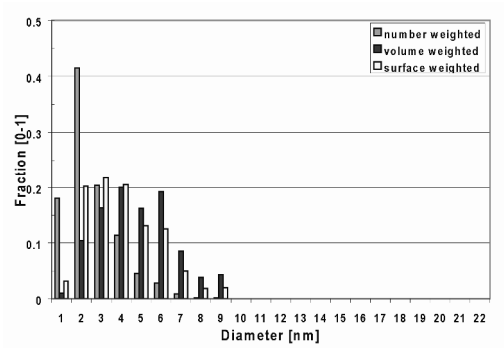

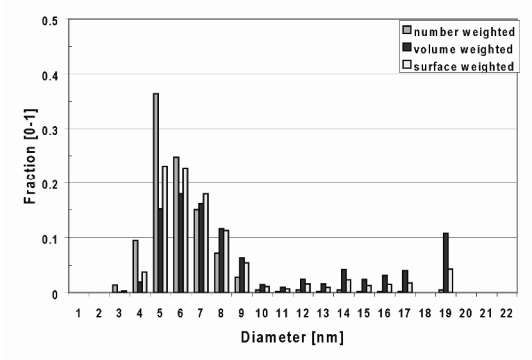

Figure 3.15. Number, surface and volume weighted particle size distributions of: (a) Au-Ti-G, (b) Au/Ti-N-30h and (c) AuN-Ti-15h.

3.4. Discussion

A high intake of Au on a support for TiO_2 requires a high number of available hydroxyl groups as adsorption centers for the gold species [23]. As shown by the ^{29}Si MAS-NMR findings, pretreatment with NH_4NO_3 significantly increased the number of hydroxyl groups (Scheme 3.1).

$$\text{Ti-O-Si} \xrightarrow[\text{pH=5}]{NH_4^+NO_3^- / H_2O} \text{Si-OH + Ti-OH}$$

Scheme 3.1. NH_4NO_3 treatment of the Ti-SBA-15 material.

According to the ICP-AES measurements, Au was completely deposited in the NH_4NO_3-pretreated Ti-SBA-15 support. In contrast, in the non-pretreated support, the amount of Au deposited was only 10% of the available Au precursor in the solution. The actual deposition mechanism should be similar to that proposed by Moreau et al. [24], who investigated Au deposition on TiO_2 by studying the effect of pH in the deposition-precipitation process and the species formed at different pH values.

When the Ti-SBA-15 support was immersed in the $HAuCl_4$ solution, the pH was 2.6. The pH was raised up to a value of 9 through the addition of Na_2CO_3 to obtain the deposited $Au(OH)_3$. In this pH range, the Si-OH groups were gradually transformed into negatively charged $Si\text{-}O^-$, but in the 4.5-6 range, the Ti-OH groups remained protonated as $Ti\text{-}OH_2^+$ [25]. In this pH range, the Au species in solutions were mainly anions $[AuCl_x(OH)_{4-x}]^-$ (x= 1-4). This negatively charged species could then be adsorbed on the protonated $Ti\text{-}OH_2^+$ groups according to Scheme 3.2.

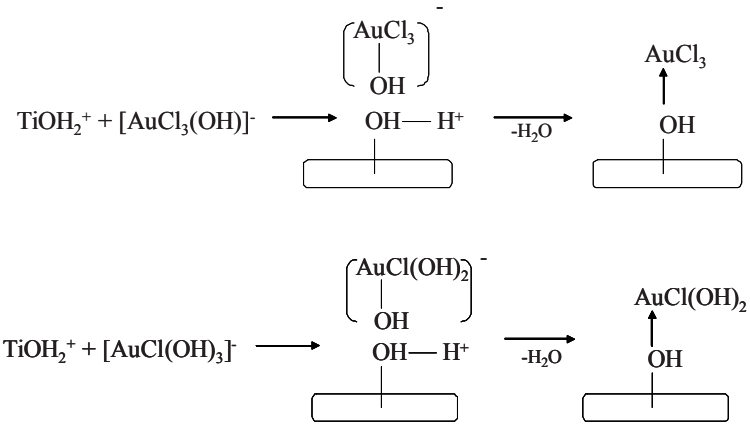

Scheme 3.2. Mechanism of $HAuCl_4$ deposition on NH_4NO_3 pretreated Ti-SBA-15 at pH < 6.

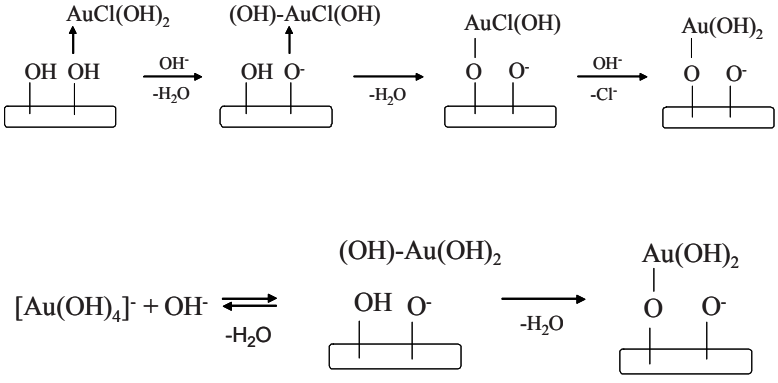

Scheme 3.3. Mechanism of $HAuCl_4$ deposition on NH_4NO_3 pretreated Ti-SBA-15 at pH > 6.

The electrostatic interaction will be stabilized by the formation of an adsorbed hydroxochloro complex of Au (Scheme 3.2). This complex will act as a nucleation center for the formation of the $Au(OH)_3$ species [26]. The formation of an Au-amine complex next to the Ti sites was proposed by Delgass et al. [2] to explain the increased Au deposition on a TS-1 support pretreated with 1 M NH_4NO_3. However, no experimental evidence for this complex was given, but comparing the water-pretreated Ti-H-30h support with the NH_4NO_3 pretreated Ti-N-n supports shows more Au adsorption on the latter. These findings suggest that along with generating a greater density of hydroxyl groups on the Ti-SBA-15 support, amine species also played a role in the homogeneous deposition of Au. Therefore, we may assume that the presence of amine species in the structure of the Ti-SBA-15 support enhanced the homogeneous dispersion of gold onto the support. Amine species may be concentrated near to the Lewis acidic Ti sites after post-synthesis NH_4NO_3 treatment of the Ti-SBA-15 support. This causes a more homogeneous deposition of Au nanoparticles in the proximity of the Ti sites. This was indicated by the results obtained for the AuN/Ti-15h sample when Au was deposited on a NH_4NO_3-treated SBA-15 and Ti was then added. In this case, Au was not homogeneously dispersed because there was no Ti on the support that could concentrate the amine species and facilitate the homogeneous deposition on Ti-OH species. At pH > 6, the surface of the Ti-SBA-15 support became negatively charged due to deprotonation of most of the hydroxyl groups. In solution, the predominant Au species were $AuCl(OH)_3^-$ and $Au(OH)_4^-$. At this pH, the already coordinated $AuCl(OH)_2$ species will react with some possible free OH groups, resulting in the formation of a -O-AuCl(OH) complex (Scheme 3.3).

The $AuCl(OH)_3^-$ and $Au(OH)_4^-$ also can react with the remaining free OH groups on the surface to produce the -O-Au bonds (Scheme 3.3). Further increase in the pH can transform these species into $Au(OH)_3$. Previous studies of the deposition of gold on TiO_2 have shown decreased Au intake at pH 9 [26]. The presence of free hydroxyl groups and amine species on the surface of the Ti-SBA-15 will lead to an enhanced adsorption of the gold species starting at a low pH value when the hydroxyl groups are protonated. This increased adsorption will occur through electrostatic interaction with anionic Au species, creating a good, uniform adsorption of Au from the solution. When the pH is increased from 6 to 9, all species will be stabilized by chemical interaction with the support (Scheme 3.3). The enhanced activity of Au/Ti-N-n catalyst for the propene epoxidation reaction compared to that of the Au-Ti-G catalyst can be associated with the differences in size and dispersion and amount of the deposited Au nanoparticles. As determined from the detailed TEM measurements, the Au particles in the Au/Ti-N-30h catalyst had a number-weighted mean diameter of 2-3 nm, much smaller than that of the Au-G catalyst. Moreover, the differences in volume-weighted mean diameter, from 5 nm (Au/Ti-N-30h) to 15 nm (Au-Ti-G), clearly suggest that apart

from the low loading of Au present in Au-Ti-G catalyst, a large percentage of the Au atoms were catalytically inactive because they were inaccessible due to the large Au nanoparticles. It is noteworthy that changes in the Au dispersion/particle size between these types of catalysts were related to the different pretreatments of the support with NH_4NO_3. As demonstrated earlier, NH_4NO_3 pretreatment led to better Au adsorption and dispersion due to an increasing number of available adsorption sites at the Ti-SBA-15 surface. Examining the catalytic data in Table 3.1 for the Au/Ti-N-n (n= 6-30 h) pretreated with NH_4NO_3 for different times reveals the greatest propene oxide yield in the sample pretreated for 30 h (Au/Ti-N-30h). Because all samples contained the same amount of Au, the difference in activity can be attributed to better dispersion of the gold particles on the support due to the increased number of adsorption sites. UV-Vis DRS spectra of the Ti-SBA-15 supports found titanium also as extra-framework octahedral species. This type of titanium species, known to be responsible for side reactions in propene epoxidation, can be partially removed during NH_4NO_3 pretreatment. Increasing the pretreatment time will then further decrease the amount of these extra-framework Ti species, resulting in an increased propene oxide yield.

3.5. Conclusions

The pretreatment of Ti-SBA-15 with NH_4NO_3 before Au immobilization was found to enhance both the gold loading and dispersion. The resulting catalyst materials have enhanced activity in the direct epoxidation of propene with H_2 and O_2 compared with untreated Au/Ti-SBA-15. The main effect of the NH_4NO_3 pretreatment is related to an increased number of Au adsorption sites at the Ti-SBA-15 surface. This can be explained by the cooperative effect between an increasing number of hydroxyl groups formed by a partial hydrolysis of the ≡Si–O–Si≡ or ≡Ti–O–Si≡ bonds in the Ti-SBA-15 support material and the concentration of amine species in the proximity of Ti sites.

References

1. B. Taylor, J. Lauterbach, W.N. Delgass, Appl. Catal. A: General, 291 (2005) 188.
2. L. Cumaranatunge, W.N. Delgass, J. Catal., 232 (2005) 38.
3. E.E. Stangland, K.B. Stevens, R.P. Andres, W.N. Delgass, J. Catal., 191 (2000) 332.
4. C. Qi, T. Akita, M. Okumura, K. Kuraoka, M. Maruta, Appl. Catal. A: General, 253 (2003) 75.
5. M. Haruta, Catal. Today, 36 (1997) 153.
6. N. Yap, R.P. Andres, W.N. Delgass, J. Catal., 226 (2004) 156.
7. D. Zhao, J. Feng, Q. Huo, N. Melosh, B.F. Chmelka, G.D. Stucky, J. Am. Chem. Soc., 120 (1998) 26024.

8. X. Gao, S.R. Bare, J.L.G. Fierro, M.A. Banares, I.E. Wachs, J. Phys. Chem. B, 102 (1998) 5653.
9. A.H. Janssen, C.-M. Yang, Y. Wang, F. Schüth, A.J. Koster, K.P. de Jong, J. Phys. Chem. B., 107 (2003) 10552.
10. H. Friedrich, J.R.A. Sietsma, P.E. de Jongh, A.J. Verkleij, K.P. de Jong, J. Am. Chem. Soc., 129 (2007) 33.
11. U. Ziese, K.P. de Jong, Appl. Catal. A: General, 260 (2004) 71.
12. K.S.W. Sing, D.H. Everett, R.A.W. Haul, L. Moscow, R.A. Pierotti, J. Rouquerol, T. Siemieniewska, Pure Appl. Chem., 57 (1985) 603.
13. P. Van Der Voort, P.I. Ravikovitch, K.P. De Jong, M. Benjelloun, E.A. Van Bavel, H. Janssen, A.V. Neimark, B.M. Weckhuysen, E.F. Vansant, J. Phys. Chem. B, 106 (2002) 5873.
14. P. Van Der Voort, P.I. Ravikovitch, K.P. de Jong, A.V. Neimark, A.H. Janssen, M. Benjelloun, E. Van Bavel, P. Cool, B.M. Weckhuysen, E.F. Vansant, Chem. Commun., (2002) 1010.
15. G. Ricchiardi, A. Damin, S. Bordiga, C. Lamberti, G. Spano, F. Rivetti, A. Zecchina, J. Am. Chem. Soc., 121 (2001) 11409.
16. S. Bordiga, S. Coluccia, C. Lamberti, L. Marchese, A. Zecchina, F. Boscherini, F. Buffa, F. Genoni, G. Leofanti, G. Petrini, G. Vlaic, J. Phys. Chem., 98 (1994) 4125.
17. D. Trong On, S. Nguyen, V. Hulea, E. Dumitriu, S. Kaliaguine, Micropor. Mesopor. Mater., 57 (2003) 169.
18. M.C. Daniel, D. Astruc, Chem. Rev., 104 (2004) 239.
19. C.A. Fyfe, G.C. Gobbi, G.J. Kennedy, J. Phys. Chem., 89 (1985) 277.
20. Z. Luan, H. He, W. Zhou, J. Klinowski, J. Chem. Soc., Faraday Trans., 94 (1998) 979.
21. L. Marchese, E. Gianotti, V. Dellarocca, T. Maschmeyer, F. Rey, S. Coluccia, J.M. Thomas, Phys. Chem. Chem. Phys., 1 (1999) 585.
22. R.J. Matyi, L.H. Schwartz, J. B. Butt, Catal. Rev. Sci. Eng., 29 (1987) 41.
23. R. Zanella, L. Delannoy, C. Louis, Appl. Catal. A: General, 291 (2005) 62.
24. F. Moreau, G.C. Bond, A.O. Taylor, J. Catal., 231 (2005) 105.
25. P. Inego, G. Aprile, M.D. Serio, D. Gazzoli, E. Sactacesaria, Appl. Catal. A: General, 178 (1999) 97.
26. G.C. Bond, C. Louis, D.T. Thompson, "Catalysis by Gold – Catalytic science series Vol. 6", Ed. G.J. Hutchings, Imperial College Press, London (2006).

Chapter 4

Propene adsorption on Au nanoparticles during the propene epoxidation with H_2 and O_2: An in-situ XANES study

Abstract

The adsorption of propene on supported Au nanoparticles has been identified as a reaction step in the propene epoxidation with H_2 and O_2 by applying a detailed analysis of in-situ measured XANES spectra. For this purpose, Au/SiO_2 catalysts were investigated since this support is more inert and propene is not converted. Propene adsorption was investigated by using the hydrogen oxidation as a probe reaction. It was shown that co-feeding of propene dramatically decreased the hydrogen oxidation rate. Since it has been reported in the literature that the hydrogen oxidation occurs exclusively over Au nanoparticles, this inhibition by propene can be attributed to adsorption of propene on the Au nanoparticles. Delta-mu analysis of the in-situ XANES spectra confirmed the adsorption of propene on the Au and the mode of adsorption was determined to be π-bonding. Comparative experiments with ethene and propane confirmed this π-bonded adsorption, since ethene similarly inhibited the hydrogen oxidation, while propane had only a minor effect. Thus the strong adsorption of propene on Au nanoparticles was found to be in agreement with published work in which it was found that Au nanoparticles were activating propene to reactively adsorb on titania to produce a bidentate propoxy species.

4.1. Introduction

Au/TiO_2 catalysts are able to highly selectively (> 90%) epoxidize propene by using a mixture of H_2 and O_2 [1]. However, for these catalysts a few important issues have to be addressed. First of all, the conversion levels (typically < 2%), the hydrogen efficiency (< 30%), and finally the stability of the more active catalysts are usually low. The best system developed by Haruta et al. produces propene oxide at a propene conversion of 10%, but loses about 40% of its activity in 4 h [2]. A mechanistic understanding of this catalyst system can be of great help in the development of better catalysts, which do not suffer from these disadvantages. The common view in the literature, is that the gold–titania catalysts are bifunctional: Au nanoparticles produce a peroxide species, which is subsequently transferred to titanium sites, which use the peroxide to epoxidize propene [3,4-6]. Indeed, in the literature it has been demonstrated that Au nanoparticles can produce hydrogen peroxide [6-9] and that titanium based catalysts are highly effective in epoxidizing propene using hydrogen peroxide [10]. Haruta et al. detected the formation of Ti hydroperoxo/peroxo and superoxo species by using in-situ UV-Vis and EPR measurements during the propene epoxidation with H_2 and O_2 over a $Au/Ti{-}SiO_2$ (Ti/Si= 3:100) catalyst. On the other hand, these species could not be detected on Au/TiO_2 catalyst [8]. They concluded that the reaction mechanism on Au/TiO_2 and $Au/Ti\text{-}SiO_2$ can be different and that the formation of hydroperoxo species on tetrahedral Ti^{4+} sites in titanosilicate materials can be one of the fundamental differences. However, a complete mechanistic picture of this system is not yet available. Recently, Oyama et al. presented a mechanistic study using $Au\text{-}Ba/Ti\text{-}SiO_2$ catalysts for the gas-phase epoxidation of propene with H_2 and O_2. They showed by using in-situ UV-Vis and XANES spectroscopy the presence of Ti-hydroperoxo species. Futhermore, these species are reacting at the same rate as the overall rate of the reaction [11].

In the literature, Au is generally thought to only play a role in the formation of the peroxide species [3,8,12]. Nijhuis et al. published work based on FT-IR spectroscopy, which showed that Au has an additional role, namely, activating propene to adsorb on titania to produce a bidentate propoxy species [13,14]. How this activation occurs, is not clear, and furthermore, if this bidentate propoxy species is indeed a reaction intermediate or rather a spectator, is also unclear. In the work of Mul et al. [15], the bidentate propoxy species is assumed to be the main species responsible for the Au/TiO_2 and Au/TS-1 catalysts deactivation. In contrast Oyama, et al. showed by in-situ FT-IR during propene epoxidation with H_2 and O_2 over the $Au\text{-}Ba/Ti\text{-}SiO_2$ catalyst that bidentate propoxy species are only spectators and that these species are strongly adsorbed on a few Ti sites that would otherwise be involved in the formation of propene oxide [11]. Although it is not clear if this bidentate propoxy species is either an intermediate or deactivating species, both roles are of importance for the catalytic activity. The manner in which Au plays a role into the activation of

propene to form the bidentate propoxy species can be either by propene which is adsorbing on the Au nanoparticles or by Au influencing the behavior of neighboring titanium sites.

From the literature, it is not clear if propene adsorbs on Au under the reaction conditions used for the epoxidation. In the work of Campbell et al. [16] on the adsorption of propene on Au nanoparticles supported on titania, propene adsorption is observed at temperatures up to 27º C, which is in agreement with the report of Davis and Goodman [17], whom observed propene adsorption at Au(111) and (100) surfaces up to 77º C. It is important to note that Campbell et al. [16] observed that propene primarily adsorbs on the perimeter of the Au nanoparticles, also interacting with the titania support. Davis and Goodman [17] made a distinction in the adsorption of propene on clean and oxygen covered Au surfaces. On clean Au surfaces propene already desorbed at -73º C, while in the presence of O_2, the desorption was delayed up to 77º C. In this latter case, part of the 'propene' desorbed in the form of oxidation products. Friend et al. [18] studied the adsorption of propene on Au surfaces covered with atomic oxygen (created on the surface by ozone decomposition) and observed oxidized hydrocarbon species on the surface up to 227º C. In this study, however, the reactive atomic oxygen species towards propene, create stronger adsorbing species, similar to what Davis and Goodman reported. It is not known if during the propene epoxidation with H_2 and O_2 oxidized propene species will be formed on Au as well.

In this **Chapter**, the hydrogen oxidation over Au/SiO_2 catalysts is used as probe reaction to obtain a better understanding into the gold-titania epoxidation system. Au/SiO_2 catalysts were chosen in order to be able to investigate the interaction of hydrocarbons with the Au nanoparticles, without them being converted into propene oxide. A low reaction temperature of 80º C was used since it has been previously shown that such catalysts are only active for propene conversion at higher temperatures [14]. Catalytic experiments are performed and combined with in-situ XANES measurements. The effect of feeding propene, as well as ethene and propane for comparison, on the catalytic activity is investigated. The in-situ XANES spectra of Au are also investigated under reaction conditions in the presence and absence of these hydrocarbons. This will provide essential information about hydrocarbon (propene) adsorption on the Au nanoparticles and the role within the propene epoxidation reaction mechanism.

4.2. Experimental

4.2.1. Catalyst Preparation

Catalysts were prepared using two types of silica, Degussa OX50 (50 m^2/g) and Davisil 645 (Grace Davison, 295 m^2/g). A catalyst was also prepared on P25 titania (Degussa, 45 m^2/g). Au was deposited on the supports by means of a deposition-precipitation method using ammonia [3]. 10 gram of support was dispersed in 100 ml of demineralized water with a magnetic stirrer. The pH was raised to 9.5 by using 2.5% NH_4OH. The target loading in Au was 1 wt%, for which 172 mg of hydrogen tetrachloroaurate(III) solution ($HAuCl_4$, Aldrich, 30 wt% solution) was diluted in 40 ml of demineralized water and added gradually over a 15 min period to the support slurry, while keeping the pH between 9.4 and 9.6 by periodically adding NH_4OH. After addition of all the Au, the solution was stirred for 1 more hour after which it was filtered and washed 3 times with 200 ml of demineralized water. The yellow catalyst was dried overnight in air at 80º C and then calcined. Calcination was carried out by heating to 120º C (5º C/min heating) for 2 h followed by 4 h at 400º C (5º C/min heating and cooling). The thus obtained catalysts had an intense dark color (brown-red for the Davisil and salmon pink/red for OX50).

4.2.2. Catalyst characterization

The Au particle size and distribution on the catalysts were determined by using the SEM and TEM micrographs, both before and after use in catalytic experiments. XRF analysis was used to determine the Au loading on the catalysts and the presence of contaminants affecting the activity (e.g., chloride).

4.2.3. Catalyst activity testing

A flow reactor was used to determine the catalytic performance of the different catalysts. The experiments were carried out with typically 0.30 g of catalyst and a gas flow of 50 Nml/min (GHSV 10,000 h^{-1}). A flow was used containing 5 vol% of H_2 and 5 vol% of O_2. Hydrogen oxidation experiments were performed with lower hydrogen and oxygen concentrations than is typically used for the epoxidation of propene with H_2 and O_2 to avoid operating too close to the explosion limits, which for hydrogen are lower compared to when no propene is present. Optionally ethene, propene or propane was added in an amount of 5 vol%. The pressure in the reactor was 1100 mbar. The analysis of the gas leaving the reactor was carried out using an Interscience Compact GC system, equipped with a Molsieve 5A and a Porabond Q column, each with a thermal conductivity detector (TCD). Gas samples were analyzed every 3 min. To make sure the catalyst was in a well defined state prior to the experiments, the catalysts were heated for 60 min at 300º C (10º C/min) in a 50 ml/min gas stream consisting of 10% of O_2 in He. In prior work [13,14,19], it

was determined that this treatment could restore the catalyst activity, even if it was deactivated during epoxidation experiments. The experiments performed with only the SiO_2 support material did not show any catalytic activity for either the propene epoxidation or the hydrogen oxidation. The catalytic tests were performed in a fully automated set-up over a period of typically 5-10 days during which multiple reaction conditions were applied, including repeat conditions to verify for catalyst deactivation.

4.2.4. In-situ X-ray absorption spectroscopy

XAFS measurements were performed to evaluate if there were any changes in the Au particles during reaction. These measurements were performed on the Au L_{III}- edge (11.9187 keV) and were carried out on beam station BM26A at the ESRF. The measurements were performed in fluorescence mode using a multi-element Ge detector for the OX50 supported catalysts and in transmission mode using gas filled ion-chambers including a monitor in order to correct for any variation in energy, for the Davisil supported catalysts. The measurements with the OX50 catalyst were performed in fluorescence mode, since the X-ray signal through the sample was too low to be reliably measured. In the experiments a 200 mg sample was loosely pressed to form a self-supporting wafer/bed mounted in a specialized cell for recording in-situ XAFS data. The XAFS spectra (R-space up to 15 Å) were recorded in normal scanning mode (ca. 40 min/spectrum) over a 48-h period under conditions comparable to those used for the catalytic activity tests (i.e. reaction temperature 80º C, gas composition 6 vol% H_2, 6 vol% O_2 and optionally 6 vol% hydrocarbon, remainder He). XAFS data were processed using an in-house developed Matlab code. As with standard XAFS processing software the data was first converted into energy *vs* absorption coefficient. The pre-edge was subtracted and the signal normalized to the post-edge background extrapolated to the edge position.

4.3. Results

4.3.1. Catalyst characterization

XRF analysis showed that the amount of chlorine present on the catalysts was below the detection limit of the system (< 6 ppm). The gold loading of the catalysts was very close to the target loading of 1 wt% for the prepared catalysts (between 0.9 and 1 wt%). Table 4.1 gives the particle sizes for the prepared catalysts after calcination and after use in catalytic experiments (> 150 h). It can be seen that the Au particle size is similar for both silica supports and that during the catalytic experiments there is no significant change in the Au particle sizes.

Table 4.1.Overview of the sizes of Au nanoparticles and related errors (95% confidence limits) of the catalyst materials.

Catalyst	State	Average size (nm)	Error (std. dev.)	Particles counted
Au/SiO_2 (OX50)	Fresh	4.0	0.2 (1.8)	233
	Spent	3.7	0.2 (1.5)	238
Au/SiO_2 (Davisil)	Fresh	3.5	0.3 (1.5)	86
Au/TiO_2 (P25)	Fresh	3.9	0.1 (1.1)	236
	Spent	4.2	0.2 (1.2)	127

The EXAFS spectra recorded of the catalysts during the reaction did not change, indicating that the state of the bulk of the Au atoms remained the same. The Fourier transforms of the EXAFS spectra contained only contributions of the Au-Au interactions (indicating only metallic gold being present) with a typical first shell coordination number of 10. The Au particle size, which could be estimated from the Au coordination in EXAFS, was found to be in agreement with the TEM results (typically 30% smaller).

4.3.2. Catalytic testing

Figure 4.1 shows the activity of the catalyst for the hydrogen oxidation. It can be seen that in the first part of the experiment after an initial activation the catalytic activity remains constant. The time it takes for the catalyst to reach about 80% of its final activity is about 30 min, which is considerably longer than the experimentally determined response time of the system to changes in the gas feed (less than 2 min). The hydrogen oxidation activity for the catalysts prepared supported on the two different types of silica (OX50 and Davisil 645) was identical. Once propene is co-fed to the catalyst, the hydrogen oxidation rate drops dramatically by a factor of 3. Propene is not converted as far as it could be determined by GC analysis of the gases leaving the reactor. Once propene is removed from the gas feed, the catalytic activity of the hydrogen oxidation recovers slowly. Comparable experiments were also performed for the hydrogen oxidation in which either ethene or propane was co-fed. Neither of the hydrocarbons was converted. For ethene, it was observed that the hydrogen oxidation dropped similarly as for propene. The activity recovery after ethene removal was considerably slower than for propene. For propane, the decrease in the catalytic conversion that could be observed was significantly less, approximately 25%. Furthermore, the catalytic activity is recovered about 4 h after the removal of the propane. Duplicate experiments were performed, which showed that for each of the hydrocarbons the extent of hydrogen oxidation inhibition was reproducible quantitatively with an identical rate of activity recovery after the hydrocarbon was removed.

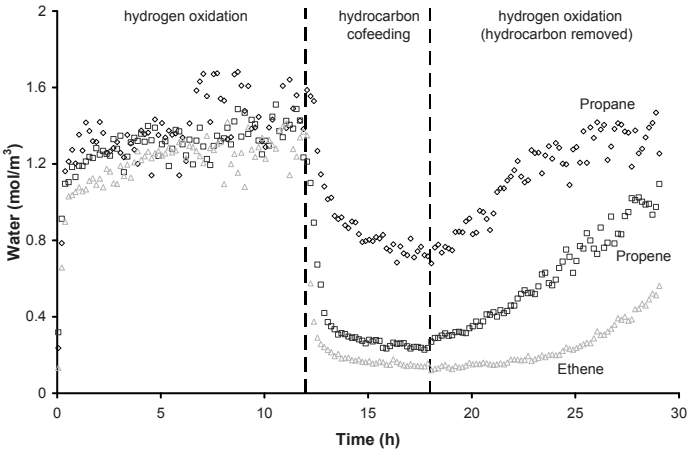

Figure 4.1. Water formation rate (as water concentration in gas phase) in hydrogen oxidation over 1 wt% Au/SiO_2 (Davisil 645) catalyst at 80° C (GHSV= 16000 h^{-1}). From 12-18 h into the experiment a hydrocarbon is co-fed in the gas phase (propane, propene, or ethene). (P= 1100 mbar, 5% H_2, O_2, hydrocarbon in He).

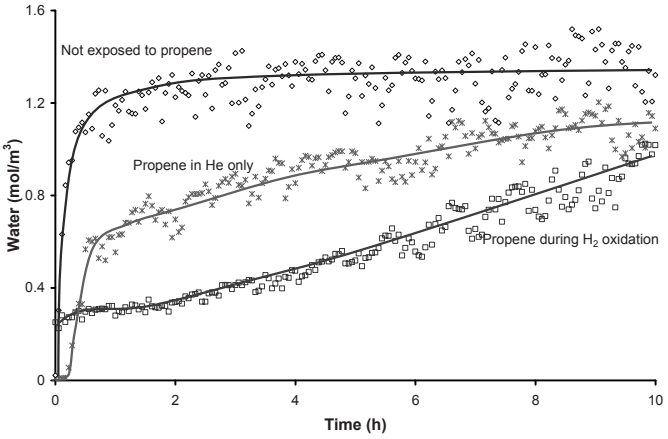

Figure 4.2. Water formation rate (as water concentration in gas phase) in hydrogen oxidation over a 1 wt% Au/SiO_2 (Davisil 645) catalyst at 80^0 C (GHSV= 16000 h^{-1}). An experiment is shown in which a fresh catalyst is used, and experiment in which a fresh catalyst is exposed to propene (5% in He at 80° C) for 6 h prior to the hydrogen oxidation, and an experiment in which before the experiment shown propene has been feed to the catalyst during the hydrogen oxidation for 6 h. (P= 1100 mbar, 5% H_2, O_2, hydrocarbon in He).

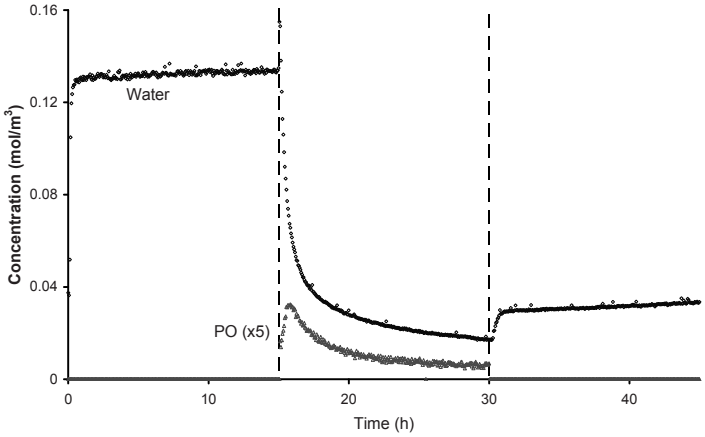

Figure 4.3. Water and propene oxide formation rate (as concentration in gas phase) in hydrogen oxidation over 1 wt% Au/TiO_2 (P25) catalyst at 50º C (GHSV= 16000 h^{-1}). In the first and final part of the experiment only the hydrogen oxidation is performed (no propene present). From 15-30 h into the experiment propene is co-fed in the gas phase and propene oxide is produced. (P= 1100 mbar, 5% H_2, O_2, hydrocarbon in He).

4.3.3. *X-ray absorption spectroscopy*

In Figure 4.4 the in-situ XAFS spectra recorded during an experimental series of a hydrogen oxidation over a Au/SiO_2 (Davisil 645) catalyst with intermediate propene co-feeding are shown. It can be seen that in the 'raw' XAFS spectra no significant changes can be observed in the spectra during the entire experiment. This indicates that even though during the reaction the catalytic activity of the Au particles is changing significantly, neither the oxidation state (metallic Au *vs* cationic) nor the size of the particles is changing significantly. In Figure 4.5, the delta-mu XANES spectra are shown of the catalyst during this activation phase. In a delta-mu XANES spectrum [20], the changes in the XANES region of the spectrum are made more pronounced by subtracting a reference spectrum of the same catalyst, usually recorded on the same sample in the same experimental run but under different conditions.

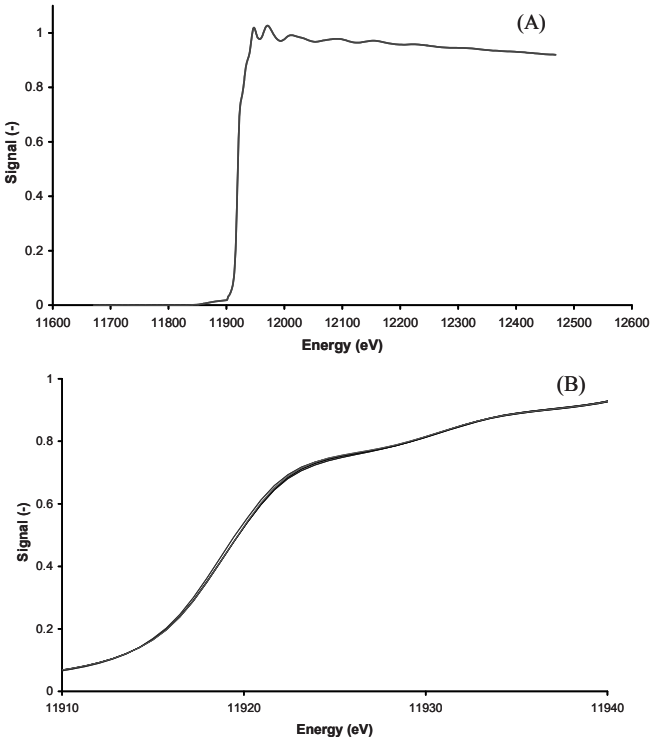

Figure 4.4. (A) XAFS Spectra of Au/SiO_2 (Davisil 645) catalysts in He over the entire recorded range from 11650 to 12500 eV. (B) Magnification of the edge region (11910-11940 eV) of the XAFS spectra in He, during the hydrogen oxidation, during propene co-feeding in hydrogen oxidation, and after propene removal in hydrogen oxidation (curves overlapping).

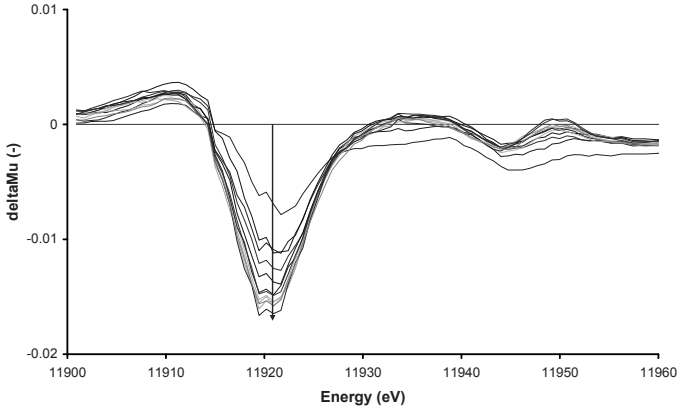

Figure 4.5. Development of features in delta-mu XANES spectrum of the Au L_{III}- edge of a Au/SiO_2 (Davisil 645) catalyst during the activation in the hydrogen oxidation reaction. The first spectrum (horizontal line) He spectrum is used as a starting position. Spectra thereafter are collected after 50 min interval for each spectrum.

The delta-mu spectra shown in Figure 4.5 are the spectra recorded with the starting spectrum (the catalyst in He) as a reference subtracted. It can be seen that the delta-mu XANES spectrum slowly develops a feature at 11920.2 eV. The intensity of this developing feature increases together with increasing catalytic activity as shown in Figure 4.5. An explanation of this feature can be given by a small shift of the edge position of 0.15 eV to a higher energy. In another experimental series measured earlier at the same beamline but recorded on the Au on OX50 silica catalyst in fluorescence mode (not shown) this shift was determined to be 0.2 eV. This shift is very small considering the energy resolution of the beamline of 0.8 eV. However, the shift is occurring over a wide range of data points and can therefore still be determined accurately numerically. Furthermore, the feature only starts to develop from the moment the H_2/O_2 feed is initiated and the development is gradual, which further supports the validity of the observation. The simultaneous measurement of a Au reference foil, placed in the beam after the sample and before a third detector (monitor) eliminates the possibility that such changes are caused by either a 'drift' in the energy calibration of the beamline.

In Figure 4.6 the delta-mu spectra are shown during the hydrogen oxidation experiment when propene is co-fed. In this figure, the XANES spectra of the catalysts in its steady state condition during the hydrogen oxidation are used as the reference.

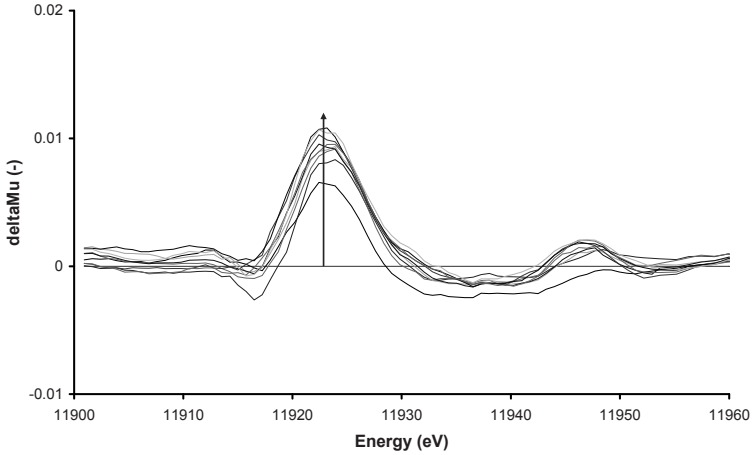

Figure 4.6. Development of features in delta-mu XANES spectrum of the Au L_{III}- edge of a Au/SiO_2 (Davisil 645) catalyst during the co-feeding of propene during the hydrogen oxidation reaction. The first spectrum (horizontal line) is the steady state spectrum during the hydrogen oxidation, which is used as a starting position (reference). Spectra thereafter are collected after 50 min interval for each spectrum.

It can be seen that in the presence of propene, a feature is appearing at 11922.4 eV, attributable to the appearance of a whiteline in the XANES spectrum. When propene is removed

from the gas-phase, this feature disappears after about 1 h. The location of this feature is over 2 eV above the edge position and again can not be explained by any shift in the position of the adsorption edge.

In Figure 4.7 the delta-mu spectra are shown for the developed feature after exposure of the Au catalyst to ethene, propene and propane. It can be seen that the features for propene and ethane are very similar. For propane, the feature is much less intense and the position is slightly shifted.

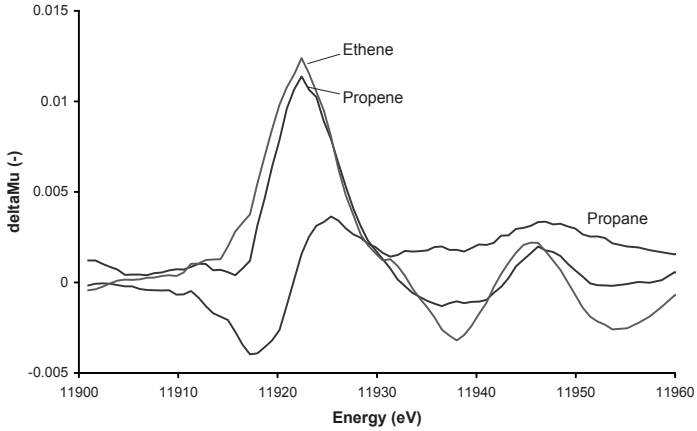

Figure 4.7. Delta-mu XANES spectra of the Au L_{III}- edge of a Au/SiO_2 (Davisil 645) catalyst during the co-feeding of propene, propane, and ethene during the hydrogen oxidation reaction. The steady state spectrum during the hydrogen oxidation prior to the hydrocarbon feeding was used as a starting position (reference).

4.4. Discussion

4.4.1. Catalytic data

In the catalytic experiments, it can be seen that the hydrocarbons containing a double bond, strongly inhibit the hydrogen oxidation over Au. Propane co-feeding only has a minor effect on the reaction rate. The most likely conclusion from these observations is that the hydrocarbons adsorb on the Au nanoparticles via an interaction with their double bond. The fact that no other reaction products other than water are observed is a clear indication that the hydrocarbon adsorption occurs via a reversible (physical) adsorption on the Au particles. Given the extent of the inhibition on the hydrogen oxidation rate, and the time it takes until the catalytic activity is restored from the moment the hydrocarbon co-feeding is stopped, this implies that the hydrocarbon adsorption is strong. If one compares the behaviour of a Au/TiO_2 catalyst exposed to a similar reaction cycle (Figure 4.3), it can be seen that the inhibiting effect of propene on the hydrogen oxidation is very similar. However, during the propene co-feeding (when the epoxidation also occurs) the catalyst deactivates

significantly. The propene oxide formation decreases and the water formation rate decreases even further. This type of deactivation is commonly observed for gold-titania epoxidation catalysts [3,19]. Upon removal of the propene from this catalyst, the hydrogen oxidation rate undergoes only a minor recovery after which the activity remains at a much lower level, indicating that in this case a deactivating species remains on the catalyst. The catalyst activity can be fully restored by a simple treatment at 300º C in 10% O_2 in He for 30 min. This proves that the deactivation is not caused by an irreversible change to the catalyst itself (e.g., sintering of the Au particles), but rather by the formation of a hydrocarbon related deactivation product. In the literature, this species is usually attributed to either propene oxide oligomers [3,4] or carbonates formed out of consecutive oxidation of propene oxide [13,19]. Although the inhibiting effect by ethene and propene is reversible, the fact that the hydrogen oxidation activity is not restored to its original level even after over 10 h of continued hydrogen oxidation after the hydrocarbon is removed, indicates that the inhibition occurs by more than a simple physical adsorption. Attempts to determine the presence of the adsorbed species by infrared spectroscopy so far were unsuccessful. After removal of the hydrocarbon, no adsorbed species could be detected on the catalyst. In the presence of the hydrocarbon, the intensity of the signal from the gaseous hydrocarbon was too strong to allow the observation of adsorbate species. In Figure 4.2, it is seen that the inhibiting effect of exposing the catalyst to propene only on the hydrogen oxidation activity is less strong than in the case when propene is co-fed during the hydrogen oxidation. A possible explanation for this might be that during the hydrogen oxidation reactive peroxo species are present on the Au nanoparticles, which would convert part of the adsorbed propene to even stronger adsorbed partially oxidized species. However, we could not prove this assumption by spectroscopic (FT-IR or XAFS) data, which would imply that the amount of such a species on the catalyst would be very low.

4.4.2. Delta-mu XANES analysis

The delta-mu XANES analysis has been principally exploited by Ramaker et al. [20] in order to interpret subtle changes in the XANES spectrum, which can be the result of the adsorption of species on small metal particles. Recently, van Bokhoven et al. [21] performed a delta-mu XANES analysis on Au/TiO_2 catalysts for the CO oxidation reaction. In this work they reported the appearance of a positive feature in the delta-mu XANES spectrum at 11920 eV when their catalyst was exposed to oxygen only, which was interpreted in terms of the formation of an activated Au-O complex on the reducible support. In our work, we observe a negative peak in the delta-mu XANES at the same position (Figure 4.5). The appearance of this negative peak during the 'activation phase' of the hydrogen oxidation, however, needs an alternative explanation. In the work of Guzman and Gates [22,23] the activity of Au-catalysts for CO oxidation is linked to the presence of cationic Au

species. A slight shift of the Au edge to a higher energy, our explanation for the negative peak in the delta-mu XANES at 11920 eV, is in agreement with the presence of an initially small amount of oxidized (positively charged) Au species being reduced. Costello et al. [24] reported on the shifting Au edge upon reduction of a Au-catalyst. Guzman and Gates [22,23] found a direct link between the catalytic activity for the CO oxidation and the presence of cationic Au in the nanoparticles, which indicates how a slight shift in the overall oxidation state can have a large effect on the catalytic performance. Upon exposure of the catalyst during hydrogen oxidation to ethene or propene, a positive feature is appearing in the delta-mu XANES spectrum at 11922.4 eV. This feature is different from the negative one at 11920 eV that appeared during the 'activation phase' in the hydrogen oxidation and not just its reversal. In the work by van Bokhoven on the CO oxidation [21] an identical feature appeared at 11922.5 eV upon exposing the catalyst to CO. In this work this feature was explained by the back-bonding of the Au d band to the $2\pi^*$ molecular orbitals of CO reducing the density of d-states, making the 2p3/2–5d dipole transition allowed. In later work by van Bokhoven et al. [25], they observed a feature which is identical to our observation in Figure 4.6 upon exposing Au and Pt catalysts to ethene. According to theoretical references obtained using calculations with the FEFF8 program, they were able to attribute the spectrum to π-bonded ethene on Au or Pt. In our work, we observe this same delta-mu XANES spectrum when we expose our Au on SiO_2 catalyst to ethene or propene. This makes it possible to conclude that also under the reaction conditions used for the hydrogen oxidation over Au, both ethane and propene are bonding to the Au particles by means of $2\pi^*$-d backbonding, which explains why they both can have a strong inhibiting effect on the hydrogen oxidation. Since propane does not have a double bond, this molecule can not π-bond to Au, which explains why its inhibiting effect is significantly less and also why in the delta-mu XANES spectrum no strong features are visible. Since in the hydrogen oxidation over Au/SiO_2, we used identical conditions as they are used for the propene epoxidation over Au/TiO_2 catalysts, it can be assumed that also during the propene epoxidation with H_2 and O_2, propene will adsorb on the Au nanoparticles. In Figure 4.2 we noticed that the inhibiting effect of propene on the hydrogen oxidation is stronger when propene is co-fed during the hydrogen oxidation than when propene is fed to the catalyst in absence of H_2 and O_2. We assume therefore, that the inhibition might be partly by adsorbed propene and partly by a stronger adsorbing species produced by a partial conversion of the propene on the Au nanoparticles in the presence of H_2 and O_2. This assumption is in line with the fact that in the delta-mu XANES spectrum we see the feature disappearing at 11922.4 eV (attributed to propene adsorbed by π-bonding) in just over 1 h time. In Figure 4.2, we can also see that when we just expose the catalyst to propene, the catalyst recovers 50% of its final activity in less than 1 h time. We were not able to find evidence of a more strongly

adsorbing 'second' inhibiting species formed in the presence of propene, H_2, and O_2 in the delta-mu XANES spectra, which would indicate that such a species would be present on the surface of the Au nanoparticles only in very small amounts. Since we did not observe any changes in either the EXAFS or the XANES of the spectra before and 1 h after the exposure of the catalyst to propene during the hydrogen oxidation, we think it is unlikely the state of the Au nanoparticles itself has changed because of this exposure to propene.

4.4.3. Implications for relevance for propene epoxidation reaction mechanism

Nijhuis et al. have reported an FT-IR spectroscopic study on the (reactive) adsorption of propene on gold-titania catalysts [13,14]. They showed that in the presence of Au nanoparticles, propene could adsorb on titania producing a bidentate propoxy species, which is the same species formed upon adsorption of propene oxide on titania. This bidentate propoxy species was only formed in the presence of Au nanoparticles. No measurable adsorption of propene occurred in the absence of these nanoparticles. O_2 and or H_2 were not required to produce this species. Two explanations were offered for the formation of this species. The first option was that propene would adsorb on Au and in an activated adsorbed form would be transferred to TiO_2 for a reactive adsorption producing the bidentate propoxy species. The second option was that the Au nanoparticles would influence the state of the neighboring titanium atoms, making them more reactive towards propene to form a bidentate propoxy species. In this work, we observed the adsorption of propene on Au nanoparticles on an inert support. Therefore, our proposal for the formation of bidentate propoxy species is that this occurs via an adsorption of propene on Au, followed by a spillover to TiO_2. Therefore, we propose a second function of the Au nanoparticles, in addition to the commonly described peroxide formation over the Au nanoparticles out of H_2 and O_2 [9,26,27]. Since in this work we did not study the epoxidation itself, it can not yet be determined whether the bidentate propoxy species formed in this manner is a reaction intermediate [13,14] or the species responsible for catalyst deactivation [15].

4.5. Conclusions

Both propene and ethene were found to strongly inhibit the hydrogen oxidation rate over Au nanoparticle catalysts. By analysis using delta-mu XANES, it was determined that both propene and ethene are π-bonding to the Au particles. Propane adsorption was not observable in the XANES analysis, which is in agreement with the minor inhibiting effect that propane has on the hydrogen oxidation rate. The inhibition of (adsorbed) propene on the hydrogen oxidation is stronger when propene is exposed to the catalyst in the presence of both hydrogen and oxygen, in comparison to the inhibiting effect propene has when it is fed to the catalyst prior to the hydrogen oxidation. This

indicates that in the presence of H_2 and O_2 a small fraction of the propene might be converted to an even stronger adsorbing species, although this remains speculative, since we could not confirm the presence of this species using direct spectroscopic measurements. The adsorption of propene on Au nanoparticles under reaction conditions typical for the propene epoxidation with O_2 and H_2 can be a key step in the epoxidation reaction mechanism. This adsorption supports the observation reported earlier [13,14] that Au nanoparticles on titania can make propene reactively adsorb on titania to produce a bidentate propoxy species. The adsorption of propene on the Au nanoparticles, significantly reduces the direct water formation over Au catalysts, which is an undesirable competitive reaction during the propene epoxidation with O_2 and H_2.

References

1. T. Hayashi, K. Tanaka, M. Haruta, J. Catal., 178 (1998) 566.
2. A.K. Sinha, S. Seelan, S. Tsubota, M. Haruta, Angew. Chem. Int. Ed., 43 (2004) 1546.
3. T.A. Nijhuis, B.J. Huizinga, M. Makkee, J.A. Moulijn, Ind. Eng. Chem. Res., 38 (1999) 884.
4. E.E. Stangland, K.B. Stavens, R.P. Andres, W.N. Delgass, J. Catal., 191 (2000) 332.
5. C. Sivadinarayana, T.V. Choudhary, L.L. Daemen, J. Eckert, D.W. Goodman, J. Am. Chem. Soc., 126 (2004) 38.
6. J. Edwards, P. Landon, A.F. Carley, G.J. Hutchings, J. Mater., Res. 22 (2007) 831.
7. P. Landon, P.J. Collier, A.J. Papworth, C.J. Kiely, G.J. Hutchings, Chem. Commun., (2002) 2058.
8. B. Chowdhury, J.J. Bravo-Suarez, N. Mimura, J.Q. Lu, K.K. Bando, S. Tsubota, M. Haruta, J. Phys. Chem. B, 110 (2006) 22995.
9. T. Ishihara, Y. Ohura, S. Yoshida, Y. Hata, H. Nishiguchi, Y. Takita, Appl. Catal. A: General, 291 (2005) 215.
10. M.G. Clerici, G. Bellussi, U. Romano, J. Catal., 129 (1991) 159.
11. J.J. Bravo- Suárez, K.K. Bando, J.Lu, M. Haruta, T. Fujitani, S.T. Oyama, J. Phys. Chem. C, 112 (2008) 1115.
12. J.Q. Lu, X.M. Zhang, J.J. Bravo-Suarez, S. Tsubota, J. Gaudet, S.T. Oyama, Catal. Today, 123 (2007) 189.
13. T.A. Nijhuis, T. Visser, B.M. Weckhuysen, Angew. Chem. Int. Ed., 44 (2005) 1115.
14. T.A. Nijhuis, T. Visser, B.M. Weckhuysen, J. Phys. Chem. B, 109 (2005) 19309.
15. G. Mul, A. Zwijnenburg, B. van der Linden, M. Makkee, J.A. Moulijn, J. Catal., 201 (2001) 128.
16. H.M. Ajo, V.A. Bondzie, C.T. Campbell, Catal. Lett., 78 (2002) 359.
17. K.A. Davis, D.W. Goodman, J. Phys. Chem. B, 104 (2000) 8557.

18. X.Y. Deng, B.K. Min, X.Y. Liu, C.M. Friend, J. Phys. Chem. B, 110 (2006) 15982.
19. T.A. Nijhuis, B.M. Weckhuysen, Catal. Today, 117 (2006) 84.
20. A. Teliska, W.E. O'Grady, D.E. Ramaker, J. Phys. Chem. B, 109 (2005) 8076.
21. N. Weiher, A.M. Beesley, N. Tsapatsaris, L. Delannoy, C. Louis, J.A. van Bokhoven, S.L.M. Schroeder, J. Am. Chem. Soc., 129 (2007) 2240.
22. J. Guzman, B.C. Gates, J. Am. Chem. Soc., 126 (2004) 2672.
23. J. Guzman, B.C. Gates, J. Phys. Chem. B, 106 (2002) 7659.
24. C.K. Costello, J. Guzman, J.H. Yang, Y.M. Wang, M.C. Kung, B.C. Gates, H.H. Kung, J. Phys. Chem. B, 108 (2004) 12529.
25. E. Bus, D.E. Ramaker, J.A. van Bokhoven, J. Am. Chem. Soc., 129 (2007) 8094.
26. G.J. Hutchings, Chem. Commun., (2008) 1148.
27. A.M. Joshi, W.N. Delgass, K.T. Thomson, J. Phys. Chem. B, 109 (2005) 22392.

Chapter 5

The role of support oxygen in the epoxidation of propene over gold-titania catalysts investigated by isotopic transient kinetics

Abstract

Transient kinetic experiments were performed on gold-titania catalysts for the epoxidation of propene using hydrogen and oxygen to investigate the reaction mechanism. A 'classical' 1 wt% Au on TiO_2 catalyst was studied, as well as a 1 wt% Au on Ti-SBA-15 catalyst. Steady State Isotopic Transient Kinetic Analysis (SSITKA) experiments were performed to provide information on the types and quantities of adsorbate species present on the catalyst during reaction, as well as on possible reaction pathways. The isotopic transients take place on a time-scale of minutes, while the isotopic switch of the unreacted feed gases proceeds in a matter of seconds. These observations indicate a slow desorption of the products from the catalysts. Slow product desorption was also indicated by the amounts of adsorbate species that were calculated to be present on the catalysts. The aim of the study, to determine if support oxygen would be playing a role in the reaction mechanism, could not be determined conclusively. For the water produced as a side product, it could be determined that support oxygen is ending up in the water, however, this can be explained by an exchange after its formation. The amount of carbon containing adsorbates present on the catalyst is high and is indicating that product desorption is a limiting step and that most likely part of the Au is present in subnanometer particles, not visible by TEM.

5.1. Introduction

Gold-titania catalysts are bifunctional as both titanium oxide and Au need to be present to have an active epoxidation catalyst [1]. The general consensus in literature is that the primary role of the Au particles is to produce a peroxide species, which is thereafter used to epoxidize propene over a titanium site. This is supported by the fact that Au nanoparticle catalysts are capable to directly produce hydrogen peroxide [2-4]. In the liquid phase titanium-based catalysts, especially TS-1, are very efficient epoxidation catalysts using hydrogen peroxide as oxidant [5]. Using UV-Vis DRS [6] and XANES [7] it has indeed been observed for gold-titania catalysts that the peroxide species produced on the Au nanoparticles are transferred to titanium sites. In addition, Nijhuis et al. [1,8] observed that Au particles catalyzed the formation of partially oxidized species on the titania surface, namely the formation of bidentate propoxy species, even in the absence of gas phase oxygen. The formation of these species is explained in **Chapter 4**. Propene is adsorbing first on the Au nanoparticle, spillovers to titanium sites with the formation of the bidentate propoxy species. One thing is not clear so far, if these partially oxidized surface species are intermediates towards propene oxide or simply spectators or even deactivating species.

In this **Chapter**, the role of support oxygen in the propene epoxidation mechanism is investigated by using Steady State Isotopic Transient Kinetic Analysis [9,10]. In the SSITKA technique, a catalyst is used in a catalytic experiment under constant reaction conditions - ideally at steady state. At one point during the experiment, the feed is switched for an identical feed, but with one (or more) of the reactants substituted for the same reactant containing an isotopic version of one of the atoms in it. In this case, $^{18}O_2$ was used to substitute non-labeled $^{16}O_2$. By examining the time and rate at which the $^{18}O_2$ appears in the products, mechanistic information can be obtained and the amount of adsorbate species on the catalyst can be calculated. A big advantage of this technique is that the amount of adsorbate species determined, is the amount of species involved in the reaction mechanism, and does not include spectator species, as can be the case for spectroscopic techniques.

5.2. Experimental

SSITKA experiments were performed on two types of Au-catalysts. The first type consisted of 1 wt% of Au on TiO_2 (P25). The preparation and performance of this catalyst are discussed by Nijhuis et al. [1]. The second catalyst, a 1 wt% Au on Ti-SBA-15 catalyst (Si/Ti= 40, NH_4NO_3 treated for 30 h) is prepared according to the method described in **Chapter 3**. Both catalysts were run at their respective optimal reaction temperature (50º C for Au/TiO_2 and 150º C for Au/Ti-SBA-15) at which they have a comparable epoxidation activity.

The gas feed during the SSITKA experiment consisted of 10 vol% of C_3H_6, H_2 and O_2 in inert. Specifically, 30 ml/min Ar was fed with 5 ml/min C_3H_6 and 5 ml/min H_2 directly to the

reactor. In addition, 5 ml/min Ar together with 5 ml/min $^{16}O_2$ was feed to the reactor through a rapid switching valve. After running the reaction at constant conditions for 30 min, the gas feed going through the switching valve was exchanged for 5 ml/min $^{18}O_2$ with 5 ml/min Ne to determine the SSITKA transient for oxygen in the feed. The switch of a small amount of Ar for Ne was made to determine possible peak broadening of the pulse response due to the flow in the catalyst bed and the gas lines. The system is designed in such a manner that it is possible to instantly make a switch from one gas feed to another, without disturbances in pressure or flow. The SSITKA experiments were run for a total of 20 min using $^{18}O_2$, to limit the consumption of the expensive gas.

The product analysis was performed using both a mass spectrometer and a gas chromatograph-mass spectrometry (GC-MS) system. The mass spectrometer was used to scan all major m/z (mass over charge) values for the most relevant components, with a time resolution for each component of 2.5 s. The GC-MS system was equipped with a 16 position gas sampling valve. The sampling valve filled sample loops from the moment the isotopic switch was made until 20 min afterwards, initially with a 30 s interval, which was increased after each loop was filled. After all sample loops were filled, they were analyzed on the system. The analysis of the experiments was only performed in a quantitative manner with respect to the isotopic composition of the major products, propene oxide, carbon dioxide, and water. The system was not calibrated for the total quantitative amounts of the product. The quantitative performance of the catalysts tested using SSITKA was determined in a dedicated set-up, which is described in **Chapters 2** and **3**. By combining the catalytic performance of the catalysts with the isotopic composition for each of the products, a quantitative analysis of the surface species could be made.

5.3. Results

The characteristics of the system were evaluated by examining the response of Ne. Figure 5.1 shows the mass spectrometer response for Ne, measured at a higher rate. It can be observed that the gas composition switch travelling through the catalyst bed is complete in about 3 s. Broader transients measured during the catalytic experiments will be caused by physico-chemical phenomena; i.e., adsorption, reaction, and desorption at the catalyst surface. Figure 5.2 shows the transients during the epoxidation for propene oxide, water, and carbon dioxide during the epoxidation over Au/TiO_2. The isotopic transients for the products are very slow. The isotopic switch from $^{16}O_2$ to $^{18}O_2$ was made after 40 min of running the epoxidation, which is close to the point where the epoxidation rate is the highest (see Figure 5.3). For both water and carbon dioxide, even after 15 min, the primary isotopic ‘versions’ produced only contained ^{16}O.

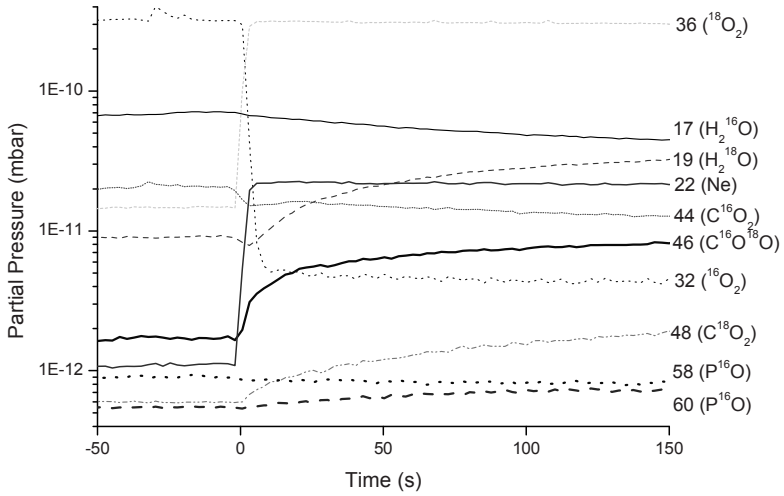

Figure 5.1. Example of SSITKA data recorded with a Mass spectrometer making the isotopic switch at t= 0. From the Ne signal, the peak broadening due to the catalyst bed/ system can be determined. Switch from $^{16}O_2$ to $^{18}O_2$ after running the propene epoxidation over a 0.3 g of 1 wt% Au/Ti-SBA-15 catalyst at 150º C for 40 min (50 Nml/min total flow rate, 10 vol% of H_2, O_2 and propene in Ar/Ne).

To evaluate if this very slow transient would be caused by a strong adsorption on the catalyst, or by a large pool of oxygen containing intermediates on the catalyst, an additional experiment was made in which over the same catalyst a SSITKA switch was performed from $^{12}CO_2$ to $^{13}CO_2$ (in Ar/Ne). This experiment is shown in Figure 5.4. The almost instantaneous switch shows that the delays observed in Figure 5.2 are not caused by adsorption on the catalyst of the CO_2 produced, but rather by a slow release/ production rate.

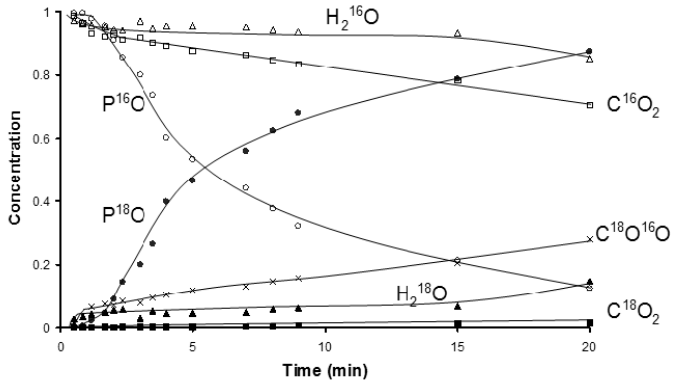

Figure 5.2. SSITKA transients for switch from $^{16}O_2$ to $^{18}O_2$ (at t= 0) after running the propene epoxidation over a 0.3 g of 1 wt% Au/TiO_2 catalyst at 50º C for 40 min (50 Nml/min total flow rate, 10 vol% of H_2, O_2 and C_3H_6 in Ar/ Ne).

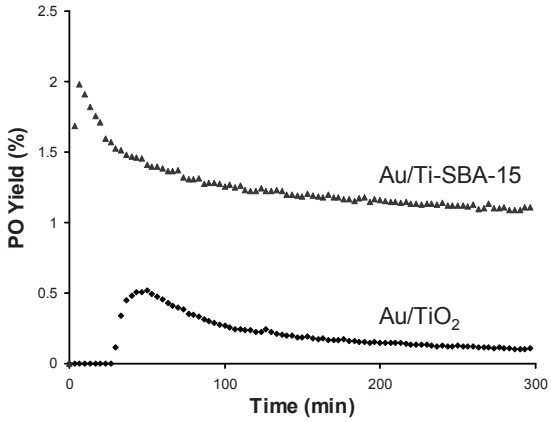

Figure 5.3. Catalytic performance of Au/TiO_2 (50^0 C) and Au/Ti-SBA-15 (150^0 C) catalysts at their optimal reaction temperature (1 wt% Au loading, 0.3 g catalyst, 50 Nml/min total flow rate, 10 vol% of H_2, O_2 and C_3H_6 in He, 1.1 bar).

The fact that in Figure 5.2 the amount of $C^{18}O_2$ produced after 15 min is still less than 1% of the CO_2 production, indicates that gas-phase oxygen does not play a direct role in the release of this product from the catalyst. Either carbonates are released slowly from the catalyst surface, or support oxygen is ending up on the CO_2 produced.

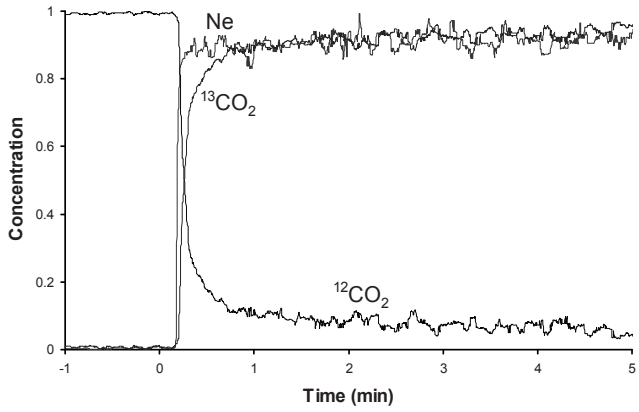

Figure 5.4. SSITKA response for a CO_2 isotopic switch over 0.5 g of 1 wt% Au/TiO_2 catalyst. Switch from $^{12}CO_2$ to $^{13}CO_2$ isotopes at t= 0, 50º C. Total flowrate 60 ml/ min, 2 vol% CO_2 in Ar (Ar/Ne after switch). CO_2 composition scaled to 1, Ne transient scaled from 0-1 for transient.

The isotopic transients for the Au/Ti-SBA-15 catalyst are shown in Figure 5.5. It can be observed that for this catalyst, the transients are a lot faster than for the Au/TiO_2 catalyst, but the transients are significantly longer than the actual gas switch breakthrough time of about 3 s. The SSITKA

switch for the Au/Ti-SBA-15 catalyst was similarly as for the Au/TiO_2 catalyst made after operating it in the epoxidation for 40 min. At this moment the activity of the catalyst was constant.

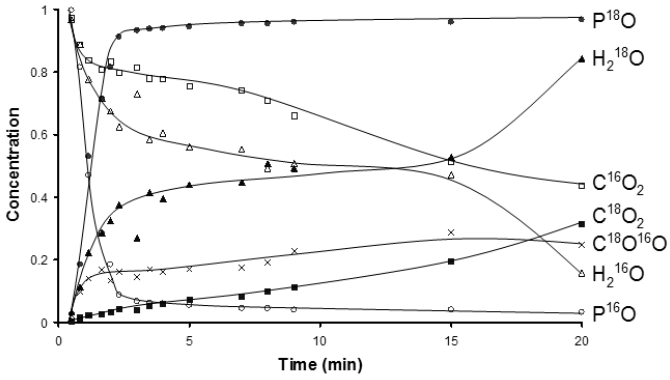

Figure 5.5. SSITKA transients for switch from $^{16}O_2$ to $^{18}O_2$ (at t= 0) after running the propene epoxidation over a 0.3 g of 1 wt% Au/Ti-SBA-15 catalyst at 150º C for 40 min (50 Nml/ min total flow rate, 10 vol% of H_2, O_2 and propene in Ar/ Ne).

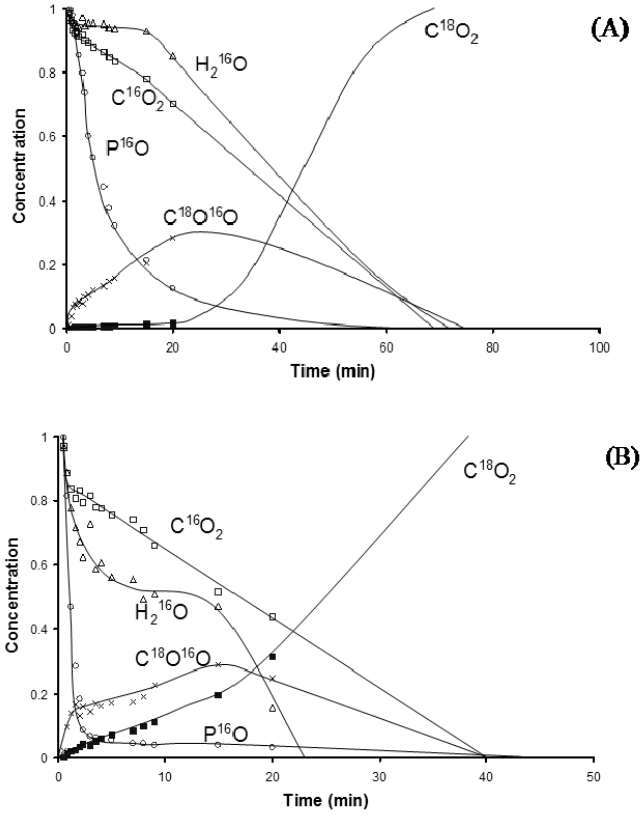

Figure 5.6. Extrapolated SSITKA responses for the experiments shown in Figures 5.2 and 5.5, used for the determination of the amounts of adsorbates on the catalysts. A) Au/TiO_2 catalyst (Figure 5.2) and B) Au/Ti-SBA-15 catalyst (Figure 5.5).

5.4. Discussion

The isotopic transients for the products in the epoxidation over the Au/TiO_2 and the Au/Ti-SBA-15 catalysts are slow. This can be explained in two ways. A first explanation is that the reaction products are produced on the catalyst surface and only desorb slowly. A second explanation is that the oxygen fed in the gas phase does not directly appear in these products, but is converted first into a different oxidizing species (e.g. a hydroperoxide), which has a significant retention / coverage on the catalyst surface. For the carbon dioxide produced, which contains two oxygen atoms, we can draw one further conclusion from the experiments. Since a large quantity of single labeled carbon dioxide is produced over a longer time, this implies that it is formed in a two-step oxidation. After the SSITKA switch, single labeled CO_2 is produced almost instantaneously, even faster than ^{18}O containing propene oxide. This indicates that a partially oxidized species is oxidized further either directly from oxygen in the gas phase, or from a rapidly formed oxidizing surface species (adsorbed atomic oxygen, adsorbed molecular oxygen, or a peroxo species). The fact that for a long time $C^{16}O_2$ is the dominant type of carbon dioxide indicates that in addition an adsorbed CO_2 precursor, which does not need further oxygen to be provided for its production, is also present in a significant amount on the catalyst. Since CO_2 adsorption itself on the catalyst is only minor (Figure 5.4), a slow decomposition of a surface carboxylate species can be the explanation for this slow response. The fact that even while $C^{16}O_2$ is still the primary type of CO_2 produced, after 20 min for the Au/Ti-SBA-15 catalyst $C^{18}O_2$ is produced/released in a larger amount than single labeled $C^{16}O^{18}O$ is an indication that at least 2 routes are present producing carbon dioxide.

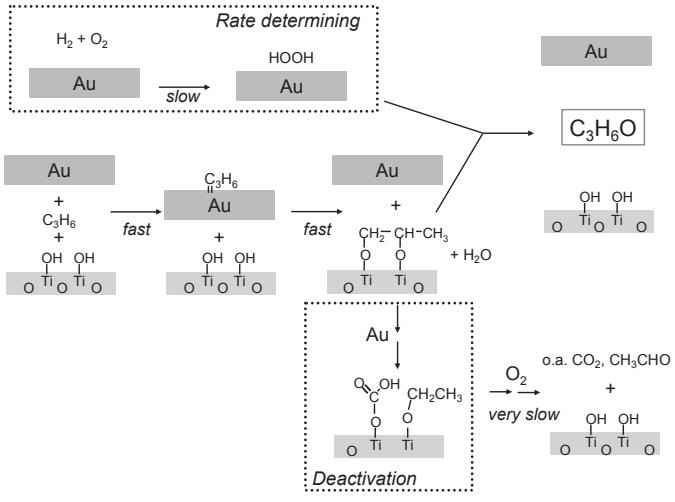

Scheme 5.1. Mechanism proposed for the epoxidation of propene over a gold-titania catalyst (adapted from Nijhuis and Wekhuysen [12]).

Considering the in-situ FT-IR studies and kinetic investigations reported by Nijhuis and Weckhuysen [12] and XANES results discussed in **Chapter 4**, we have proposed a reaction mechanism for the epoxidation of propene over gold-titania catalysts. This mechanism is shown in Scheme 5.1. In this scheme, the formation of a bidentate propoxy species on the catalyst support is occuring via the first the adsorption of propene on Au, followed by a spillover to titania as it was evidenced by XANES. The oxygen in this bidentate propoxy species was thought to be originating from the catalyst support. The main argument for this proposition is that the formation of this species was observed using FT-IR spectroscopy upon exposing a gold-titania catalyst to propene in the absence of oxygen in the gas phase [1,8]. The current observations are in agreement with this first step in the mechanism. Since the TiO_2 supported catalyst has a large amount of oxygen in the support available, the appearance of ^{18}O in the propene oxide support can be delayed for a long time. The Ti-SBA-15 supported catalyst only has a relatively small amount of reducible titania present, which explains why labeled oxygen appears a lot faster in the propene oxide produced. An additional explanation for this difference is a decreased adsorption strength of the bidentate propoxy species [12] when it is formed on a catalyst with titania dispersed on/in a silica support. In this case the bidentate propoxy species is only able to interact with one Ti-site, with the other 'leg' of the bidentate species binding to a Si. Deactivation of the catalyst, as well as formation of carbon dioxide, was explained by a consecutive oxidation of the bidentate propoxy species [1,8]. The oxidized species formed, would be strongly adsorbed on the catalyst and only desorb slowly. In the SSITKA experiments we do indeed observe that the isotopic transient for the titania supported catalyst is extremely slow. In the mechanism in Scheme 5.1, it can be observed that, as the C-C bond between the two legs of the bidentate propoxy species is broken in the route towards complete oxidation, two partially oxidized species are produced. The consecutive oxidation and desorption of these two species at different rates, can be the explanation for the minimum of two routes towards CO_2 formation that it was identified from the SSITKA.

For the titania supported catalyst, it is clearly visible that $H_2{}^{18}O$ is observed as a product prior to ^{18}O labeled propene oxide. This indicates that at least part of the water produced is a primary product, while propene oxide is not. This is in agreement with the common idea that first H_2O_2 is produced, which thereafter epoxidizes propene over a titanium site, and also with our proposed alternative route in which H_2O_2 (Scheme 5.1) is required for the reactive desorption of propene oxide from the catalyst. To do a more quantitative interpretation of the adsorbates playing a role during the reaction, we extrapolated the SSITKA transients to completion (i.e. a complete switch of the oxygen atoms in the products to oxygen-18). These extrapolated curves are shown in Figure 5.6. The area under these curves was determined, in this way providing a hold-up for the respective species on the catalyst. These hold-ups for the species on the catalysts are for actual

reaction intermediates and will not include spectator species, because of the nature in which SSITKA experiments are performed spectator species remaining inactive on the catalyst surface are not observed. The integrated areas under the extrapolated curves might have a relatively large error, since the extrapolations are just made 'by eye', but they will provide a good indication for the amount of these species. In Table 5.1, these areas are given.

Table 5.1. Integrated areas for the isotopic composition of ^{16}O containing products after the isotopic switch in the SSITKA experiments.

	Au/TiO_2	Au/Ti-SBA-15	
Propene oxide ^{16}O	8.0	2.0	min
$C^{16}O^{18}O$	16*	7.5	min
$C^{16}O_2$	40	20	min
$H_2{}^{16}O$	700*	15	min

- The accuracy of these values is lower due to the extrapolation made (possible error estimated to be up to 50% of this value)

Table 5.2. Catalytic data for both Au-catalysts and calculated amounts of adsorbate species using the catalytic data and the information provided in Table 5.1.

	Au/TiO_2	Au/Ti-SBA-15	
Temperature	323	423	K
Total flowrate	50	50	ml/min
Propene flow	5	5	ml/min
Propene flow	200	200	µmol/min
Conversion	0.5	1.5	%
Propene converted	1.0	3.0	µmol/min
PO selectivity	99	90	%
PO produced	1.0	2.7	µmol/min
CO_2 selectivity	1	10	%
CO_2 produced	0.01	0.9	µmol/min
Hydrogen efficiency	15	3	%
Water produced	6.6	90	µmol/min
PO adsorbed	**7.9**	**5.5**	µmol
CO_2 adsorbed – type 1 (precursor for $C^{18}O^{16}O$)	**0.48**	**7.1**	µmol
CO_2 adsorbed – type 2 (precursor for $C^{16}O_2$)	**2.4**	**36.0**	µmol
H_2O adsorbed	**4620**	**1360**	µmol

When a comparison is made between the amount of PO-16, which leaves the catalyst after the SSITKA switch (for both catalysts about 8 μmol), and the number of titanium sites on both catalysts (248 μmol for TiO_2 and 125 μmol for Ti-SBA-15), one can see that considerable more sites are available than the amount of propene oxide that is observed. However, for the epoxidation, both Au and Ti sites are a requirement. The number of Ti sites in the direct vicinity of a Au particle, assuming uniform spherical Au particles of 4 nm in size completely surrounded by Ti, is calculated to be 0.3 μmol, which is considerably lower. Possible explanations for the larger amount of PO-16 can be:

- Propene adsorbs after it is produced reversibly at other sites at the catalyst, not in the vicinity of a Au particle. This assumption is supported by thermogravimetrical adsorption experiments we published previously [1]. On P25 titania 1.5 wt% propene oxide adsorbs at 50º C (corresponding to 78 μmol for 0.3 g catalyst), of which 0.1 wt% adsorbs reversibly (5.1 μmol).
- The support provides oxygen for the epoxidation. This can only be the case for the TiO_2 support, since for Ti-SBA-15 only Ti is reducible, not Si. The number of reducible sites for Ti-SBA-15 is therefore by far insufficient.
- A large number of smaller Au particles, which could not be observed by TEM must be present. Small Au particles are indeed reported to be highly active in the epoxidation [13].

A supporting indication for this assumption is the fact that in EXAFS analysis of our catalysts (**Chapter 2**) we consistently obtained smaller average Au particle sizes for EXAFS compared to TEM. For the Au/TiO_2 catalyst, this was 1.5 nm compared to 4 nm. However, a Au particle of 1.5 nm still consists of about 100 atoms, which means that the amount of (reaction) sites in the neighborhood of Au particles will still not be sufficient to have been the sites where the PO-16 was adsorbed.

The amount of $H_2{}^{16}O$ released from the catalysts after the switch to $^{18}O_2$ needs different explanations for the two catalysts studied. For the TiO_2 supported catalyst, this amount of water is almost 20 times larger than the total number of sites available for the adsorption of water. The most likely explanation for this large amount of ^{16}O present in the water produced must therefore be that it is originating from the titania. It cannot be determined from these experiments, however, if the support oxygen ends up in the water when the water is produced, or if it is exchanging with the support afterwards (see Scheme 5.2). For rutile type titania this isotopic exchange of oxygen in water with support oxygen in the titania has been confirmed experimentally [14]. A similar exchange can be expected for the P25 support (85% anatase, 15% rutile) used in this study. For the Ti-SBA-15 supported catalyst, the specific surface area is considerably higher. For this catalyst, the

^{16}O containing water leaving the reactor after the SSITKA switch can either have been adsorbed physically or it can have been produced by an exchange with surface O or OH.

Table 5.3. Physical data on the Au-catalysts and calculated numbers of adsorption sites available.

	Au/TiO_2	Au/Ti-SBA-15	
Weight in reactor	0.300	0.300	g
Surface area	50	490	m^2/g
Surface area	15	147	m^2
Si/Ti ratio	-	40	-
Ti content	-	3.2	wt%
Ti sites[1]		125	µmol
Ti sites[2]	16.6	-	$\mu mol/m^2$
Si sites[2]		13.6	$\mu mol/m^2$
Ti sites	248		µmol
Si sites		2000	µmol
Au loading	1	1	wt%
Au in reactor	3	3	mg
Au particle avg. size	4	4	nm
Au atoms	15.2	15.2	µmol
Au particles[3]	7.7	7.7	nmol
Ti neighbor sites	0.31	0.31[4]	µmol

[1] Ti is deposited by grafting, it is therefore assumed that all Ti is on the surface
[2] based on bulk density of anatase and quartz, respectively
[3] assuming spherical particles
[4] assuming the Au particles only have Ti/O atoms as immediate neighbors. A circle equal to the particle diameter is taken for this site calculation

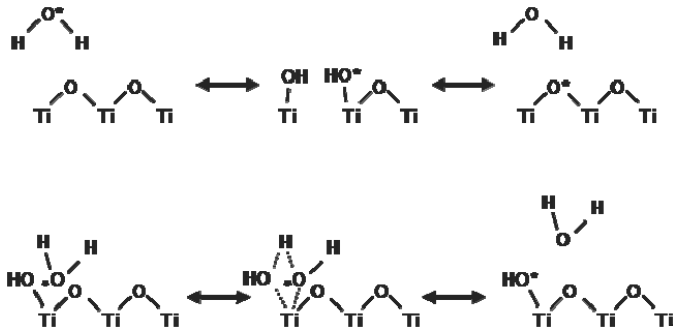

Scheme 5.2. Proposed mechanisms for exchange of oxygen in the water produced by the catalyst with oxygen from the support.

For CO_2 it can be observed from the SSITKA experiment shown in Figure 5.4 that the delay in response of the signal is primarily caused by a slow formation, rather than from a physical adsorption. It can also be observed that for the Ti-SBA-15 catalyst the exchange of oxygen from CO_2 produced with the support is minor. If such an exchange would be occurring at a significant rate, it would not be possible that $C^{18}O_2$ would be present in a larger concentration as a product than $C^{16}O^{18}O$ while $C^{16}O_2$ is still the primary product. As a consequence, the isotopic composition of the CO_2 as it is observed in the experiments must be identical or at least close to that of the isotopic composition released from the sites where it is produced.

The quantity of ^{16}O containing CO_2 liberated from the catalysts after the SSITKA switch is quite large, especially for the Ti-SBA-15 supported catalyst. To explain this, one needs to consider that the CO_2 response due to adsorption on the catalyst is only delayed very little (Figure 5.4) and that Au particles are responsible for the complete oxidation (no oxidation by the support itself) [1,15]. The 43 μmol of ^{16}O containing carbon dioxide that the Ti-SBA-15 supported catalyst produces after the SSITKA switch should therefore originate from reaction or adsorption sites near Au particles. The number of sites directly neighboring Au particles (taking the observed TEM particle size of 4 nm), however, is only 0.3 μmol (which assumes all sites are Ti sites, in reality a large number will be Si). Even if a larger perimeter would be taken than only the directly adjoining sites, this number will be considerably smaller than 43 μmol. It would be possible that these sites would contain adsorbed ^{16}O containing intermediates and that an exchange with the support oxygen would provide some more ^{16}O, however, since the Si of the support is not reducible and the amount of additional ^{16}O needed is quite significant, such an exchange is less likely to be a sufficient explanation. The most probable explanation is that apart from the visible 4 nm Au particles, also a large number of TEM invisible small Au particles are present, as is supported by our EXAFS data (**Chapter 2**). The TEM microscope used for the determination of the Au particle size has a lower detection limit for Au particles of approximately 1 nm in size. The EXAFS data, providing an averaged particle size for all Au atoms, indicate an average particle size of 1.0 nm. If one would hypothesize a bimodal distribution of 4 nm Au particles (TEM visible) and TEM invisible single Au atoms on the catalyst, one can calculate that about 1/3rd of the Au atoms would be present as single atoms on the catalyst (i.e. about 5 μmol), which will greatly increase the number of possible Ti neighboring sites and bring this more in agreement with the calculated number of adsorbates. Similar calculations can be done for small Au clusters. The catalytic activity of small 6-10 atom Au clusters was recently discussed by Ojeda and Iglesia [16] and Lee et al. [17]. For example, if one would assume the TEM 'invisible' Au would consist of 0.4 nm large 6 atom Au clusters [18], it can be calculated that about half of the Au present would be in the form of these 0.4 nm clusters (1.2 μmol). A larger amount of reaction sites on the catalyst for propene epoxidation and for complete

combustion explained by the presence of a large amount of small Au particles/single Au atoms, is therefore a feasible explanation.

A general remark is needed on the calculations of sites and adsorbate species that have been made. The catalysts used will almost certainly contain many different types of Au and Ti sites. In the calculations, we have lumped all these different sites together since we are not able to make a distinction between them from the experiments performed.

5.5. Conclusions

SSITKA experiments showed that the amount of reaction intermediates on the catalyst surface is very high for the Au/TiO_2 and Au/Ti-SBA-15 catalysts. The total amounts of adsorbates are of the same order of magnitude as the total amount of adsorption sites available on the catalyst, which indicates that product desorption is likely to be the rate limiting factor. This assumption is also supported by the slow isotopic transients that are observed. The main aim of this study was to determine if support oxygen plays a role in the formation of propene oxide. However, this question cannot be answered conclusively.

Carbon dioxide is produced via at least two different pathways. The amount of ^{16}O containing propene oxide produced after the SSITKA isotopic switch is larger than the calculated number of sites at which it is produced, which can be an indication that support oxygen is ending up in the product, however, strong but reversible propene oxide adsorption on the catalyst can also explain the delayed SSITKA response. Given the commonly accepted view that both the epoxidation and complete combustion only proceed near the Au particles on the support, the amount of ^{16}O containing propene oxide and carbon dioxide produced after the SSITKA switch indicates that the catalyst contains also a significant amount of sub-nanometer sized Au particles, providing additional reaction sites.

The amount of labeled oxygen in the water, which is produced as a co-product, is large. For the Ti-SBA-15 supported catalyst, this can be explained by water adsorption on the entire support, including the Si-OH sites. For the Ti-supported catalysts, the adsorbed amount is considerably larger than the available surface area for adsorption of water. For this catalyst, support oxygen must be ending up in the water produced, which can either happen by a role of support oxygen in its formation, or by an exchange with the support afterwards.

References

1. T.A. Nijhuis, T. Visser, B.M. Weckhuysen, J. Phys. Chem. B, 109 (2005) 19309.
2. J. Edwards, P. Landon, A.F. Carley, G.J. Hutchings, J. Mater. Res., 22 (2007) 831.

3. T. Ishihara, Y. Ohura, S. Yoshida, Y. Hata, H. Nishiguchi, Y. Takita, Appl. Catal. A: General, 291 (2005) 215.
4. P. Landon, P.J. Collier, A.J. Papworth, C.J. Kiely, G.J. Hutchings, Chem. Commun., (2002) 2058.
5. M.G. Clerici, G. Bellussi, U. Romano, J. Catal., 129 (1991) 159.
6. B. Chowdhury, J.J. Bravo-Suarez, N. Mimura, J.Q. Lu, K.K. Bando, S. Tsubota, M. Haruta, J. Phys. Chem. B, 110 (2006) 22995.
7. J.J. Bravo-Suarez, K.K. Bando, J. Lu, M. Haruta, T. Fujitani, S.T. Oyama, J. Phys. Chem. C, 112 (2008) 1115.
8. T.A. Nijhuis, T. Visser, B.M. Weckhuysen, Angew. Chem. Int. Ed., 44 (2005) 1115.
9. S.L. Shannon, J.G. Goodwin, Chem. Rev., 95 (1995) 677.
10. R.J. Berger, F. Kapteijn, J.A. Moulijn, G.B. Marin, J. De Wilde, M. Olea, D. Chen, A. Holmen, L. Lietti, E. Tronconi, Y. Schuurman, Appl. Catal. A: General, 342 (2008) 3.
11. T.A. Nijhuis, B.M. Weckhuysen, Catal. Today, 117 (2006) 84.
12. G. Mul, A. Zwijnenburg, B. van der Linden, M. Makkee, J.A. Moulijn, J. Catal., 201 (2001) 128.
13. B. Taylor, J. Lauterbach, W.N. Delgass, Appl. Catal. A: General, 291 (2005) 188.
14. T. Wu, W.E. Kaden, S.L. Anderson, J. Phys. Chem. C, 112 (2008) 9006.
15. J.Q. Lu, X. M. Zhang, J.J. Bravo-Suarez, S. Tsubota, J. Gaudet, S.T. Oyama, Catal. Today, 123 (2007) 189.
16. M. Ojeda, E. Iglesia, Chem. Commun., (2009) 352.
17. S. Lee, L.M. Molina, M.J. López, J.A. Alonso, B. Hammer, B. Lee, S. Seifert, R.E. Winans, J.W. Elam, M.J. Pellin, S. Vajda, Angew. Chem. Int. Ed., 48 (2009)1467.
18. J. Guzman, B.C. Gates, Nano Lett., 1 (2001) 689.

Chapter 6

Towards a reaction mechanism for the propene epoxidation with O_2 and H_2 over Au/Ti-based catalysts

Abstract

A comprehensive overview on mechanistic studies of the propene epoxidation with H_2 and O_2 over Au/Ti-based catalysts will be presented. This will be done by highlighting and comparing the various kinetic and as well spectroscopic studies available in the open literature in an attempt to arrive at a more general view on the nature of the active sites, related reaction intermediates and deactivation products. The chapter ends with some concluding remarks emphasizing the different challenges ahead of us in understanding this intriguing catalytic system.

6.1. Introduction

The propene epoxidation reaction with a mixture of O_2 and H_2 over Au/Ti-based catalysts is an active subject of research. A considerable effort has been made to understand the relationship between catalyst structure and performance. An improvement in the activity and stability of Au/Ti-based catalysts has been obtained by using microporous and mesoporous silicious supports with well-dispersed Ti instead of a pure TiO_2 support for the deposition of Au [1-9] as was for example shown in **Chapters 2** and **3** of this PhD thesis. The activity per amount of Au could be increased when a very low Au loading was deposited on these titanosilicate supports [10]. The explanation of the catalytic activity of Au is a subject of controversy, but the general agreement is that a major factor determining the catalytic activity is the size of the Au nanoparticles [1]. Nevertheless, the

fundamental reason for this particle size effect remains unresolved since a variation of the Au particle size also results in a variation of the Au-support contact area, which can induce possible electronic effects on the Au nanoparticles [11-13]. Furthermore, it is now accepted that both a titania-containing support and Au are important in generating a reasonable epoxidation activity. In this **Chapter**, the theoretical, kinetic and spectroscopic studies on the epoxidation of propene with H_2 and O_2 over Au/Ti-based catalysts in the open literature will be discussed together with our own characterization investigations in order to arrive at a better understanding of the active sites, the role of potential reaction intermediates and deactivation products as well as the related propene epoxidation mechanism. This will be done by subsequently discussing (a) the role of Au and TiO_2 in the propene epoxidation reaction; (b) highlighting the different kinetic and spectroscopic studies currently available; (c) the role of the Au/Ti interface; and (d) the proposed deactivation and reaction propene epoxidation mechanisms. The chapter ends with some concluding remarks emphasizing the different challenges ahead of us in understanding this intriguing catalytic system.

6.2. Role of Au and Ti in the propene epoxidation reaction

6.2.1. Formation of H_2O_2 from H_2 and O_2 on Au nanoparticles

One of the functions of Au in the epoxidation of propene with H_2 and O_2 over Au/Ti-based catalysts is the synthesis of H_2O_2. Experimentally, it has been shown that supported Au catalysts can be very selective for the formation of H_2O_2 from H_2 and O_2 mixtures. The group of Hutchings reported for the first time that Au deposited on supports, such as Al_2O_3 and ZnO, is active for the synthesis of H_2O_2 [14]. At 2º C and 3.7 MPa using methanol as a solvent, Au/Al_2O_3 was the most selective (53%) and active catalyst (1530 $mmol_{H_2O_2}\, g_{cat}$ h). However, it was also found that Pd is acting as a good promoter. Furthermore, the group of Haruta reported that the H_2O_2 production from H_2 and O_2 over Au catalysts is influenced by the acid-base properties of the support and the size of Au nanoparticles [15]. Over Au/MgO and Au/SiO_2-Al_2O_3, the rates of H_2O_2 formation were extremely low. The higher activity of Au/SiO_2 for the H_2O_2 synthesis compared to Au/TiO_2 catalyst under pressurized conditions was explained to be related with the weak interaction between Au and SiO_2 in contrast to the strong interaction between Au and TiO_2. The activity of Au/MCM-41 and Au/SiO_2 catalysts was found to be dependent on the Au particle size. The amount of H_2O_2 produced decreases with increasing Au nanoparticle diameter. Moreover, Au particles of 30 nm produced no H_2O_2 [15].

6.2.1.1. Kinetic studies on the synthesis of H_2O_2 on Au nanoparticles

Supported by kinetic and Density Functional Theory (DFT) studies, a reaction mechanism for H_2O_2 formation from H_2 and O_2 over Au/SiO_2, Au/TS-1 and Au/S-1 catalysts was proposed by Barton and Podkolzin [16]. The reaction mechanism described by the rate expression (Equation 6.1) is shown in Scheme 6.1.

$$r_{H_2O} = \frac{kK_{OOH}K_{O_2}P_{O_2}\sqrt{K_{H_2}P_{H_2}}P_{H_2}}{\left(1 + K_{O_2}P_{O_2} + \sqrt{K_{H_2}P_{H_2}} + K_{OOH}K_{O_2}P_{O_2}\sqrt{K_{H_2}P_{H_2}}\right)\left(1 + \sqrt{K_{H_2}P_{H_2}}\right)} \quad (6.1)$$

1. O_2 (gas) + * ↔ O_2* 2. H_2 (gas) + 2 *↔2H* 3. H_2(gas) +2 □ ↔ 2H□ 4. O_2* + H□ ↔ OOH* + □ Rate-determining step OOH* + H_2 (gas)+ □ → H_2O_2* + H□ 5. H_2O_2* + * → 2OH* 6. OH* + H* → H_2O* + * 7. H_2O* → * + H_2O	Scheme 6.1. Reaction mechanism for the H_2O synthesis over Au catalysts based on a two-site model as developed by Barton and Podkolzin [16].

DFT calculations with Au_5, Au_{13}, Au_{55} clusters and Au(111), Au(211) periodic slabs were used to evaluate the thermodynamic stability and reactivity of surface species. The measured apparent power-law kinetic parameters were similar for all Au-based catalysts with a H_2 order of 0.69-0.82, O_2 order of 0.1-0.2 and an activation energy of 37-41 kJ/mol. The introduction of H_2O in the inlet stream (~ 3 vol%) did not affect the reaction orders. The similarity between the reaction orders and activation energies between the Au-based catalysts, suggests a common reaction mechanism. Furthermore, the differences in catalyst activity are related to differences in Au particle size. The DFT calculations indicated that Au nanoparticles with similar size as Au_{13} cluster can activate H_2 and O_2 to generate H_2O_2, which is then decomposed to H_2O. Smaller particles are less reactive due to the instability of the OOH intermediate, whereas larger particles are less reactive due to the instability of adsorbed oxygen. The Au particles inside the pores of MFI supports (TS-1, S-1) are limited to the size of a Au_{13} cluster. Thus, the lowest catalytic activity of Au/SiO_2 (amorphous SiO_2) compared to Au/TS-1 and Au/S-1 could be explained from the dependence of the catalytic activity on the size of Au nanoparticles. The reaction mechanism proposed for the water synthesis on Au-based catalysts needs to involve two different surface sites in order to have a good fit between the theoretical kinetic model and the experimental data. A 'one-site-system' has been

excluded on the basis of results obtained from the computational studies and from the values of formations and stabilization energies of all the intermediates. Computational studies indicated that hydrogen can be stabilized by the surface and that splitting of a hydrogen molecule is facilitated by stabilization of one of its atoms by the surface. This suggests that an additional surface site is required for the formation of H_2O_2 (Scheme. 6.1). Calculations with Au (211) support the conclusions that on one type of surface sites O_2, OOH and H will compete for adsorption and on another type of surface sites only adsorption of hydrogen will occur [16].

Therefore, the proposed reaction mechanism for H_2O_2 formation depicted in Scheme 6.1 includes two types of active sites. One site is capable of nondissociative adsorption of O_2 and dissociative adsorption of H_2 and the other one is capable only for dissociative adsorption of H_2. The formation of adsorbed H_2O_2, which is then decomposed to H_2O, is proposed to be the rate determining step according to DFT calculations [16]. The kinetics of the H_2 oxidation over Au-based catalysts has also been explored by Nijhuis and Weckhuysen [17] as a way to understand the reaction mechanism for propene epoxidation. This kinetic modeling used the power-rate law expression derived by Barton and Podkolzin [16] as a starting point in the kinetic fitting. The kinetic model was extended with an Arhenius expression for the rate constant and a Langmuir adsorption term for the H_2O inhibition, reducing the number of active sites available for the reaction. The extension of the model of Barton and Podkolzin [16] was made to account for the strong inhibiting effect of water that Nijhuis and Weckhuysen [17] observed for the activity of Au-based catalysts in the propene epoxidation reaction. In the Figure 6.1 it is observed that the catalytic activity is 4 times lower in an experiment in which a small amount of water is added to the gas feed. The reactor was modelled as a plug flow to take into account this strong inhibition by the water produced

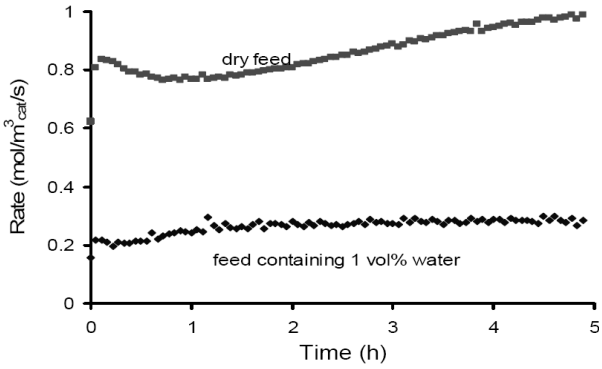

Figure 6.1. H_2 oxidation over Au/SiO_2 (GHSV = 10000 h^{-1}, T = 80º C, 6% H_2; 6% O_2 in He) with a 'dry' feed and a gas feed containing 1 vol% of H_2O. Reproduced from Nijhuis and Weckhuysen [17].

The kinetic model was able to describe very well the catalytic measurements of 1 wt% Au/TiO_2, 0.15 wt% Au/Sil-1, 0.45 wt% Au/Sil-1 and 1 wt% Au/SiO_2. Considering the similarities

between the catalysts, a single kinetic expression was developed having more theoretical background than the empirical power-rate low (Equation 6.2).

$$r_{H_2O} = k_0 \cdot e^{\frac{-E_a}{R \cdot T}} \cdot \frac{K_{H_2}C_{H_2}}{\left(1 + K_w C_{H_2O} + \sqrt{K_{H_2}C_{H_2}}\right)^2} \cdot \frac{K_{O_2}C_{O_2}}{1 + K_{O_2}C_{O_2}} \qquad (6.2)$$

Table 6.1. Kinetic Parameters Determined by Modelling of Catalytic Experiment with Langmuir-Hinshelwood Type Model (Equation 6.2) [17].

	Au/TiO_2 (1 wt%)	Au/Sil-1 (0.15 wt%)	Au/Sil-1 (0.45 wt%)	Au/SiO_2 (1 wt%)
No. of observations	46	24	33	16
k (10^6 mol/m^3/s)	294			
E_a (kJ/mol)	51.3			
K_{H2} (m^3/mol)	0.15			
K_{O2} (m^3/mol)	2.2			
K_w (m^3/mol)	3.1			
Relative activity	4.0	1	1.5	5.1
Avg dev. (%)	5.6	7.7	9.0	6.4

In the Langmuir-Hinshelwood type kinetic expression oxygen has its own adsorption site, different from the one of H_2 and H_2O since the reaction order in O_2 is close to zero. Dissociative adsorption of H_2 is also assumed [16]. H_2 is competing with H_2O on the same adsorption sites because the order in H_2 is close to 1. The model introduced some parameters that described the differences in available Au surface and Au loadings between the catalysts. The kinetic parameters determined by modelling of catalytic experiments with the Langmuir-Hinshelwood model (Equation 6.1) are described in Table 6.1. Very good fits were obtained for all catalysts under investigation, suggesting that H_2 oxidation over supported Au nanoparticles occurs exclusively on Au nanoparticles and the support is not involved in the reaction, since the kinetics and the kinetic parameters are support independent. The differences among the activities of Au-based catalysts are related with the variation in Au particle size [17]. H_2O was found to strongly decrease the rate of H_2 oxidation because is competing on the same adsorption sites with H_2. Therefore, if H_2O is present it will strongly decrease the amount of absorbed H_2 and decrease the H_2 efficiency of the oxidation process.

6.2.1.2. Spectroscopic evidence for the role of Au in the formation of hydroperoxo species

In-situ UV-Vis and EPR provided evidence on the role of Au in the formation of hydroperoxide species during the epoxidation of propene with O_2 and H_2 over Au/Ti-SiO_2 and Au/TS-1 catalysts [18]. During in-situ UV-Vis measurements, besides the typical charge-transfer band due to tetrahedral Ti^{4+} species (at around 233-222 nm) and the Au plasmon resonance band (at around 556-500 nm), another absorption band in the 360 nm region was observed.

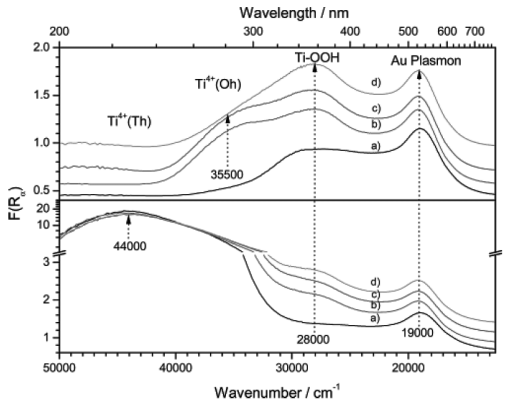

Figure 6.2. In-situ UV-Vis spectra during propene epoxidation on a Au/Ti-SiO_2 catalyst (Bottom: $BaSO_4$ referenced, and Top: Ti-SiO_2 referenced): (a) under Ar at 25° C before propene epoxidation, (b) under $C_3H_6/O_2/H_2/Ar$ (1/1/1/7 in volume) at 150° C for 120 min, (c) under $C_3H_6/O_2/H_2/Ar$ (1/1/1/7 in volume) at 150° C for 270 min, (d) under Ar at 25° C after propene epoxidation. Offsets are used for clarity. Reproduced from Chowdhury et al. [18].

This is illustrated in Figure 6.2, and it can be observed that the intensity of this 360 nm band was increasing during the propene epoxidation reaction with H_2 and O_2. The formation of this band around 360 nm is associated with the formation of Ti-OOH species upon interaction of H_2O_2 with Ti^{4+} [19, 20]. When the epoxidation reaction was performed over Ti/SiO_2 supports no absorption band characteristic to Ti-OOH was observed, suggesting that the role of Au is to form hydroperoxo species. With EPR a signal attributable to ($O_2^{\bullet -}$) was observed after the epoxidation of propene with H_2 and O_2 over Au/Ti-SiO_2. The EPR signal was not observed for the samples before propene epoxidation reaction. The lack of the EPR peak attributable to Ti^{3+} indicated that ($O_2^{\bullet -}$) may reside on Au, Ti^{4+}, or more likely at the Au-Ti^{4+} interface [21]. Au is facilitating the formation of paramagnetic ($O_2^{\bullet -}$) species, which during the trapping procedure spillover to Ti^{4+} to form superoxo-adsorbed species. The appearance of superoxo/hydroperoxo species when Au is present highlights the important role of Au nanoparticles on the formation of Ti-hydroperoxo species. These species are considered to be a reaction intermediate in the epoxidation of propene with H_2 and O_2 [31]. On the other hand, the formation of Ti-OOH species was not observed on Au/TiO_2. This suggests that the reaction mechanism of Au/TiO_2 may be different than the one of Au/Ti-SiO_2 for

the propene epoxidation reaction with H_2 and O_2. The formation of Ti-OOH species on tetrahedral Ti^{4+} can be one of the main differences. Based on the experimental results and literature reports, the group of Haruta proposed a mechanistic model for the formation of superoxo/hydroperoxo species on Au supported titanosilicates in Scheme 6.2 [18].

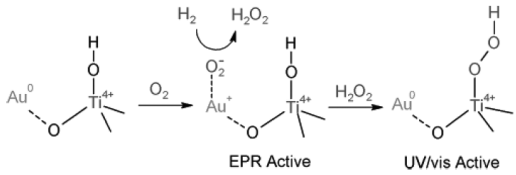

Scheme 6.2. Possible mechanistic model for the formation of hydroperoxo species on Au/titanosilicates. Reproduced from Chowdhury et al. [18].

6.2.2. Role of Au nanoparticles in propene adsorption and activation

Another function of Au in the propene epoxidation reaction with H_2 and O_2 is to influence the adsorption behavior of propene towards the formation of the bidentate propoxy species. In-situ XANES spectroscopy has been used to investigate the adsorption of propene on supported Au nanoparticles [22]. This study is described in great detail in **Chapter 4** of this PhD thesis. Au on silica catalysts were used in this study since SiO_2 is a more inert support and propene is not converted into propene oxide. Propene adsorption was investigated by using the H_2 oxidation as a reaction probe. It was observed that co-feeding of propene during H_2 oxidation reaction dramatically decreased the H_2O formation rate. The adsorbed propene could be very slowly removed from the Au/SiO_2 surface. More than 12 h of flushing with H_2 and O_2 were necessary to restore the initial activity of the catalyst in the hydrogen oxidation. By applying the delta-mu XANES analysis method it was found that propene is π bonding to the Au particles, which explains the strong inhibiting effect on the H_2 oxidation [22]. The physically adsorbed propene could be easily removed from the Au/SiO_2 surface because the activity for the H_2 oxidation reaction was recovered in a short time [22].

The adsorption of propene was also investigated with FT-IR spectroscopy [23-26]. Propene was found to reversibly adsorb on a bare TiO_2 support, but the adsorption was irreversible on an Au/TiO_2 catalyst, as shown in Figure 6.3. The irreversible adsorption of propene was considered to originate from the presence of Au on the TiO_2 support. The bands at 1050-1150 cm^{-1}, characteristic to C-O-Ti stretching vibrations for primary and secondary atoms, indicates that adsorbed species remain on the titania support after propene adsorption and not on the Au. When the propene oxide is adsorbed on TiO_2, similar species are generated as the ones formed upon adsorption of propene on

Au/TiO_2. Bidentate propoxy species are produced upon both, adsorption of propene oxide on TiO_2 and of propene on Au/TiO_2 catalyst [24].

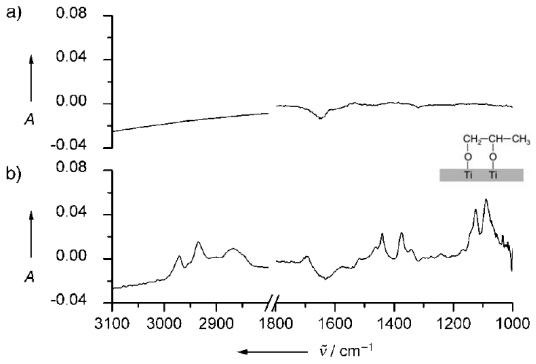

Figure 6.3. FT-IR spectra of adsorbed species on (a) TiO_2 and (b) a Au/TiO_2 catalyst after adsorption and subsequent desorption of propene (50° C; 100 spectra averaged). Reproduced from Nijhuis et al. [24].

To understand the similarities and differences between Au/TiO_2 and $Au/Ti\text{-}SiO_2$ catalysts, propene oxide adsorption experiments were carried out on SiO_2 and $Ti\text{-}SiO_2$ supports [25]. The FT-IR results are shown in Figure 6.4.

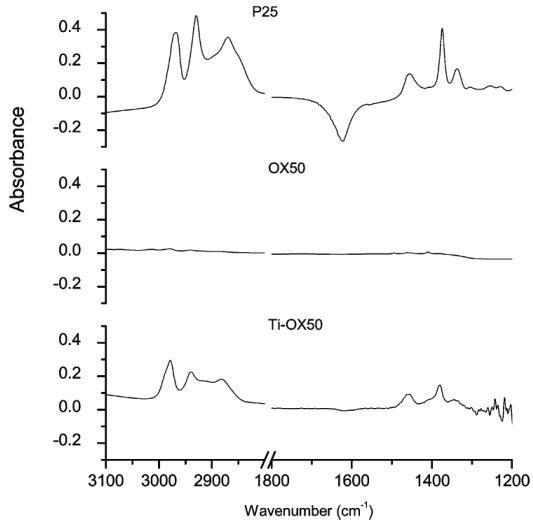

Figure 6.4. Propene oxide adsorption followed by desorption in He for different catalyst supports: P25 TiO_2, OX50 SiO_2, and Ti dispersed on OX50 SiO_2 (measured at 50° C) (20 spectra averaged). Reproduced from Nijhuis et al. [25].

Propene oxide is reversibly adsorbed on SiO_2, but on $Ti\text{-}SiO_2$ bidentate propoxy species are formed. The characteristic FT-IR bands of bidentate propoxy species are shifted to a higher energy than the ones on TiO_2, probably because these species are bonded with the primary carbon to a Ti site and with the secondary carbon to a Si site [25]. For a $Au/Ti\text{-}SiO_2$ catalyst the adsorption of propene caused the formation of a small amount of bidentate propoxy species compared to a Au/TiO_2 catalyst. This is because the $Au/Ti\text{-}SiO_2$ catalyst contains a small amount of well dispersed Ti. The presence of irreversible adsorbed species on both Au/TiO_2 and $Au/Ti\text{-}SiO_2$ catalysts may indicate that the reaction mechanism for both catalysts might be similar [25]. The FT-IR

spectroscopic results are in line with the in-situ XANES analysis [22, 24, 25]. Bidentate propoxy species are formed only in the presence of Au nanoparticles as no measurable adsorption of propene occurred in the absence of Au. Therefore, based on XAFS and FT-IR results it was proposed that bidentate propoxy species are produced via the adsorption of propene on Au, followed by a spillover to Ti. Thus, a second function of the Au nanoparticles was proposed, in addition to the earlier described peroxide formation out of H_2 and O_2 [27, 28].

6.2.3. Role of surface Ti sites in the propene epoxidation reaction

The role of Ti in the propene epoxidation reaction with H_2 and O_2 is generally associated with the ability of performing the epoxidation reaction, since it was experimentally observed that titanium-silicates can epoxidize propene with diluted H_2O_2 [29, 30]. Furthermore, as it was discussed above, the role of Ti is to stabilize the bidentate propoxy species [24, 25]. Based on the in-situ FT-IR results, Nijhuis et al. [24, 25] considered that the epoxidation reaction is taking place on Ti sites and that the bidentate propoxy species are reaction intermediates. The propene epoxidation reaction mechanism over Au/Ti-SiO_2 catalysts was also investigated by the group of Oyama, who used in-situ UV-Vis spectroscopy in combination with in-situ XANES spectroscopy [31]. On the basis of spectroscopic results, the propene epoxidation reaction over Au/Ti-SiO_2 was considered to occurr on Ti, but with Ti-OOH species as reaction intermediates. All the spectroscopic investigations and the related discussions on the propene epoxidation mechanism with H_2 and O_2 over Au/Ti-based catalysts will be discussed in separate sections. In what follows, we will discuss the activity of Ti in the liquid phase epoxidation of propene with H_2O_2.

6.2.3.1. Role of surface Ti sites in the epoxidation of propene with H_2O_2

Titanium incorporated into different silica frameworks is active and selective for the epoxidation of various alkenes and alkanes [32, 33]. Titanium silicalite-1 (TS-1) is able to catalyze the epoxidation of propene by H_2O_2 with a high rate using methanol or a methanol/ water mixture as solvent. The selectivity to propene oxide is very high (> 96%) and the yield is quantitative with respect to H_2O_2 [29]. Besides TS-1, various micro- and mesoporous materials containing titanosilicates have been synthesised and tested. Examples include TS-2 [34], Ti-ZSM-48, [35], Ti-β [36-38], Ti-MCM-41 [39-40], Ti-MCM-48 [41],Ti-SBA-15 [42, 43] and Ti-TUS-1 [44].

The surface of titanosilicate materials is characterized by the coordination of Ti and surface -OH groups present in the form of silanols and titanols. Tetrahedrally coordinated, isolated Ti^{4+} ions are considered to be the active sites [45]. This assumption is supported by the catalytic activity of homogeneous titanium silsesquioxane complexes in the olefin epoxidation reaction [46, 47]. The

principal problem of heterogeneous catalysts is that the catalytic surface contains a large range of structurally different catalytic sites which are difficult to be distinguished with the spectroscopic techniques. In the recent years, advanced in-situ spectroscopic techniques have added considerable knowledge to the structure of the active sites and the nature of reaction intermediates in TS-1 and Ti-MCM-41 during catalysis [19, 48-67]. In-situ XAFS investigations [52, 61] have revealed that Ti^{4+} has a four-fold coordination in both TS-1 and Ti-MCM-41, most of the Ti in the former has a closed tetrapodal $Ti(OSi)_4$ structure, whereas Ti in the Ti-MCM-41 has an open tripodal $Ti(OSi)_3(OH)$ structure. A mixture of $(-SiO)_4Ti$, $(-SiO)_3Ti(-OH)$ and $(-SiO)_2Ti-(OH)_2$ sites probably exists in the titanosilica materials where the Ti have been isomorphously substituted into the framework (Scheme 6.3). Species I will not exist in the grafted Ti^{4+} silica materials.

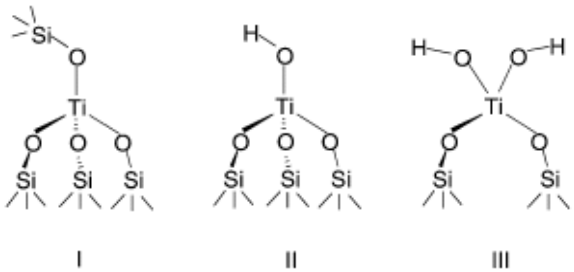

Scheme 6.3. Proposed models of tetrahedral Ti sites in dehydrated porous titanosilicates. Reproduced from Barker et al. [61].

All these structural characteristics are influencing the catalytic activity and selectivity of the titanosilicate materials. Srinivas and Ratnasamy [68, 69] reported a detailed EPR investigation of Ti^{3+} in TS-1, Ti-MCM-41, ETS-4 and ETS-10 materials. Ti^{4+} was reduced to Ti^{3+} by dry hydrogen. The presence of two types of tetrahedral Ti, differing in their reducibility, tetrapodal in TS-1 and tripodal in Ti-MCM-41 was evidenced by EPR spectroscopy. It was also found that it is more difficult to reduce Ti in a tetrahedral coordination geometry (TS-1 and Ti-MCM-41) than in an octahedral geometry (ETS-10 and ETS-4). Counterions and additives, such as Pt and Cs, were found to influence the redox properties of Ti^{4+} ions. The presence of Pt in TS-1 and Ti-MCM-41 enhances the reduction of Ti^{4+} in contrast to Cs^+ ions, that are stabilising Ti^{4+} ions due to their basic properties.

The acidic character of TS-1 was evidenced in acid-catalyzed reactions, such as the formation of diols in epoxidation reactions [70] and the rearrangement of cyclohexanone oxime to caprolactam [71]. In the oxidation reactions with H_2O_2, the acidity can be generated in-situ by coordination of H_2O_2 to the Ti sites [72]. Zhuang et al. [73] demonstrated using a combination of ^{31}P and ^{1}H MAS NMR spectroscopy the presence of both Lewis and Brönsted acidic sites in TS-1. The presence of Ti in the framework results in the formation of new OH groups, namely titanols, which are more acidic than silanols in silicalite-1. The dehydrated TS-1 and other titanosilicates do

not have Brönsted acidity. Zecchina et al. [74] identified the Lewis acidic character of Ti^{4+} ions with pyridine as a probe molecule. FT-IR indicated that dehydrated TS-1 and Ti-MCM-41 with similar Ti contents posses only Lewis acid sites. The characteristic FT-IR bands of Lewis acidic sites disappeared when the temperature was increased beyond 125º C for TS-1 and 250º C for Ti-MCM-41 indicating a higher acid strength in Ti-MCM-41 than in TS-1 material. The number of acid sites estimated from FT-IR band intensities was higher on Ti-MCM-41 than in TS-1.

6.2.3.2. Reaction intermediates in the propene epoxidation with H_2O_2

Spectroscopic investigations suggest that the coordination number of Ti increases from tetra- to penta- and six-fold coordination on contact with H_2O_2 [48-67]. More specifically, UV-Vis and EPR have indicated that the nature of the oxo intermediates formed on contact with H_2O_2 depend on the local structure and coordination of Ti. Tetrapodal structures seem to generate oxo species, their concentration correlates with activity in the epoxidation of alkenes. The structure of titanium peroxo/superoxo species formed on the surface during the catalytic reaction is influencing the dissociation mode of the O-O bond in H_2O_2. The oxo ion/radical formed during the H_2O_2 dissociation determines the selectivity in oxidation reactions. The heterolytic O-O bond dissociation acts for instance in the epoxidation of alkenes and the hemolytic O-O bond dissociation is responsible for the oxidation of alkenes and side chains in alkyl aromatics [75]. The conversion of propene into its oxide implies the selective transfer of a peroxygen atom O(–I) by a heterolytic mechanism, without modification of the formal oxidation state or oxidation number of the metallic centre.

Clerici et al. were the first who proposed that a Ti-OOH group is the active site for the selective oxidation of hydrocarbons with H_2O_2 on TS-1 [33, 76, 77]. Using alcohols as solvents they proposed that the complex formed from the coordination of the alcohol to the end-on Ti-OOH (Scheme 6.4, species II), is the key intermediate in the alkene epoxidation. Formation and stability of this complex is influenced by the type of the alcohol and acid/base properties of the reaction mixture. The solvent is considered to act as a co-catalyst, stabilizing the Ti-OOH intermediate.

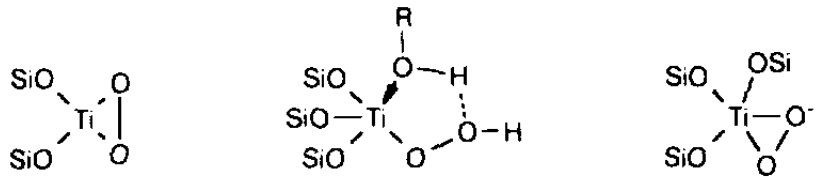

I II III

Scheme 6.4. Proposed structures of Ti sites interacting with H_2O_2. Reproduced from Clerici et al. [29].

The stability of this complex is influencing the kinetics and yield of the epoxidation [29]. Species I was proposed by Jacobs et al. as the key intermediate in TS-1 catalysis [32]. The group of Clerici [29] could not explain the formation of these species from the relationship between solvent effects and kinetics. Species III are considered to be inert to reactions with olefins since the presence of a negative charge greatly reduces their electrophylic properties.

By considering species II as the active intermediate, two possible reaction mechanisms for the epoxidation of lower olefins have been proposed in the open literature. They are outlined in Scheme 6.5. Both mechanisms were derived on the basis of steric arguments, but unfortunately not experimentally verified. The first mechanism proposed by Chong and Sharpless [78] (Scheme 6.5, mechanism 1) with the olefin approaching the oxygen from the back side and along the O-O bond axis was not in agreement with the steric arguments proposed by Clerici et al. [29] as the alkyl groups of the olefin will be in close proximity with framework siloxane bonds.

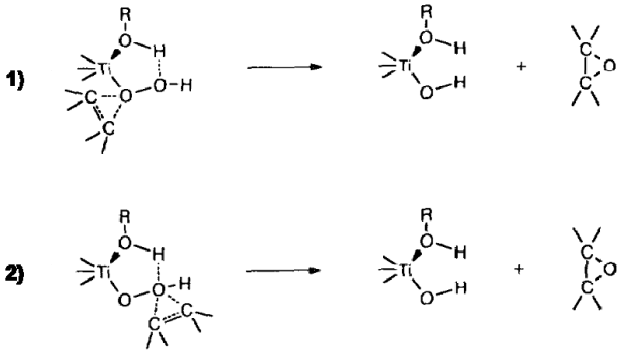

Scheme 6.5. Proposed reaction mechanisms of the olefin epoxidation with H_2O_2/solvent over TS-1 catalysts. Reproduced from Clerici et al. [29].

The second mechanism of the olefin epoxidation with H_2O_2 over TS-1 was considered more likely. It assumes that distal oxygen is present at the centre of the zeolitic channel, minimizing in this way the interaction of the olefin with the catalyst surface. Theoretical calculations have been performed in order to establish which of the oxygen atoms from the Ti-OOH moiety is preferentially attacked [79].

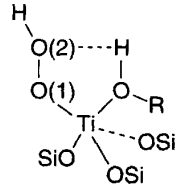

Scheme 6.6. Representation of the structure of HOO-Ti-(OSi≡)$_3$-ROH species (Ti(η^1OOH)(ROH). Reproduced from Neurock et al. [66].

The results are not in agreement with the epoxidation reaction mechanism proposed by Clerici et al. (Scheme 6.5, mechanism 2). The interaction with O(2) from Scheme 6.6 was found to be repulsive regardless of the direction of attack. Ethene attack at the oxygen bound to Ti-O(1) was attractive

and occurred through a back-side attack of ethene to the O(1) of the -OOH group. Based on these results, the oxygen closest to the titanium centre is involved in alkene epoxidation [79].

Combined DFT and EXAFS investigations have provided evidence of the nature of the oxo intermediates formed by the interaction of *tert*-butyl hydroperoxide (TBHP) with Ti-MCM-41 catalyst [61]. The structures and energetics of a range of possible oxygen-donating species on the surface of Ti-MCM-41 have been computationally investigated (Scheme 6.7). EXAFS data obtained from the interaction of TBHP with Ti-MCM-41 were compared with the theoretical results.

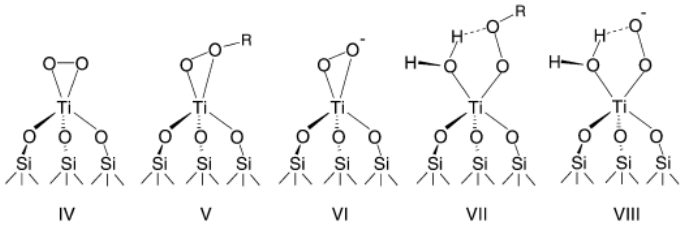

Scheme 6.7. Postulated models for Ti–peroxo species in dehydrated, porous titanosilicate, R= H or ^{t}Bu when ROOH=H_2O_2 or TBHP. Reproduced from Barker et al. [61].

The DFT calculations for the Ti(η^2-O_2) and Ti(η^2-OO^-) clusters showed that their energy is with 300 kJ/mol higher than of the reactants (Ti-OH cluster, H_2O_2 and H_2O) and thus unlikely to form under mild reaction conditions, typically employed for catalytic oxidations. Furthermore, these DFT results were in agreement with the experimental data.

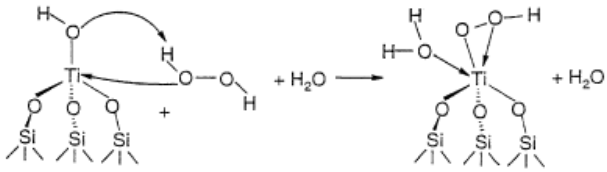

Scheme 6.8. Representation of the formation of Ti (η^2-OOH)· H_2O upon the interaction of HO-Ti-(OSi≡)$_3$ with H_2O_2/H_2O. Reproduced from Barker et al. [61].

In the EXAFS studies performed on the TBHP/Ti-MCM-41 system, the Ti(η^2-O_2) and Ti(η^2-OO^-) clusters could not be identified.

From DFT calculations, Ti(η^2-OOH) cluster was found to be more stable than its respective reactants (Ti-OH cluster, H_2O_2 and H_2O), -19 kJ/mol for five- coordinate (η^2-OOH). When water is

coordinated to the Ti(η^2-OOH), the energy is -44 kJ/mol lower than that of reactants indicating that the preferential coordination mode is six (Scheme 6.8).

The DFT calculations for the Ti(η^1-OOH) cluster showed that is likely to be stable within H_2O_2/titanosilicate system. The formation energies are -41 and -65 kJ/mol for five- and six-coordinate Ti(η^1-OOH) clusters relative to a tetrahedral Ti site with one molecule of H_2O_2 and one of H_2O. This indicates that six-coordination of the Ti (η^1-OOH) complexes is the preferential one (Scheme 6.9) [61].

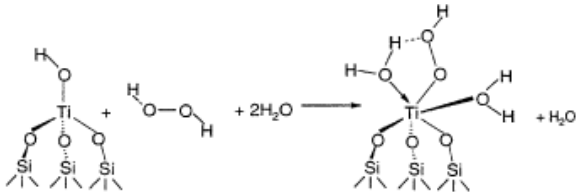

'Ti-OH' + H_2O_2 + 2H_2O → 'Ti(η^1-OOH)(O(H)H) · H_2O' + H_2O

Scheme 6.9. Representation of the formation of Ti (η^1-OOH)(O(H)H)· H_2O upon the interaction of HO-Ti-(OSi≡)$_3$ with H_2O_2/H_2O. Reproduced from Barker et al. [61].

DFT calculations and EXAFS obtained from the interaction of Ti-MCM-41 with TBHP indicated that the oxygen donating species are the six-coordinated Ti(η^2-OOH) and Ti(η^1-OOH) complexes. Both five- and six-coordinated (i.e. dehydrated and hydrated) η^2-O_2, η^2-OO^- and η^1-OO^- type species did not fit with the EXAFS as well with DFT results [61].

The equilibrium between the Ti(η^2-OOH) and Ti(η^1-OOH) complexes in the titanosilicates was investigated in-situ with high resolution XANES spectroscopy [67]. The formation of side-on Ti-η^2-peroxo complex by the interaction of H_2O_2/H_2O solution with activated TS-1 catalyst was evidenced from XANES measurements. The formation of the side-on Ti-η^2-peroxo complex drastically modified all the XANES features, the pre-edge feature decreases from 0.9 to 0.16 in intensity, evidencing the loss of tetrahedrally symmetry. Two prominent and well defined features appear now in the edge around 4984 and 4995 eV, which is the fingerprint of a side-on Ti-η^2-peroxo complex (Figure 6.5). When the water is removed from the H_2O_2/H_2O treated TS-1 sample, the features of the side-on Ti-η^2-peroxo complex almost disappear. By reexposure of the sample to water the features of the side-on Ti-η^2-peroxo complex are almost completely restored. The spectra of anhydrous H_2O_2 exposed TS-1 is very similar with the one after the evacuation of water. When the anhydrous H_2O_2 treated TS-1 is exposed to water, the XANES spectra presents the features of the side-on Ti-η^2-peroxo complex [67]. Based on these results an equilibrium between the end-one Ti-η^1-hydroperoxo complex and the side-on Ti-η^2-peroxo complex is proposed (Scheme 6.10).

Dosing TBHP in a decane solution on Ti-MSA (anhydrous mesoporous material with Ti^{4+} exposed on the surface of the pores) results in a similar spectrum as the one obtained upon the interaction of anhydrous H_2O_2 with TS-1, in both the XANES and EXAFS regions. When the Ti-MSA is exposed to a TBHP solution diluted with H_2O, the characteristic features of the side-on Ti-η^2-peroxo complex are observed. Such features are more evident when the Ti-MSA is treated with a H_2O_2/H_2O solution. The EXAFS results evidenced that this interaction causes irreversible extraction of the Ti species.

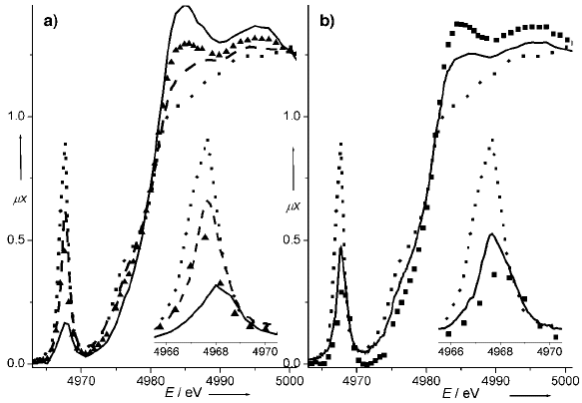

Figure 6.5. High-resolution XANES spectra collected at liquid-nitrogen temperature on the TS-1 catalyst under different conditions. The two parts refer to two different experiments for which the reported set of spectra has been recorded in the time sequence. a) Activated TS-1 catalyst (dotted line ……); after contact with H_2O_2/H_2O solution (solid line —); after sublimation of H_2O by evacuation at 77 K (dashed line ------); after subsequent contact with water (scattered squares ▲). b) Activated TS-1 catalyst (dotted ….); after contact with "anhydrous" H_2O_2 from the gas phase (solid line —); after subsequent contact with water (scattered squares ■). Reproduced from Prestipino et al. [67].

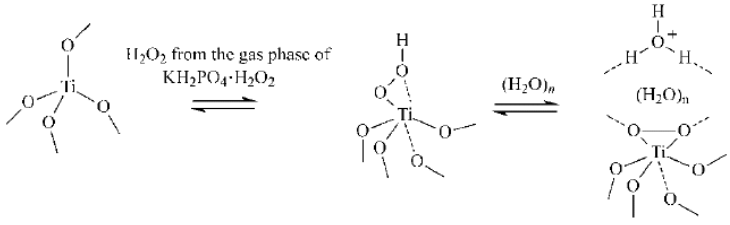

Scheme 6.10. Representation of the equilibria between TiO_4 framework species and η^1-complexes inside TS-1 channels upon dosage of anhydrous H_2O_2 (left) and between η^1 - and η^2 -complexes upon hydration (right). Reproduced from Prestipino et al. [67].

These results explain why mesoporous Ti-silicates are unsuitable catalysts for the epoxidation reaction with H_2O_2/ H_2O compared to TS-1. The catalytic properties of TS-1 under

such conditions are explained by a reversible formation of η^2-side-on peroxo complex. The amount of water is a key factor for the change of η^1-end-on into η^2-side-on complex. The reaction intermediate for the olefin epoxidation could be the η^1-end-on complex if it assumed (a) the hydrophobic character of TS-1 together with the presence of olefins in the channels as the dominant species and (b) that water is present in a very low amount [67].

The interaction of H_2O_2 with titanosilicates was also investigated by Ratnasamy et al. [19, 55, 65] using a combination of UV-Vis and EPR spectroscopy. The formation of diamagnetic peroxo/hydroperoxo species $Ti(O_2H)$ was observed in the UV-Vis spectra, while paramagnetic superoxo species $Ti(O_2^{\bullet -})$ were observed in the EPR spectra. The formation of similar oxo species in the reaction of H_2 and O_2 over TS-1, instead of H_2O_2 as the oxidant, was also evidenced with EPR, as shown in Figure 6.6.

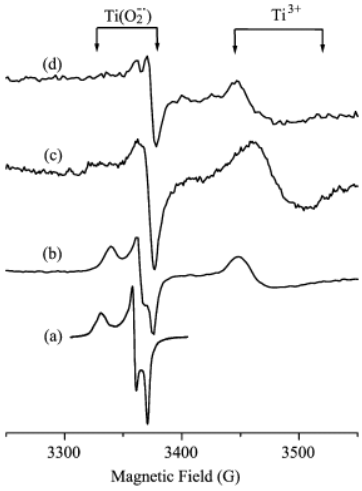

Figure 6.6. EPR spectra of $Ti(O_2^{\bullet -})$ and Ti^{3+} ions at 80 K. (a) Pd(2)-TS-2 + H_2O_2; (b) Pt(0.015)-TS-1 +H_2 + O_2 (treated at 400º C); (c) Pd(2)-TS-1 + H_2 + O_2 (treated at 50º C); and (d) TS-1 + H_2 + O_2 (treated at 50º C). For clarity, spectra (c) and (d) are shown at four and five times the actual gain. Spectral regions corresponding to $Ti(O_2^{\bullet -})$ and Ti^{3+} ions are marked. Reproduced from Shetti et al. [19].

The superoxo species were not formed in the presence of O_2 on the TS-1, Ti-MCM-41, Pd-TS-1, and Pt-TS samples. The presence of Pd ions in the TS-1 was found to facilitate the reducibility of Ti^{4+} ions and promoted the formation of the diverse titanium oxo species at lower temperatures. When Pd(Pt)-TS-1 samples were brought in contact with H_2 + O_2, Ti^{4+} was reduced to Ti^{3+} by H_2 (Figure 6.6). The Ti^{3+} ions generates $Ti(O_2^{\bullet -})$ species upon interaction with O_2. The reduction and reoxidation of Ti ions in TS-1, which requires temperatures of 200º C or higher, is facilitated by Pd or Pt and occurs even at 50º C (Figure 6.6). Both the amount of Ti^{4+} that is reduced and the amount of $Ti(O_2^{\bullet -})$ species that is formed are dependent on the Pd content. The maximum concentration of the paramagnetic titanium oxo species were formed at a loading of 2 wt% Pd [19].The UV-Vis bands observed upon interaction of TS-1 and Pd-TS-1 with H_2O_2 were associated with the formation of $Ti(O_2^{\bullet -})$ superoxide and $Ti(O_2H)$ hydroperoxo/peroxo species. The position and the relative intensities of these bands are different in TS-1 compared to Pd-TS-1. The intensity

ratio ($Ti(O_2H)/Ti(O_2^{\bullet -})$) was higher for Pd-TS-1 compared to TS-1, which evidences the influence of additives, such as Pd, in promoting the formation of various titanium oxo species.

The formation of Ti-OOH species upon the interaction of H_2O_2 with Ti in TS-1 has been spectroscopically observed by Lin and Frei [20]. The Ti-OOH species were found to photodissociate efficiently under irradiation with visible or near UV light. In-situ FT-IR monitoring of the phototriggered or thermally induced oxidation of ethene and propene molecules lead to direct observation of reaction of the Ti-OOH species.

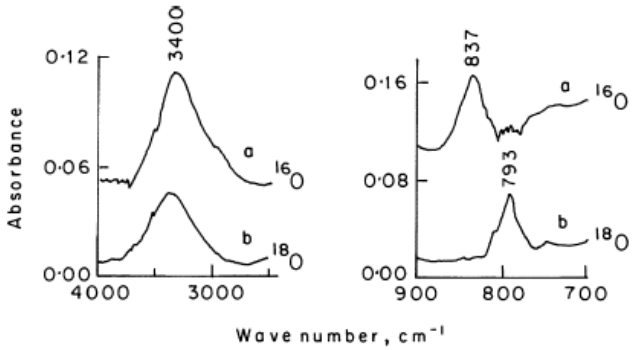

Figure 6.7. Infrared difference spectra before and after loading of $H_2{}^{16}O_2$ (curve a) and $H_2{}^{18}O_2$ (curve b) into TS-1 followed by 12 h evacuation (1025 mbar). Reproduced from Lin and Frei [20].

The absorption band at 837 cm^{-1}, corresponding to the O-O stretching vibrations, could be detected upon loading $H_2{}^{16}O_2$ onto the TS-1 material. This band was shifted to 793 cm^{-1} when $H_2{}^{18}O_2$ was loaded on TS-1 (Figure 6.7). The vibration at 3400 cm^{-1} was assigned to hydrogen-bonded OH groups of Ti-OOH. These bands could not be observed when the same experiment was performed on a bare silicalite-1 support [20]. Hence, the two FT-IR absorption bands were suggested to originate from a side-on hydroperoxo species (η^2-$Ti(O_2H)$ interacting with framework Ti (Scheme 6.11). The η^2-$Ti(O_2H)$ was found to be stable for a long time at room temperature. Also, ab-initio and DFT cluster calculations predicted that Ti-OOH is the most stable Ti peroxo specie [54,80,81]. Lin and Frei [20] proposed that tetrapodal framework Ti sites are converted into $(Si\text{-}O)_3TiOOH$ after the exposure of the dehydrated TS-1 material to H_2O_2, as illustrated in Scheme 6.11. In the case of the tripodal framework $(SiO)_3Ti\text{-}OH$, substitution of OH by OOH was suggested to occur rather than opening of the Ti-O-Si bridges. The formation of Ti-OOH centres adjacent to a Si-OH group was therefore proposed to occur on both tetra- and tripodal Ti sites. The UV-Vis spectrum of a H_2O_2 treated TS-1 sample revealed a band at 360 nm and a tail at 550 nm, which were still visible even after evacuation of H_2O_2. Upon irradiation of the H_2O_2 loaded TS-1 sample with 355 nm light of a Nd: YAG laser or the visible emission of a conventional tungsten source, the intensities of the

UV-Vis absorption band and the FT-IR bands at 837 cm^{-1} and 3400 cm^{-1} decreased [20]. At the same time, new FT-IR bands were observed at 3676 cm^{-1}, 1629 cm^{-1} and at 960 cm^{-1}. The photodissociation results points that Ti-OOH disproportionate into Ti-OH and O. The original coordination environment of Ti will be restored by the recondensation of this Ti-OH group with adjacent Si-OH with the regeneration of Si-O-Ti and H_2O. This was evidenced by using isotopic labelled $H_2{}^{18}O_2$. After condensation of the Ti-OH species with Si-OH, the resulted water was found to contain labelled ^{18}O [20].

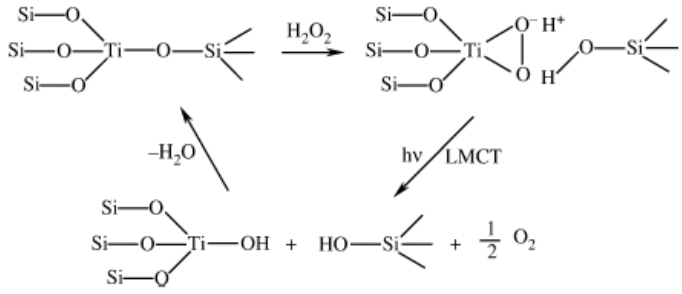

Scheme 6.11. Formation of Ti (η^2-OOH) upon the interaction of HO-Ti-$(OSi\equiv)_3$ with H_2O_2. Reproduced from Lin and Frei. [20].

The epoxidation of propene with H_2O_2 over TS-1 was similarly investigated. The loss of characteristic bands of adsorbed propene and Ti-OOH at 873 cm^{-1} and 3400 cm^{-1} is observed on a very short time scale from the loading of propene over the H_2O_2 treated TS-1 sample. New absorption bands are also observed upon the interaction of propene with Ti-OOH and were attributed to the propene oxide product. The presence of ^{18}O in the propene oxide molecule was confirmed when $H_2{}^{18}O_2$ treated TS-1 was exposed to propene [20]. The shift of the FT-IR absorption bands characteristic for labelled propene oxide in comparison with unlabelled one was a clear indication that propene oxide is formed upon oxygen abstraction from the Ti-OOH during interaction with propene. The propene epoxidation did not occur in the absence of a H_2O_2 loaded TS-1 material. The main conclusion was that Ti-OOH groups are reaction intermediates in the propene epoxidation over TS-1. Loading of the propene oxide over the H_2O_2 loaded TS-1 catalyst resulted in the conversion of propene oxide to propionaldehyde. This suggest that the slow growth of aldehyde upon spontaneous reaction of propene in H_2O_2 treated TS-1 sieve is due to thermal rearrangement of the accumulating propene oxide. It was concluded that the spontaneous epoxidation of propene by Ti-OOH is completely selective and that only one peroxo ligand is formed per Ti centre. The higher reactivity of Ti-OOH in propene epoxidation compared to ethene epoxidation was explained considering the orbital interactions and electron densities of the double bond. The activity of Ti-OOH towards olefin epoxidation is influenced by the interaction of the

π*(OO) orbital with the π*(CC) of the olefin double bond. Upon this interaction an O transfer from the Ti-OOH to C=C occurs. The electrophilic nature of the O transfer explains why the epoxidation is faster in the case of propene compared with ethene. The double bond of propene is electron richer compared to ethene, due to the inductive effect of the methyl group and that is enhancing the electophilic O transfer [20].

6.2.3.3. Summary

Significant efforts have been made to identify the reaction intermediates in the catalytic epoxidation reaction of propene with H_2O_2 over titanosilicates materials. Spectroscopic techniques have identified hydroperoxo species such Ti(η^2-OOH) and Ti(η^1-OOH) complexes and superoxo structures such as Ti($O_2^{\bullet -}$) on titanosilicates upon interaction with H_2O_2 [48-67]. The participation of the titanium oxo species in the epoxidation of propene with H_2O_2 have been revealed by FT-IR [20]. Titanosilicate materials in the dehydrated state do not possess Brønsted acidity, but the hydroperoxo species generated from the interaction with H_2O_2 have Brønsted acidity. This can cause side reactions, such as for example the isomerization of propene oxide to propionaldehyde [73,74]. Therefore, besides propene epoxidation, which is the dominant reaction, side reactions attributed to the Brønsted acidity of the Ti(O_2H) group may also occur decreasing the overall selectivity towards the desired epoxide. Direct confirmation of the participation of Ti sites in the propene epoxidation reaction with H_2 and O_2 over Au/Ti-based catalysts have been obtained from UV-Vis, FT-IR and XAFS spectroscopies [18,24,25,31]. In analogy to the propene epoxidation reaction over titanosilicates, Ti-hydroperoxo species were also considered to be a reaction intermediate in the epoxidation of propene with H_2 and O_2 over Au/Ti-SiO_2 catalysts [31]. Bidentate propoxy species produced upon adsorption of propene on Ti sites have been identified with in-situ FT-IR. These species are considered to be the precursors of the propene oxide production [24-26], although not all researchers share this opinion [23]. However, although all these studies point towards the direct role of Ti sites in the propene epoxidation reaction with H_2 and O_2, the reaction pathway over Au/Ti-based catalysts is still under discussion.

6.3. Kinetic studies of propene epoxidation mechanism with H_2 and O_2 over Au/Ti-based catalysts

In all mechanistic studies on the epoxidation of propene over Au/Ti-based catalysts, bi-functionality has been considered as an essential part of this catalytic system. As already shown in the previous sections of this chapter, the role of Au in the epoxidation reaction is generally attributed to the synthesis of H_2O_2 since this reaction was both experimentally observed [14, 15, 82,

83] and computationally verified [17, 84]. Furthermore, as previously discussed, the role of surface Ti sites is associated with the ability to perform the epoxidation reaction [29, 30]. The synthesis of Au/Ti-SiO_2 catalysts with improved catalytic stability compared to the classical Au/TiO_2 catalysts, allowed the possibility of studying the kinetics of the propene oxide and water synthesis mechanism since in this case the kinetic analysis can be performed under steady-state conditions.

6.3.1. Kinetic studies on the propene epoxidation mechanism over Au/Ti-SiO_2 catalysts

The kinetic experiments with mixtures of $O_2/H_2/C_3H_6$ need to be carefully performed due to safety considerations, which imply operating outside the explosion conditions. The group of Delgass proposed an epoxidation mechanism based on the kinetic analysis results of propene epoxidation over Au/TS-1 in the absence of significant deactivation [85]. The catalysts used in this study where Au/TS-1 with low Au loadings ranging from 0.02-0.06 wt% and Si/Ti molar ratio between 36 and 143. The kinetic analysis consisted of a factorial design of kinetic experiments that allowed the examination of a large number of non-flammable reaction conditions centred around the standard reaction mixture 10/10/10/70 vol% $O_2/H_2/C_3H_6$/diluent.

Table 6.2. Different power-rate low expressions for the formation of propene oxide, CO_2 and H_2O.

6.3.	$\mathbf{r_{PO} = k_{PO}\,[H_2]^{0.60\pm0.03}[O_2]^{0.31\pm0.04}[C_3H_6]^{0.18\pm0.04}}$	[85]
6.4.	$\mathbf{r_{PO} = k_{PO}[H_2]^{0.52}[O_2]^{0.24}[C_3H_6]^{0.36}}$	[87]
6.5.	$\mathbf{r_{CO_2} = k_{CO_2}\,[H_2]^{0.39}[O_2]^{0.21}[PO]^{0.22}}$	[87]
6.6	$\mathbf{r_{H_2O} = k_{H_2O}[H_2]^{0.67}[O_2]^{0.16}[PO]^{0.030}}$	[87]

The activation energy was found to be catalyst specific and ranged from 35 to 54 kJ/mol. These values are similar to the activation energies for water synthesis [16]. The experimental results from the evaluation of all studied Au/TS-1 catalysts showed that the propene oxide production rate could be approximated using power-rate law expression (Table 6.2, equation 6.2) where the reaction follows the Langmuir-Hinshelwood formalism. A two-site reaction mechanism was proposed for the Au/TS-1 catalyst, as outlined in Scheme 6.12. Initially, the role of Au was assumed to be related only with the formation of the hydroperoxo species and and the Au sites were denoted as S_1. Propene was considered to mainly adsorb on Ti sites, denoted as S_2. The proposed rate determining step is shown in sequence 6 of the reaction mechanism from Scheme 6.12. H_2 appears to be incapable of adsorbing on a bare Au surface, its adsorption being promoted by the presence of O_2 on the surface, as suggested by Taylor et al. [85]. It was also suggested by Haruta and co-workers that an oxygen-covered Au surface is needed to begin the catalytic cycle [86]. Considering that all

the other steps of the reaction mechanism are at quasi-equilibrium, a power-rate law for the propene oxide synthesis (Table 6.2, Equation 6.3) was derived. The apparent order of H_2 was twice as high as the one of O_2. The elementary steps proposed to occur over Au sites could not be explained from the values of the fractional orders. According to the Langmuir-Hinshelwood formalism, propene oxide rate saturation should be obtained for both high H_2 and O_2 partial pressures. These results reconfirm the hypothesis of Barton and Podkolzin where H_2 oxidation involves two different reaction sites, one of which is responsible only for H_2 adsorption or stabilization [16].

H_2O_2 synthesis on one type of Au site (DFT) 1. $O_2 + S_1 \leftrightarrow O_2–S_1$ 2. $H_2 + O_2–S_1 + S_1 \leftrightarrow HOO–S_1 + H–S_1$ 3. $O_2 + 2H–S_1 \leftrightarrow HOO–S_1 + H–S_1$ 4. $H_2 + HOO–S_1 + S_1 \leftrightarrow HOOH–S_1 + H–S_1$ Propene epoxidation involving Au and Ti sites 5. $C_3H_6 + S_2 \leftrightarrow C_3H_6– S_2$ 6. $C_3H_6– S_2 + HOOH–S_1 \rightarrow H_2O– S_2 + PO– S_2$ 7. $PO– S_2 \leftrightarrow PO + S_2$ 8. $H_2O–S_1 \leftrightarrow H_2O + S_1$	Scheme 6.12. Reaction mechanism for the epoxidation of propene over Au/TS-1 catalysts based on DFT calculations and experimentally determined reaction orders. According to Taylor et al. [85].

A three active sites mechanism working in concert was found to explain both the experimental and theoretical results, but it was considered that the introduction of three active sites was lacking any mechanistic insight, especially regarding where the actual formation of propene oxide occurs. A one site mechanism in which H_2O_2 or hydroperoxy species formed on Au sites spillover to Ti sites followed by the reaction with adsorbed propene could not be made consistent with the experimentally reaction orders. The migration of hydroperoxy species to Ti followed by an epoxidation will force the H_2 and O_2 to have similar values for the reaction orders. The positioning of the OOH species on a Au site and propene on adjacent Ti site is therefore necessary in order to reproduce the experimentally observed orders. In conclusion, the mechanism proposed by this group assumes formation of hydroperoxy species on Au site and adsorption of propene on a Ti site. The formation of propene oxide is proposed to occur on adjacent Au and Ti sites. This step determines the rate of the epoxidation reaction. This proposed mechanism is somewhat different from what has been suggested to be the mechanism of TS-1 catalysts for the propene epoxidation with H_2O_2. In that case, the propene was not coordinating to Ti of the TS-1 as is proposed to occur for the Au/TS-1 for the gas phase propene epoxidation.

Another kinetic study using a factorial design of the propene epoxidation reaction was carried out at 150^0 C over a stable Ba-doped, mesoporous Au/Ti-TUD catalyst. The power-rate law

and various Langmuir-Hinshelwood models were fitted to the kinetic data [87, 88]. Based on the kinetic experiments the rate of propene oxide formation could be described by the power-law expression from Table 6.2, equation 6.4. The power-rate law for CO_2 (Table 6.2, equation 6.5) indicates that CO_2 is mainly produced from propene oxide, H_2 and O_2. The CO_2 rate formation was also calculated considering propene instead of propene oxide. The small fractional order obtained for propene (0.073) compared with that of propene oxide (0.22) indicates that propene oxide is mainly involved in the CO_2 formation. For the H_2O formation (Table 6.2, equation 6.6), values of the exponents indicate that H_2O is mainly produced from the reaction of H_2 and O_2. The H_2 and O_2 dependencies are similar to those reported for the H_2O formation [16]. The apparent activation energies values determined in this kinetic study for the H_2O, CO_2 and propene oxide formation were 51, 80 and 43 kJ/mol. The value of the activation energy of 43 kJ/mol for the propene oxide formation is close to the 37-41 kJ/mol, previously obtained for the H_2O formation [16].

The power-rate law expression for the propene oxide formation on Au/Ti-TUD was in agreement with a reaction mechanism involving three active sites, two Au sites and one Ti site. The mechanism is illustrated in Scheme 6.13.

H_2O_2 synthesis on one two type of Au sites (DFT) 1. $O_2 + * \leftrightarrow O_2*$ 2. $H_2 + \bullet \leftrightarrow 2H\bullet$ 3. $O_2* + H\bullet \leftrightarrow HOO* + \bullet$ 4. $HOO* + H_2 + \bullet \rightarrow H_2O_2 + * + H\bullet$ Propene epoxidation involving Ti site 5. $H_2O_2 + Ti(OH) \leftrightarrow Ti(OH)(HOOH)$ 6. $Ti(OH)(HOOH) \leftrightarrow Ti(OH_2)(OOH)$ 7. $Ti(OH_2)(OOH) + C_3H_6 \leftrightarrow Ti(OH_2)(OOH)(C_3H_6)$ 8. $Ti(OH_2)(OOH)(C_3H_6) \rightarrow Ti(OH_2)(OH)(C_3H_6O)$ 9. $Ti(OH_2)(OH)(C_3H_6O) \leftrightarrow Ti(OH) + H_2O + C_3H_6O$	Scheme 6.13. Reaction mechanism for the epoxidation of propene over Au/Ti-TUD catalysts based on DFT calculations and experimentally determined reaction orders. According to Lu et al. [87]. • -reaction site one * -different site two

In the proposed mechanism two irreversible steps (sequence 4 and 8, Scheme 6.13) are determining the overall rate of the epoxidation reaction. One step is involved in the H_2O_2 synthesis on a Au site and the other step is involved in the epoxidation of propene with OOH species on Ti site. This group considers that the synchronization of the catalytic cycles on Au and Ti sites as proposed by Delgass [85] is an unnecessary requirement because the epoxidation step is known to occur much faster than the synthesis of H_2O_2 [30,89].

To better understand the meaning of the exponent values from the power-rate law of the propene oxide formation, independent adsorption measurements of the reactants were carried out by

the group of Oyama at the same reaction temperature [88]. From the temperature-programmed desorption measurements it was determined that Au enhances the adsorption of O_2 and C_3H_6 on Ti sites probably by a spillover mechanism. The amount of adsorbed reactants was found to decrease in the order $O_2 > C_3H_6 > H_2$.

Several kinetic models were proposed to describe the propene oxide formation rate. Most of them included generalized expressions of the power-rate law and few introduced more details associated with the proposed mechanism [87, 88]. All kinetic equations considered the Langmuir-Hinshelwood formalism, since all the reactants are assumed to adsorb on the catalyst surface. The previously described power-rate law gave a good fit, with a higher probability and was also in accordance with the adsorption data, but such an empirical equation cannot provide too much information about the reaction mechanism. A kinetic equation, which was based on a reaction mechanism, involving three active sites for H_2, O_2 and propene adsorption, where H_2 adsorption is considered as dissociative, was found to result in a good fit and could also be confirmed by the calorimetric adsorption data.

Using a more complex adsorption mechanism based on Frumkin-Temkin formalism, which involves a nonuniform surface, described also very well the propene oxide formation rate. This model was found to have a high statistical probability and was confirmed by the adsorption data. All the above kinetic models were not considering any chemical reaction on the surface of the catalyst and were taking into account only the adsorption of the reactants.

The group of Oyama [88] considered for their investigation some models that were derived from the reaction mechanism proposed by their own group and by the Delgass group [85]. The propene oxide rate expression derived by Delgass from sequence 6 (Scheme 6.12) was found to have a good statistical probability, but it was impossible to be confirmed or rejected by the calorimetric adsorption data. The difficulty to correlate the adsorption data with the kinetic study is related to the fact that in the propene oxide rate expression an exponent is used to describe two equilibrium constants for the formation of H_2O_2 from H_2 and O_2. Since in the adsorption studies O_2 and H_2 were found at the opposite ends of the trend ($O_2 > C_3H_6 > H_2$), the combination of these two equilibrium constants did not allow the comparison with the equilibrium constant of propene.

Another kinetic model was derived and a rate expression was formulated based on the reaction mechanism presented in Scheme 6.13. In the rate expression for the propene oxide formation, Oyama et al. [88] introduced the consumption of H_2O_2 to H_2O as an addition to the reaction mechanism from the Scheme 6.13. Three separate rate expressions were resolved simultaneously to provide the propene oxide formation rate. The processes considered were:

1. H_2O_2 synthesis on Au nanoparticles according to the mechanism of Barton and Podkolzin [16].
2. Separate adsorption steps for H_2O_2 and propene on Ti with a rate determining step in formation of propene oxide.
3. The decomposition of H_2O_2 to H_2O considered to be a first order reaction.

These steps are schematically given in Figure 6.8.

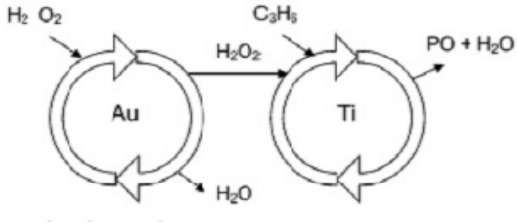

Figure 6.8. Schematic representation of a proposed epoxidation reaction mechanism where three separate reactions are simultaneously contributing to the overall rate for the propene oxide formation. Reproduced from Bravo-Suárez et al. [88].

This model offered a good fit and a high statistical probability, but as in the case of the previous model it could not be confirmed by the adsorption data. It is important to be mentioned that this model can be simplified to an identical rate equation as the one derived from the model proposed by the group of Delgass [85]. These results indicate that a reaction mechanism can not be validated from the rate expression only since different reaction models and assumptions can lead to the same mathematical expression. It is also important to mention that the adsorption measurements were performed for individual gases, but the rate parameters were expressed for the reaction conditions.

6.3.2. Kinetic studies on the epoxidation mechanism over Au/TiO_2 catalysts

The challenge in studying the kinetics of the Au/TiO_2 catalyst is related to the fact that this catalyst system is deactivating much faster than Au/Ti-SiO_2. Therefore, the measurements cannot be performed under steady-state conditions. Nevertheless, a reaction model has been developed by Nijhuis et al. [90]. In this model, it is considered that Au nanoparticles activate propene adsorption on Ti with the formation of a bidentate propoxy species as well as produces H_2O_2. Furthermore, the peroxide species produced on Au promotes the desorption of the bidentate propoxy species from the catalyst surface with the formation of propene oxide. The determination of the activation energy or kinetic constant of this catalytic system is, however, difficult. As shown in Figure 6.9, at low temperature, the products are observed after almost 30 min from the beginning of the epoxidation reaction, because of the slow desorption from the catalyst surface. Also the catalytic activity of Au/TiO_2 is decreasing gradually.

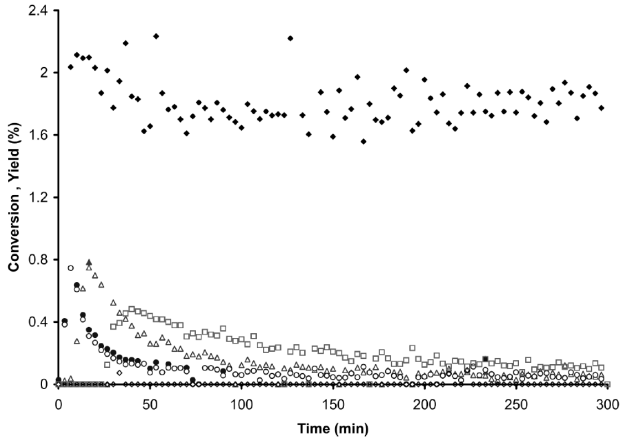

Figure 6.9. Catalytic performance of Au/TiO_2. Conversion (closed symbols) and yield (open) at 50º C (□), 70º C (Δ), 90º C (○), and 150º C (●) (pressure 1.1 bar, GHSV 9000 $m^3_{gas}/(m^3_{cat}h)$) (yield and conversions largely overlap for experiments at 50º C and 70º C). Reproduced from Nijhuis et al. [90].

By comparing the steady-state activity of Au/TiO_2 at different temperatures, the propene oxide production rate appears to be higher at lower temperatures, resulting in a negative value of the apparent activation energy. This is not likely because at the beginning of the catalytic cycle, the propene oxide production is increasing with increasing temperature. Since Au/TiO_2 is deactivating quite fast, the apparent negative activation energy can be explained by the fact that the activation energy of the deactivation process is higher than the activation energy of the epoxidation. Thus, the kinetic model developed by Nijhuis et al. considers both the reaction and catalyst deactivation processes for the calculation of the kinetic parameters [90]. In the kinetic model, the catalytic experiments at temperatures lower than 100º C were considered since it is known that at higher temperatures, the selectivity of Au/TiO_2 catalysts is decreasing. This is causing the amount of propene oxide formed to be close to zero and makes the kinetic evaluation very difficult. In this model, the rate determining steps of the epoxidation reaction are considered to be the propene oxide desorption and formation of the peroxide species on Au [91, 92]. In the other kinetic models discussed above, the rate determining steps were considered to be the H_2O_2 formation on Au and the epoxidation reaction on Ti. Based on the FT-IR results, the predominant species on the Au/TiO_2 catalyst surface is considered to be adsorbed propene oxide in the form of bidentate propoxy species [24-26]. If one would assume that peroxide species need to be formed to aid desorption of propene oxide/bidentate propoxy and that the formation of these peroxide species would be the rate-determining step, this does imply that the concentration of the peroxide species is very low and its formation is actually the rate determining step. As a consequence, the rate determining step in this mechanism is actually in agreement with most other reports in literature.

Based on all this, a reaction mechanism has been proposed as given in Scheme 6.14. According to this mechanism, lattice oxygen (equation 1, Scheme 6.14) participates into the

oxidation of hydrocarbon molecules in a similar manner as the Mars-van Krevelen mechanism, in which lattice oxygen is replenished by gas-phase oxygen. In the FT-IR measurements it was observed that these bidentate propoxy species are formed in the absence of any source of oxygen ande only source of oxygen that could be involved in the formation of the bidentate propoxy species was considered to be the oxygen from the TiO_2 support [24].

1. $C_3H_6 + 2Ti_{Au} + 2\ O_{TiO_2} \longrightarrow BPS_{Au}$
2. $H_2 + O_2 + Au \longrightarrow Au\text{-}HOOH$
3. $Au\text{-}OOH + BPS_{Au} \longrightarrow PO + H_2O + Au + 2\ Ti_{Au} + 2\ O_{TiO_2}$
4. $BPS_{Au} + x\ O_{TiO_2} \longrightarrow 2\ Ti_{Au}\text{-}Carbox$
5. $PO + 2\ Ti_{Au} + O_{TiO_2} \longrightarrow BPS_{Au}$
6. $PO + 2\ Ti_{Ti} + O_{TiO_2} \longrightarrow BPS_{Ti}$

C_3H_6 gas phase propene
BPS bidentate propoxy species
Ti Titania site (Ti-O-Ti)
O lattice oxygen
PO gas phase propene oxide
Carbox carbonate/ carboxylate species
X value> 0 (oxygen consumed for BPS oxidation)
Subscript

Au neighboring Au particle
Ti on the bulk Ti no neighboring Au
TiO_2 (oxygen) originating from Ti support

Scheme 6.14. Schematic representation of a proposed mechanism for the propene epoxidation reaction over Au/TiO_2 catalysts. Reproduced from Nijhuis et al. [90].

Oxidation of the bidentate propoxy species to carbonate and carboxylate species (sequence 4, Scheme 6.14) was observed with FT-IR [24]. For the determination of the kinetic parameters, the concentration of propene oxide from the gas phase as well as adsorbed and reacted on was considered. The concentration of the reactants was assumed to be constant. A plug flow reactor was considered to explain best the results of the strong adsorption of propene oxide on the Au/TiO_2 surface. Different equations were solved to determine the transient behavior of the Au/TiO_2 catalyst in the reactor. The site regeneration step was integrated in an equation to calculate the residual activity of the catalyst due to the desorption of few deactivating species and to determine the concentration of the side products.

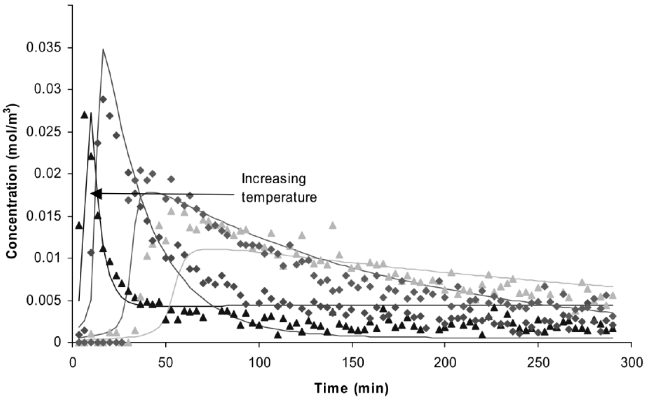

Figure 6.10. Comparison between measured and modeled behavior of 1 wt% Au/TiO_2 catalyst for the epoxidation of propene at different reaction temperatures (GHSV = 9000 $m^3_{gas}/(m^3_{cat}\ h)$, T = 42º C- 93º C). Reproduced from Nijhuis et al. [90].

This proposed model, which includes catalyst reactivation, can well describe the measured catalytic performance. The only problem is that at higher reaction temperatures the model overpredicts the propene oxide production, as shown in Figure 6.10. The proposed reaction model is in line with the kinetic equations, but the same equations are also valid if another mechanism in which propene is oxidized on Ti by the peroxide species formed on Au is modeled. The propene oxide will readsorb and further oxidized to carbonate and carboxylate species.

6.4. Spectroscopic studies of the propene epoxidation with O_2 and H_2 over Au/Ti-based catalysts

The reaction mechanism of propene epoxidation with H_2 and O_2 over Au/Ti-based catalysts was investigated by Nijhuis et al. using in-situ FT-IR spectroscopy [24-26]. Intense FT-IR bands (Figure 6.11) corresponding to the formation of the bidentate propoxy species appeared in a short time from the beginning of the propene epoxidation reaction. These bands were also observed when the Au/TiO_2 was simply exposed to propene in He, but their intensities were much lower than that of bidentate propoxy species formed during propene epoxidation reaction [24]. The bidentate propoxy species formed during epoxidation reaction were slowly oxidized on the Au/TiO_2 surface. However, the rate at which the bands intensity of the bidentate propoxy species decreased in intensity was higher than the formation of the oxidized species, indicating that desorption of some bidentate propoxy species occurred.

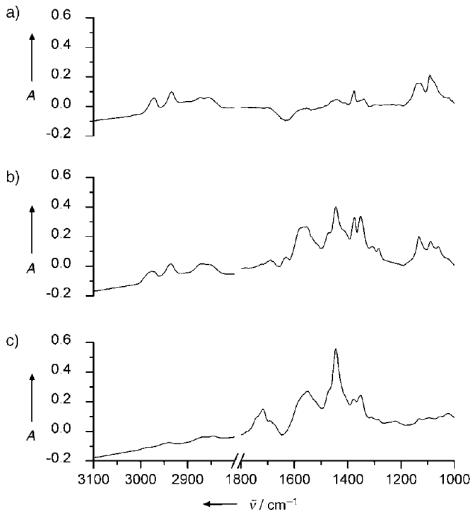

Figure 6.11. FT-IR spectra recorded after 3 min under a gas stream comprising 10% propene, 10% H_2, 10% O_2, and He (50^o C). a) 3 min after removal of propene; b) after 3 h; c) 30 min after the temperature was increased to 100^o C (50 spectra averaged). Reproduced from Nijhuis et al. [24].

Increasing the temperature to 100º C in the presence of H_2 and O_2 resulted in the complete disappearance of the C-O-Ti vibrations of the bidentate propoxy species and only the corresponding

carbonate and carboxylate bands remained. This was not the case when a similar experiment was performed in a He stream [24]. This was considered to be an indication that H_2 and O_2 facilitates the desorption of the bidentate propoxy species, possibly by producing peroxo species. It was considered that desorption could not occur because of the H_2O formation from H_2 and O_2 since gravimetrical experiments showed that H_2O could not displace adsorbed propene oxide [25]. It was not clear if propene oxide is produced after desorption of bidentate propoxy species, but because it is the only carbon containing product that was observed during the propene epoxidation over Au/TiO_2 at 50º C it was assumed that propene oxide is formed upon desorption of bidentate propoxy species.

Even if the formation of the peroxide species was not observed by Nijhuis [25] using Raman and FT-IR these species where considered to be produced by Au based on literature reports [16, 17]. The peroxide species were considered to aid the desorption of the propene oxide from the catalyst surface. Therefore, the reaction intermediates in the propene epoxidation reaction over Au/Ti-based catalysts were considered to be the peroxide species and bidentate propoxy species.

The group of Oyama [31] performed in-situ FT-IR under propene epoxidation conditions over a Au/Ba-Ti-TUD catalyst. The FT-IR bands characteristic to bidentate propoxy species, formate and acetate species were also detected on this catalyst material. The intensity of the FT-IR bands characteristic to these species did not increase during the epoxidation reaction. These species were formed at the beginning of the catalytic reaction, correlating with the initial decrease in activity before the catalyst reached a steady-state situation. Therefore, bidentate propoxy species were not considered to be reaction intermediates. The results suggest that the bidentate propoxy species strongly adsorb on a few adjacent Ti sites that would otherwise be involved in the formation of propene oxide [31]. It was concluded that propene oxide production via reaction of bidentate propoxy species adsorbed on Ti-O-Ti sites, proposed by Nijhuis et al. for Au/TiO_2 [25,26,90], is very unlikely to occur on the Au/Ba-Ti-TUD catalyst. This catalyst contains small loadings of Au and Ti highly dispersed and mostly isolated in the TUD framework, which is different than Au/TiO_2, which contains 10 times higher Au loading compared to Au/Ba-Ti-TUD.

In a recent study, the group of Iglesia [93] provides experimental evidence for the ability of Au/TiO_2 to form hydroperoxy species. As well, the hydroperoxide species are considered to be reaction intermediates. Au/TiO_2 at 300-350 K was able to produce propene oxide with a selectivity of ~ 80 % by using a H_2O/O_2 mixture instead of H_2 and O_2. Both H_2O and O_2 are necessary to form the hydroperoxy species considered to be the intermediates in the propene epoxidation reaction. Au/TiO_2 did not form any propene oxide from C_3H_6/O_2 and C_3H_6/H_2O reactant mixtures. In the literature, it was showed that O_2/H_2O mixtures can form HOO* species via the microscopic reverse of elementary steps for H_2O_2 decomposition [14]. The formation of hydroperoxy species was

explained to occur by coupling their kinetics with the propene epoxidation steps that scavenge HOO* intermediates to form propene oxide [93].

In-situ UV-Vis spectroscopy in combination with in-situ Ti K-edge XANES measurements during the propene epoxidation with H_2 and O_2 over a Au/Ba-Ti-TUD were reported by Bravo-Suárez et al. [31]. They identified the formation of Ti-OOH species during this reaction. The hydroperoxo species are considered to be true intermediates in the epoxidation reaction [94]. During the in-situ UV-Vis diffuse reflectance measurements of the Au/Ba-Ti-TUD catalyst for 8 h of reaction in the presence of a $C_3H_6/H_2/O_2/Ar$ = 1/1/1/7 gas mixture it was observed that a band in the 400-264 nm region of the spectra is appearing and is also growing in intensity. Deconvolution of this absorption band yields a major band centered at 330 nm assigned to Ti-hydroperoxo species and bands centered at 275 nm and 307 nm due to the water coordination to Ti. In Figure 6.12, it is shown that the intensity of the absorption band at 330 nm, corresponding to Ti-OOH species, is much lower when the spectra are recorded during epoxidation reaction compared to hydrogen oxidation.

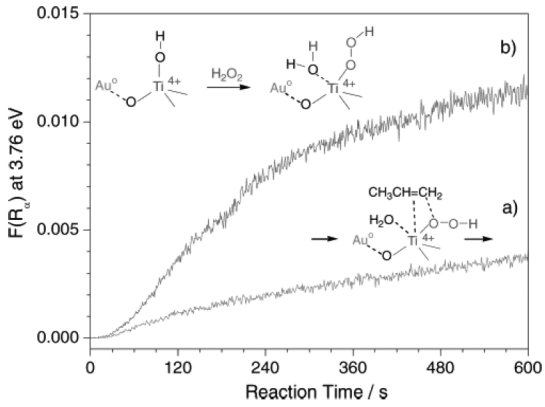

Figure 6.12. In-situ UV-Vis spectroscopy results at 3.76 eV (330 nm) for Au-Ba/Ti-TUD (9) under (a) $C_3H_6/H_2/O_2/Ar$) 1/1/1/7 (bottom) and (b) $H_2/O_2/Ar$) 1/1/8 (top) at 150º C and 0.1 MPa during the first 600 s of reaction. Reference is sample at 150º C under Ar flow before reaction. Reproduced from Bravo-Suárez et al. [94].

The low intensity of the band at 330 nm during the propene epoxidation was explained to be the result of the reaction between Ti-OOH species and adsorbed propene [31]. Nevertheless, the low intensity could be also explained by propene adsorbing on the Au sites. The H_2O_2 formation will be inhibited by the presence of adsorbed propene on Au sites, thus the intensity of the band corresponding to Ti-OOH species will be low. We have observed, as discussed in detail in **Chapter 4** of this PhD thesis, that H_2O formation rate is strongly inhibited when propene is co-fed during H_2 oxidation over Au/SiO_2 and Au/TiO_2 catalysts. The in-situ XANES results revealed that propene is π-bonding to Au nanoparticles during the epoxidation reaction and, therefore, is competing on the same sites with H_2O_2 formation [22]. The intensity of the absorption band centered at 330 nm was observed to quickly drop when the sample was flushed with Ar after the H_2 oxidation reaction. This

was related with the decomposition of the hydroperoxo species. Furthermore, the intensity of this band decreased even further when propene was flushed over the Au/Ba-Ti-TUD catalyst. In-situ XANES spectroscopy measurements at the Ti-K-edge provides information on both the oxidation state and local geometry of Ti. The intensity of the pre-edge peak was used to measure the increase in the coordination of Ti due to the adsorption of reactants. An increase in coordination of Ti due to the adsorption of reactants decreases the intensity of the pre-edge peak in direct proportion to the adsorbed amount. This was used to measure the coverage θ. The coverage was defined as the fractional decrease in the pre-edge peak area from its value before the introduction of reactants [31]. The results of the coverages on tetrahedral Ti sites in the first 1.5 h of the H_2 oxidation and epoxidation reactions are presented in the Figure 6.13.

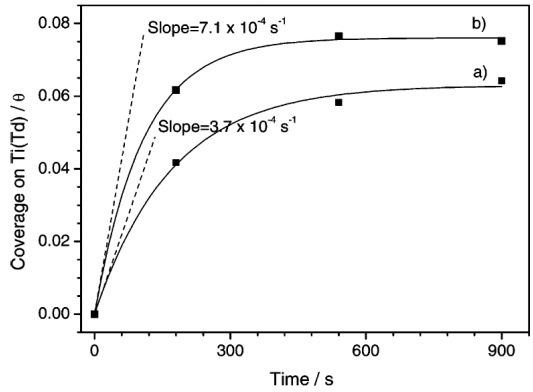

Figure 6.13. Coverage on 4-fold coordinated Ti (θ, fractional decrease of pre-edge peak area in the Ti K-edge XANES spectra) for Au-Ba/Ti-TUD under (a) $C_3H_6/H_2/O_2/Ar$ = 1/1/1/7 (bottom) and (b) $H_2/O_2/Ar$ = 1/1/8 (top) at 150^o C and 0.1 MPa during the first 900 s of reaction. Reproduced from Bravo-Suárez et al. [94].

The higher coverage values under H_2 oxidation conditions were explained to be the result of the Ti-hydroperoxo species formation. The lower coverage values under propene epoxidation conditions were explained to be due to the reaction of Ti-OOH species with propene. The coverages of the tetrahedral Ti^{4+} sites during H_2 oxidation and epoxidation reaction were used to calculate the rate of reaction of the hydroxide species in the propene epoxidation. The decomposition of these species was also estimated from the UV-Vis diffuse reflectance spectroscopy measurements. The net rate of the epoxidation reaction was calculated to be 3.4 x $10^{-4}s^{-1}$. This value was determined from Figure 6.13 by using the values of the Ti coverage θ. The calculated rate was close to the TOF value of 2.5 x $10^{-4}s^{-1}$ determined at steady state conditions for the Au/Ba-Ti-TUD catalyst. Based on these results Ti-hydroperoxide species were considered to be true reaction intermediates in the propene epoxidation with H_2 and O_2 [31].

6.5. Importance of the Au/Ti interface and deactivation of Au/Ti-based catalysts

The importance of the presence of both Au and Ti in a catalytic system to selectively catalyze the propene epoxidation reaction was evidenced by Iglesia et al. [93]. Propene oxide could

not be synthesized by using $C_3H_6/O_2/H_2$ and $C_3H_6/O_2/H_2O$ over a physical mixture of a Au/Al_2O_3 catalyst and a bare TiO_2 support. It was considered that Au and Ti must be in close proximity since propene oxide could not be synthesized otherwise. Thus, the catalytic epoxidation reaction over Au/TiO_2 must take place at the interface between Au and Ti. The group of Campbell [94] underlined as well the importance of the Au/Ti interface as being the energetically most favorable site for propene adsorption and reaction. The adsorption of propene on rutile TiO_2(110) and on Au islands dispersed on TiO_2(110) at -153º C has been studied by using temperature programmed desorption (TPD), X-ray photoelectron spectroscopy (XPS) and He^+ low energy ion scattering spectroscopy (LEIS) [94]. The results point towards the existence of three sites for propene adsorption: On the top of Au islands, on the TiO_2 (110) surface and at the edges of the Au islands at the Au/Ti interface. Their model suggests that propene hits the surface and because the molecule is mobile it is ending up at the lowest energy sites, which are located at the perimeter of the Au islands. At the lowest doses of propene, all molecules landing on bare TiO_2 (110) and on top of Au islands migrates to the energetically most favorable sites at the Au/Ti interface. At higher doses of propene and with these Au/Ti perimeter sites filled, the propene molecules leading either on the TiO_2 (110) surface or the Au islands tops get trapped there. It was shown that the size of Au islands does significantly affect the binding energy of propene. The particle size effect observed for propene epoxidation rates was considered to be at least partially due to the effect of Au island size on the propene binding energy. Oxygen adsorption experiments [95] point towards stronger binding on smaller, thinner Au islands. Thus, the Au particle size effect observed for propene epoxidation rates is related with the binding energy of both oxygen and propene. Based on these observations it was suggested that, in the epoxidation reaction the oxidant produced on Au islands reacts with propene adsorbed at the Au/Ti interface [94].

Although Au/TiO_2 catalysts are able to epoxidise propene very selectively using O_2 and H_2 under mild conditions, catalyst instability is one of the major problems of these materials. FT-IR spectroscopic studies revealed that the accumulation of carbonates and carboxylates species on the surface of the catalyst during epoxidation reaction is responsible for the deactivation of Au/TiO_2 [24-26]. Bidentate propoxy species over time are undergoing consecutive oxidation to carbonates and carboxylates (Figure 6.14) when propene is adsorbed on Au/TiO_2, even when the catalyst is kept in He. This oxidation was considered to be catalyzed by Au since the formation of carbonate and carboxylate species did not occur on bare TiO_2 by adsorbing propene oxide. The carboxylate species could be completely removed only by heating the catalyst in the presence of O_2 at temperatures higher than 300º C [24-26]. The carbonates/carboxylates could not be observed on the $Au/Ti\text{-}SiO_2$ (OX-50), which is an indication that not only Au is participating into the formation of

these species. Since the formation of these species was observed to occur when propene was adsorbed on Au/TiO_2 in He this may imply that oxygen from TiO_2 support is contributing to the oxidation of bidentate propoxy species.

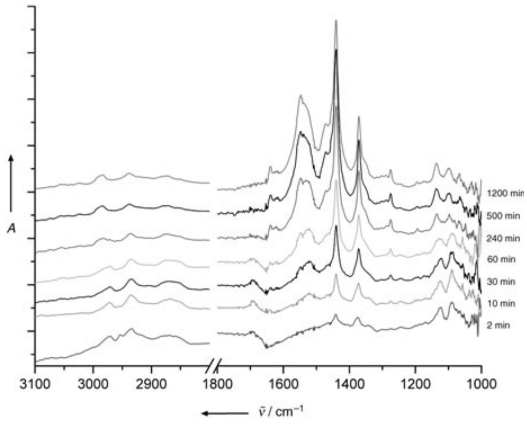

Figure 6.14. Gradual oxidation of a bidentate propoxy species on the Au–titania catalyst. Spectra were recorded from 2 to 1200 min after exposure of the catalyst to propene for 2 min (50° C; 10 spectra averaged). Reproduced from Nijhuis et al. [24]

This suggests that contrary to Au/TiO_2, the oxygen from the support of $Au/Ti\text{-}SiO_2$ is not participating in the oxidation of the bidentate propoxy species. The accumulation of high amounts of bidentate propoxy species strongly adsorbed on Ti-O-Ti sites as well as their oxidation to carbonates and carboxylates is contributing to the deactivation of Au/TiO_2 catalysts [24-26,96].

6.6. Proposed reaction mechanisms for the epoxidation of propene with H_2 and O_2

It is of interest to connect the knowledge provided by the many theoretical, kinetic and spectroscopic studies reported in the open literature and to see the similarities and differences between the differently proposed reaction mechanisms for the propene epoxidation with H_2 and O_2 over Au/TiO_2 catalysts. The true mechanism may even be a combination of what has been proposed so far. An initial attempt to do so is given in Scheme 9.15 and is mainly based on the work of the Nijhuis and co-workers.

The reaction mechanism consists of the following steps:

1. Propene is first adsorbed on Au;
2. Propene spillover on titania to produce adsorbed bidentate propoxy species. These species are formed with oxygen from the support;
3. Hydrogen and oxygen produce hydroperoxide species on Au; and

The peroxide species aids in desorption of the bidentate propoxy species from the catalyst, producing propene oxide and water and restoring the catalyst in its original state. Propene oxide is containing the oxygen from the support.

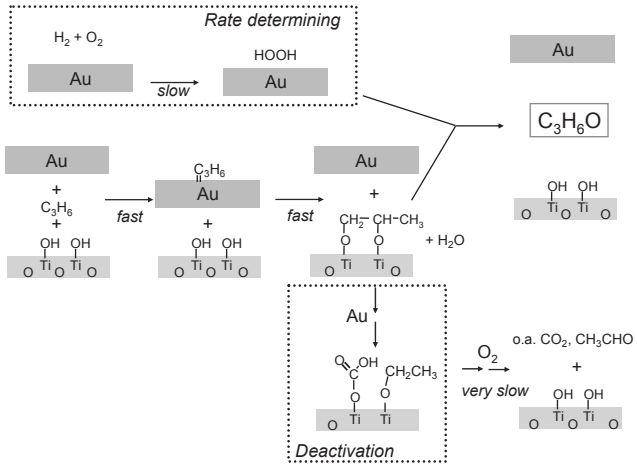

Scheme 6.15. Mechanism proposed for the epoxidation of propene over a Au-titania catalyst, as discussed in Chapter 4.

In this model it is considered that the role of Au is to adsorb and activate propene, that will spillover to titania to form bidentate propoxy species, as discussed in **Chapter 4** of this PhD thesis, and also to form H_2O_2 out of H_2 and O_2. The adsorption of propene on Au nanoparticles was experimentally identified by using in-situ XANES spectroscopy [22]. Secondly, the formation of bidentate propoxy species as propene adsorbs on titania sites near Au particles was identified with FT-IR [24]. In this mechanism, lattice oxygen is assumed to participate to the oxidation of propene since in FT-IR it was observed that the bidentate propoxy species are formed in the absence of gas phase O_2 [26]. The third step, the synthesis of H_2O_2, is assumed to occur on Au sites. This assumption is based on experimental results where it was showed that supported Au catalysts are selective in the formation of H_2O_2 from H_2 and O_2 [14, 15, 82]. In the fourth step, H_2O_2 species are used to desorb the bidentate propoxy species to produce propene oxide, as has been deduced from FT-IR experiments [24, 26]. As a side reaction, the bidentate propoxy can be oxidized further and this reaction is catalyzed by Au nanoparticles. The oxidation of the bidentate propoxy species is one of the causes of catalyst deactivation. The surface species formed by this consecutive oxidation are strongly adsorbed and only desorb very slowly or during catalyst regeneration by heating the catalyst in the presence of O_2 [26].

The group of Oyama [31] proposed a different mechanism than the one described above, in which based on their theoretical, kinetic and spectroscopic results lead to a reaction pathway outlined in Scheme 6.16. This reaction mechanism consists of the following reaction steps:

1. Synthesis of H_2O_2 from H_2 and O_2 on Au nanoparticles;
2. Formation of Ti-hydroperoxo or peroxo species from hydrogen peroxide on tetrahedral Ti sites;

3. Reaction of propene with the Ti-hydroperoxide species to form propene oxide; and
4. Decomposition of H_2O_2 into H_2O.

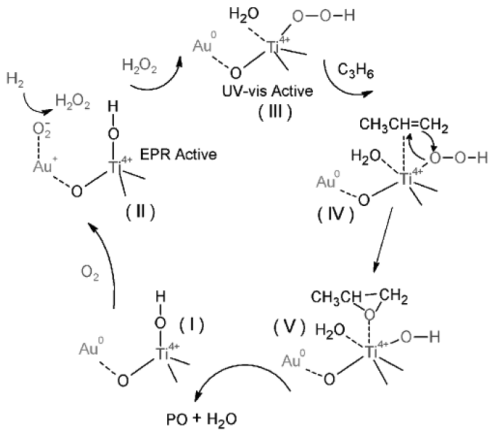

Scheme 6.16. Possible sequence of steps for propene epoxidation with H_2 and O_2 on Au-supported titanosilicates. Reproduced from Bravo-Suárez et al. [31].

The first step in this reaction mechanism is based on EPR measurements. The formation of ($O_2^{\bullet -}$) species was explained to be facilitated by Au since no paramagnetic species were formed on the support alone [18]. Under reaction conditions Ti-hydroperoxo species can be formed by the transfer of H_2O_2 from the Au surfaces to Ti^{4+} sites. The second step, the formation of Ti-hydroperoxide species during the propene epoxidation over an Au/Ti-SiO_2 was evidenced with in-situ UV-Vis spectroscopy [31]. The UV-Vis bands characteristic of Ti-OOH species did not appear when the epoxidation reaction was carried out on the titanosilicate support alone. These observations underline the role of Au on the hydroperoxo species formation and propene oxide production, since no propene oxide could be synthesized on a bare titanosilicate support. The Ti-OOH species are considered to be intermediates in this reaction becuase it was demonstrated that this species reacts at the same overall rate of reaction. The coordination of propene to Ti^{4+} sites was not spectroscopically observed. The third step, the epoxidation reaction was assumed to take place on Ti sites. This step was considered to occur because the value of the reaction rate of 3.4 x 10^{-4} s^{-1} calculated from the coverage of tetrahedral Ti^{4+} sites during the epoxidation is very close to the TOF of 2.5 x 10^{-4} s^{-1} of a Au/Ti-SiO_2 catalyst determined at steady-state [31].

Although significant progress has been achieved in studying the mechanism of Au/Ti-based catalysts, it is still not very clear which are exactly the intermediates and spectators observed during reaction. In the two reaction mechanisms discussed above it is assumed that one of the key role of Au is to produce peroxide species. However, in the proposed mechanisms, these peroxide species were considered to have different functions. Bravo-Suárez et al. [31] suggested that the role of peroxo species is to directly react with adsorbed propene towards the formation of propene oxide. It is important to be mentioned that these species and propene oxide were formed only when Au was

present on the titanosilicate support. The formation of Ti-OOH species upon interaction of H_2O_2 with TS-1 has been also evidenced with UV-Vis, FT-IR and EPR spectroscopy [20]. The loss of characteristic bands of propene and Ti-OOH during the liquid phase epoxidation of propene with H_2O_2 and the formation of new bands characteristic to propene oxide indicated that these species are directly involved in the epoxidation of propene with H_2O_2. This study also evidenced the presence of an oxygen from the peroxo species in the propene oxide when $H_2{}^{18}O_2$ treated TS-1 was exposed to propene. Considering these findings there is no doubt that Ti-OOH species are formed after interaction with in-situ produced H_2O_2 to Ti sites during the propene epoxidation with H_2 and O_2 over Au/Ti based catalysts. Even if the group of Oyama considered that Ti-OOH species are reaction intermediates and that the epoxidation reaction is taking place on Ti^{4+} sites there is to the best of our knowledge no experimental evidence about the coordination of propene to these sites and where the epoxidation reaction is taking place [31]. In view of the kinetic results the epoxidation reaction can take place not only on Ti sites but also on the Au/Ti interface.

On the other hand, Nijhuis and co-workers have considered that the role of peroxo species is to aid the reactive desorption of the bidentate propoxy species to produce propene oxide. This assumption originates from the fact that in the in-situ FT-IR measurements it was observed that these species are partly desorbed and partly oxidized in the presence on O_2 and H_2, thus indicating that desorption of these species is occurring. Due to the fact that the bidentate propoxy species were generated in the absence of any oxygen source, it was assumed that oxygen from the support is participating to the oxidation of propene with the formation of bidentate propoxy species, which are considered to be the precursors of propene oxide. However, it is unclear if indeed the oxygen from the support is ending up in propene oxide. This could not be determined conclusively from the SSITKA measurements, which are discussed in **Chapter 5** of this PhD thesis.

It was also observed that the bidentate propoxy species formed on Au/TiO_2 catalyst undergo oxidation, in He atmosphere, to carbonates/carboxylates, which indicates that support oxygen is probably used to oxidize these species [24]. The oxidation of bidentate propoxy species towards carbonates/carboxylate was also considered to be catalyzed by Au, since the bidentate propoxy species did not undergo oxidation on bare TiO_2 support. The observation that on $Au/Ti\text{-}SiO_2$ catalyst, carbonates/carboxylates did not form in a He atmosphere suggests that the oxygen from the $Ti\text{-}SiO_2$ support is not involved in the oxidation of bidentate propoxy species. It is somehow unclear why the carbonates/carboxylates are formed only on a Au/TiO_2 catalyst and not on a $Au/Ti\text{-}SiO_2$ catalyst, because this reaction was observed to occur only in the presence of Au on TiO_2. This might be due to different catalytic sites on the surface on these materials as well different number of reducible sites and probably different Au/TiO_2 interactions. Temperature-programmed desorption

measurements of propene and propene oxide adsorbed on Au/TiO_2 and $Au/Ti\text{-}SiO_2$ catalysts confirmed that the site density for adsorption is much higher on TiO_2 than on the titanosilicate support [31]. The group of Oyama [31] detected as well with in-situ FT-IR spectroscopy the formation of bidentate propoxy species and of formate and acetate species on Au/Ba-Ti-TUD catalyst under working conditions. However, the spectroscopic results suggested that the bidentate propoxy species are just spectators and they adsorb strongly only on Ti-O-Ti sites that would otherwise be involved in the formation of propene oxide.

In both mechanisms, it was suggested that the formation and accumulation of carbonates/carboxylates on the surface is responsible for the Au/TiO_2 catalyst deactivation. Although these species are formed on $Au/Ti\text{-}SiO_2$, they are produced in lower amounts than on the Au/TiO_2 surface, because $Au/Ti\text{-}SiO_2$ contains a low number of Ti-O-Ti sites, Ti being well dispersed in the SiO_2 support. Combining all the spectroscopic results, the role of Au in the propene epoxidation was suggested to be associated with the production of H_2O_2, propene adsorption and activation towards formation of bidentate propoxy species and with the synthesis of propene oxide. The role of surface Ti sites was assumed to be related with ability of performing epoxidation reaction and with the stabilization of the bidentate propoxy species.

6.7. Concluding remarks and Future Perspectives

Au/Ti-based materials have shown to be promising catalysts for the epoxidation of propene with H_2 and O_2. However, the complexity of the Au/Ti-based catalysts makes it difficult to understand the true nature of their catalytic activity. It is known that Au nanoparticles of less than 5 nm in size are active in the propene epoxidation, but the reason for this activity evokes still a lot of questions. Variation of the Au particle size results in the variation of the Au–support contact area, which can modify the chemisorption properties of the supported Au nanoparticles and most probably the energetics of the Au/Ti interface.

Despite all detailed kinetic investigations, there is still insufficient information to allow the formulation of a unifying and detailed reaction mechanism. Although there seems to be a consensus based on spectroscopic results why Au/Ti-based catalysts are partially or completely losing their catalytic activity during the epoxidation reaction, there is not yet clear evidence on how propene oxide is produced. Propene oxide is proposed to be formed from the desorption of the bidentate propoxy species or from the reaction of hydroperoxo species with propene. It is still under discussion if the bidentate propoxy species are intermediates or just spectators and arguments in favour of both hypothesis are put forward in the literature. Furthermore, it has still to be determined where exactly the propene epoxidation reaction is taking place, i.e., at the interface between Au and Ti or at Ti sites, or maybe simply both. In other words, new spectroscopic, surface science and

theoretical approaches have to be developed for further understanding the epoxidation reaction mechanism. Such studies should be extended to catalyst materials that contain well-defined Au and Ti sites. New Au/Ti-based catalysts need therefore to be prepared by using new synthesis methods that will allow to precisely control the Au particle size as well as their particle size dispersion. As recently shown by the Iglesia group [93] new oxidant mixures may be used as well for the propene epoxidation reaction, which may give new information regarding the reaction mechanism. In other words, understanding how exactly the epoxidation reaction is occurring on Au/Ti-based catalysts, on which sites the molecules are efficiently adsorbed, and where the catalytic reaction is taking place, may allow to prepare more efficient Au/Ti-based catalyst materials in the years to come.

References

1. N. Yap, R.P. Andres, W.N. Delgass, J. Catal., 226 (2004) 156.
2. E.E. Stangland, B. Taylor, R.P. Andres, W.N. Delgass, J. Phys. Chem. B, 109 (2005) 2321.
3. B. Taylor, J. Lauterbach, W.N. Delgass, Appl. Catal. A: General, 291 (2005) 188.
4. B.S. Uphade, M. Okumura, S. Tsubota, M. Haruta, Appl. Catal. A: General, 190 (2000) 43.
5. B.S. Uphade, Y. Yamada, T. Akita, T. Nakamura, M. Haruta, Appl. Catal. A: General, 215 (2001) 137.
6. B.S. Uphade, T. Akita, T. Nakamura, M. Haruta, J. Catal., 209 (2002) 331.
7. E. Sacaliuc, A.M. Beale, B.M. Weckhuysen, T.A. Nijhuis, J. Catal., 248 (2007) 235.
8. E. Sacaliuc-Parvulescu, H. Friedrich, R. Palkovits, B.M. Weckhuysen, T.A. Nijhuis, J. Catal., 259 (2008) 43.
9. A.K. Sinha, S. Seelan, M. Okumura, T. Akita, S. Tsubota, M. Haruta, J. Phys. Chem. B, 109 (2005) 3956.
10. G.C. Bond, C. Louis, D.T. Thompson, "Catalysis by Gold – Catalytic Science Series Vol. 6", Ed. G.J. Hutchings, Imperial College Press, London (2006).
11. M. Valden, X. Lai, D.W. Goodman, Science, 281 (1998) 1647.
12. G.C. Bond, D.T. Thompson, Gold Bull., 33 (2000) 41.
13. M. Haruta, Gold Bull., 37 (2004) 27.
14. P. Landon, P.J. Collier, A.J. Papworth, C.J. Kiely, G.J. Hutchings, Chem. Commun., (2002) 2058.
15. M. Okumura, Y. Kitagawa, K. Yamagcuhi, T. Akita, S. Tsubota, M. Haruta, Chem. Lett., 32 (2003) 822.
16. D.G. Barton, S.G. Podkolzin, J. Phys. Chem. B, 109 (2005) 2262.
17. T.A. Nijhuis, B.M. Weckhuysen, Prep. Pap.-Am. Chem. Soc., Div. Petr. Chem., 52 (2007) 292.

18. B. Chowdhury, J.J. Bravo-Suárez, N. Mimura, J.Q. Lu, K.K. Bando, S. Tsubota, M. Haruta, J. Phys. Chem. B, 110 (2006) 22995.
19. V.N. Shetti, P. Manikandan, D. Srinivas, P. Ratnasamy, J. Catal., 216 (2003) 461.
20. W. Lin, H. Frei, J. Am. Chem. Soc., 124 (2002) 9292.
21. M. Okumura, J.M. Coronado, J. Soria, M. Haruta, J.C. Conesay, J. Catal., 203 (2001) 168.
22. T.A. Nijhuis, E. Sacaliuc, A.M. Beale, A.M.J. van der Eerden, J.C. Schouten, B.M. Weckhuysen, J. Catal., 258 (2008) 256.
23. G. Mul, A. Zwijnenburg, B. van der Linden, M. Makkee, J. Moulijn, J. Catal., 201 (2001) 128.
24. T.A. Nijhuis, T. Visser, B.M. Weckhuysen, Angew. Chem. Int. Ed., 44 (2005) 1115.
25. T.A. Nijhuis, T. Visser, B.M, Weckhuysen, J. Phys. Chem. B, 109 (2005) 19309.
26. T.A. Nijhuis, B.M. Weckhuysen, Catal. Today, 117 (2006) 84.
27. G.J. Hutchings, Chem. Commun., (2008) 1148.
28. A.M. Joshi, W.N. Delgass, K.T. Thomson, J. Phys. Chem. B, 109 (2005) 22392.
29. M.G. Clerici, G. Bellussi, U. Romano, J. Catal., 129 (1991) 159.
30. D.H. Wells, W.N. Delgass, K.T. Thomson, J. Am. Chem. Soc., 126 (2004) 2956.
31. J.J. Bravo-Suárez, K.K. Bando, J.Lu, M. Haruta, T. Fujitani, S.T. Oyama, J. Phys. Chem. C, 112 (2008) 1115.
32. D.R.C. Huybrechts, L.D. Bruycker, P.A. Jacobs, Nature, 345 (1990) 240.
33. M.G. Clerici, P. Ingallina. J. Catal., 140 (1993) 71.
34. J.S. Reddy, R. Kumar, P. Ratnasamy, Appl. Catal., 58 (1990) L1.
35. D.P. Serrano, L. Hong-Xin, M.E. Davis, J. Chem. Soc., Chem. Commun., (1992) 745.
36. A. Corma, M.A. Camblor, P. Esteve, A. Martinez, J. Pérez-Pariente, J. Catal., 145 (1994) 151.
37. M.A. Camblor, M. Costantini, A. Corma, L. Gilbert, P. Esteve, A. Martinez, S. Valencia, Chem. Commun., (1996) 1339.
38. J.C. van der Waal, P.J. Kooyman, J.C. Jansen, H. van Bekkum, Micropor. Mesopor. Mater., 25 (1998) 43.
39. A. Corma, M.T. Navarro, J. Pérez-Pariente, J. Chem. Soc., Chem. Commun., (1994) 147.
40. P.T. Tanev, M. Chibwe, J.T. Pinnavaia, Nature, 368 (1994) 321.
41. K.A. Koyano, T. Tatsumi, Chem. Commun., (1996) 145.
42. M.S. Morey, S. O'Brien, S. Schwarz, G.D. Stucky, Chem. Mater., 12 (2000) 898.
43. Z. Luan, L. Kevan, Micropor. Mesopor. Mater., 44/45 (2001) 337.
44. Z. Shan, J.C. Jansen, L. Marchese, T. Maschmeyer, Micropor. Mesopor. Mater., 48 (2001) 181.
45. J.K.F. Buijink, J.J.M. van Vlaanderen, M. Crocker, F.G.M. Niele, Catal. Today, 93–95 (2004) 199.
46. M. Crocker, R.H.M. Herold, A.G. Orpen, M.T.A. Overgaag, Chem. Commun, (1997) 2411.

47. M. Crocker, R.H.M. Herold, A.G. Orpen, M.T.A. Overgaag, J. Chem. Soc. Dalton Trans., (1999) 3791.
48. V. Bolis, S. Bordiga, C. Lamberti, A. Zecchina, G. Petrini, F. Rivetti, G. Spanò, Micropor. Mesopor. Mater., 30 (1999) 67.
49. V. Bolis, S. Bordiga, C. Lamberti, A. Zecchina, G. Petrini, F. Rivetti, G. Spanò, Langmuir, 15 (1999) 5753.
50. G. Ricchiardi, A.J.M. de Man, J. Sauer, Phys. Chem. Chem. Phys., 2 (2000) 2195.
51. J.L. Grieneisen, H. Kessler, E. Fache, A.M. Le Govic, Micropor. Mesopor. Mater., 37 (2000) 379.
52. D. Gleeson, G. Sankar, C.R.A. Catlow, J.M. Thomas, Spanò, S. Bordiga, A. Zecchina, C. Lamberti, Phys. Chem. Chem. Phys., 2 (2000) 4812.
53. Q. Zhao, X. Bao, Y. Wang, L. Lin, G. Li, X. Guo, X. Wang, J. Mol. Catal. A: Chemical, 157 (2000) 265.
54. G. Sankar, J.M. Thomas, C.R.A. Catlow, C.M. Barker, D. Gleeson, N. Kaltsoyannis, J. Phys. Chem. B, 105 (2001) 9028.
55. K. Chaudhari, D. Srinivas, P. Ratnasamy, J. Catal., 203 (2001) 25.
56. C. Li, G. Xiong, J. Liu, P. Ying, Q. Xin, Z. Feng, J. Phys. Chem. B, 105 (2001) 2993.
57. G. Ricchiardi, A. Damin, S. Bordiga, C. Lamberti, G. Spanò, F. Rivetti, A. Zecchina, J. Am. Chem. Soc., 123 (2001) 11409.
58. S. Bordiga, A. Damin, F. Bonino, G. Ricchiardi, C. Lamberti, A. Zecchina, Angew. Chem. Int. Ed., 41 (2002) 4734.
59. A. Damin, S. Bordiga, A. Zecchina, C. Lamberti, J. Chem. Phys., 117 (2002) 226.
60. A. Damin, F. Bonino, G. Ricchiardi, S. Bordiga, A. Zecchina, C. Lamberti, J. Phys. Chem. B, 106 (2002) 7524.
61. C.M. Barker, D. Gleeson, N. Kaltsoyannis, C.R.A. Catlow, G. Sankar, J.M. Thomas, Phys. Chem. Chem. Phys., 4 (2002) 1228.
62. A. Damin, S. Bordiga, A. Zecchina, K. Doll, C. Lamberti, J. Chem. Phys., 118 (2003) 10183.
63. S. Bordiga, A. Damin, F. Bonino, G. Ricchiardi, A. Zecchina, R. Tagliapietra, C. Lamberti, Phys. Chem. Chem. Phys., 5 (2003) 4390.
64. F. Bonino, A. Damin, S. Bordiga, C. Lamberti, A. Zecchina, Langmuir, 19 (2003) 2155.
65. D. Srinivas, P. Manikandan, S.C. Laha, R. Kumar, P. Ratnasamy, J. Catal., 217 (2003) 160.
66. P. Ratnasamy, D. Srinivas, H. Knözinger, Adv. Catal., 48 (2004) 1.
67. C. Prestipino, F. Bonino, S. Usseglio, A. Damin, A. Tasso, M.G. Clerici, S. Bordiga, F. D'Acapito, A. Zecchina, C. Lamberti, Chem. Phys. Chem., 5 (2004) 1799.

68. R. Bal, K. Chaudhari, D. Srinivas, S. Sivasanker, P. Ratnasamy, J. Mol. Catal. A: Chemical, 162 (2000) 199.
69. K. Chaudhari, R. Bal, D. Srinivas, A.J. Chandwadkar, S. Sivasanker, Micropor. Mesopor. Mater., 50 (2001) 209.
70. D.R.C. Huybrechts, I. Vaesen, H.X. Li, P.A. Jacobs, Catal. Lett., 8 (1991) 237.
71. H. Ichihashi, H. Sato, Appl. Catal. A: General, 221 (2001) 359.
72. G. Bellussi, A. Carati, M.G. Clerici, G. Maddinelli, R. Millini, J. Catal., 133 (1992) 220.
73. J. Zhuang, Z. Yan, X. Liu, X. Han, X. Bao, U. Mueller, Catal. Lett., 83(2002) 87.
74. A. Zecchina, G. Spoto, S. Bordiga, M. Padovan, G. Leofanti, G. Petrini, Stud. Surf. Sci. Catal., 65 (1991) 671.
75. G. Belussi, C. Perego, in "Handbook of Heterogeneous Catalysis" (G. Ertl, H. Knözinger and J. Weitkamp, Eds.), Vol. 5, p. 2329. Wiley, New York, 1997.
76. M.G. Clerici, Appl. Catal., 68 (1996) 249.
77. M.G. Clerici, Top. Catal., 15 (2001) 257.
78. A.O. Chong, B.K. Sharpless, J. Org. Chem., 42 (1977) 1589.
79. M. Neurock, L.E. Manzer, Chem. Commun., (1996) 113.
80. E. Karlsen, K. Schoffel, Catal. Today, 32 (1996) 107.
81. P.E. Sinclair, C.R.A. Catlow, J. Phys. Chem. B, 103 (1999) 1084.
82. J.K. Edwards, B.E. Solsona, P. Landon, A.F. Carley, A. Herzing, C.J. Kiely, G. Hutchings, J. Catal., 236 (2005) 69.
83. C. Sivandinarayana, T.V. Choudhardy, L.L. Daemen, J. Eckert, D.W. Goodman, J. Am. Chem. Soc., 126 (2004) 38.
84. D.H. Wells, W.N. Delgass, K.T. Thomson, J. Catal., 225 (2004) 69.
85. B. Taylor, J. Lauterbach, G.E. Blau, W.N. Delgass, J. Catal., 242 (2006) 142.
86. T. Hayashi, K. Tanaka, M. Haruta, J. Catal., 178 (1998) 566.
87. J. Lu, X. Zhang, J.J. Bravo-Suárez, S. Tsubota, J. Gaudet, S.T. Oyama, Catal. Today, 123 (2007) 189.
88. J.J. Bravo-Suárez, J. Lu, C.G. Dallos, T. Fujitani, S.T. Oyama, J. Phys. Chem. C, 111 (2007) 17427.
89. X. Liu, X. Wang, X. Guo, G. Li, Catal. Today, 93 (2004) 505.
90. T.A. Nijhuis, T.Q. Gardner, B.M. Weckhuysen, J. Catal., 236 (2005) 153.
91. T.A. Nijhuis, B.J. Huizinga, M. Makkee, J.A. Moulijn, Ind. Eng. Chem. Res., 38 (1999) 884.
92. A. Zwijnenburg, M. Makkee, J.A. Moulijn, Appl. Catal. A: General, 270 (2004) 49.
93. M. Ojeda, E. Iglesia, Chem. Commun., (2009) 352.
94. H.M. Ajo, V.A. Bondzie, C.T. Campbell, Catal. Lett., 78 (2002) 359.

95. L. Gamble, M.B. Hugenschmidt, C.T. Campbell, Catal. Lett., 63 (1999)143.

96. F. Sun, S. Zhong, J. Nat. Gas. Chem., 15 (2006) 45.

Chapter 7

Summary

The gas-phase epoxidation of propene over Au/Ti-based catalysts is an intriguing scientific topic, not only because of the industrial importance of the production of propene oxide, but also because this reaction offers fundamental insights into the working principles of Au-based catalysis. The propene epoxidation with H_2 and O_2 over Au/Ti-based catalysts is a simple process since a single reactor is needed. It can in principle become a potential competitor for the new H_2O_2-PO process. This may become possible when the activity and hydrogen efficiency of Au/Ti-based catalysts will be improved. However, a fundamental understanding of the reaction mechanism is necessary for developing more efficient Au/Ti-based propene epoxidation catalysts. The aim of this PhD thesis was to shed futher insight into the mechanism of Au/Ti-based catalysts for the epoxidation of propene with O_2 and H_2. The first effort of the research has focused on the synthesis of Au/Ti-based catalysts with well-defined sites. **Chapter 2** deals with the synthesis, characterization and catalytic activity study of new Au/Ti-SBA-15 catalysts in the propene epoxidation with H_2 and O_2. Two different methods have been used for the synthesis of Ti-SBA-15 supports. The characterization results showed that the preparation method is crucial for the amount of isolated tetrahedral sites that is obtained in the Au/Ti-SBA-15 materials. It was found that Au/Ti-SBA-15 prepared by grafting Ti in the SBA-15 structure contains a higher absolute amount of tetrahedral Ti than the ones prepared by a hydrothermal method of preparing a Ti-SBA-15 support. Moreover, we observed that the deposition of Au is influenced by the amount of Ti present in or on the support. Au particles were larger in the grafted Au/Ti-SBA-15 samples that in the hydrothermal prepared ones. The catalytic activity of Au/Ti-SBA-15 catalysts was found to be dependent on the

amount and dispersion of Ti as well on the Au particle size. In **Chapter 3** we have investigated the influence of a post-synthesis NH_4NO_3 treatment of Au/Ti-SBA-15 catalysts in order to explain the beneficial effect on the catalytic activity for the direct epoxidation of propene with H_2 and O_2. Using ^{29}Si MAS NMR, FT-IR spectroscopy, XRD, N_2-sorption, UV-Vis DRS and TEM, we have evaluated this effect on the morphology of the Au/Ti-SBA-15 materials. We observed from TEM micrographs that highly dispersed Au particles with a mean diameter of 2-3 nm are deposited on NH_4NO_3 treated Ti-SBA-15 supports. Without this treatment, mainly large Au particles were deposited predominantly on the outer surface of Ti-SBA-15. With the ^{29}Si MAS NMR and FT-IR results we were able to explain why Au is homogeneous deposited in the channels of NH_4NO_3 treated Ti-SBA-15 support. The existence of a large number of surface hydroxyl groups together with ammonium species on the surface support have a beneficial effect on the homogeneous deposition of Au. It was concluded that the superior activity of treated Au/Ti-SBA-15 materials is related to the increased number of Au adsorption sites. The in-situ XAFS investigations on the adsorption of propene on Au nanoparticles are reported in **Chapter 4**. Propene adsorption was investigated by using hydrogen oxidation as a probe reaction. Propene was found to strongly inhibit the direct water formation rate over Au-catalyst, which is an undesired side reaction during the epoxidation of propene with H_2 and O_2. The delta-mu XANES analysis results confirmed that propene is π-bonding to the Au particles. It was concluded that the adsorption of propene is a key step in the epoxidation mechanism over Au/Ti-based catalysts. In **Chapter 5** we reported the Steady State Isotopic Kinetic Analysis results performed on Au/TiO_2 and Au/Ti-SBA-15 catalysts to investigate the reaction mechanism for the epoxidation of propene using O_2 and H_2. These experiments were performed to investigate if the support oxygen is playing a role in the production of propene oxide. It was observed that the isotopic response of the products over Au/Ti-SBA-15 is much faster compared to Au/TiO_2 catalysts, although both responses are slow compared to the isotopic switch. The amount of intermediates calculated from these experiments was high on the catalyst surface of both Au/TiO_2 and Au/Ti-SBA-15 catalysts and indicated that the products are slowly desorbed from the catalyst surface. Based on the transient responses of $C^{16}O_2$, $C^{16}O^{18}O$ and $C^{18}O_2$ produced on both Au/Ti-based catalysts we proposed that the CO_2 is produced in at least two ways. Two partially oxidized species can be produced by the breaking of C-C bonds of the two legs of bidentate propoxy species. Further oxidation of these species can explain the two routes towards CO_2 formation. However, it was not possible to determine if the support oxygen is playing a role in the formation of propene oxide. We reviewed all the mechanistic studies on the epoxidation reaction with O_2 and H_2 over Au/Ti-based catalysts in **Chapter 6**. More specifically, we have discussed in combination with our results all the theoretical, kinetic and spectroscopic studies

reported in the literature in order to better understand the active sites, the role of potential reaction intermediates and deactivation products as well as the related propene epoxidation mechanism. Despite of all investigations so far there is still not sufficient information to allow for the formulation of a unifying and detailed reaction mechanism, leaving sufficient room for future characterization studies.

Samenvatting

De gasfase epoxidatie van propeen over goud-titaan gebaseerde katalysatoren is een intrigerend wetenschappelijk onderwerp, niet alleen vanwege de industriële relevantie van de productie van propeenoxide, maar ook omdat deze reaktie de mogelijkheid biedt om een fundamenteel inzicht te verkrijgen in de werking van goud katalysatoren. De propeen epoxidatie met waterstof en zuurstof over goud/titaan gebaseerde katalysatoren kan in een eenvoudig proces met een enkele reaktor worden uitgevoerd en het biedt de mogelijkheid om een concurrent te worden van het nieuwe waterstofperoxide-propeenoxide proces. Deze mogelijkheid zal zich voordoen indien de waterstof efficiëntie van goud/titaan katalysatoren wordt verbeterd. Een fundamenteel begrip is echter nodig van het reaktiemechanisme om efficiëntere goud/titaan gebaseerde propeen epoxidatie katalysatoren te ontwikkelen. Het doel van dit promotieonderzoek is om dit inzicht in het reaktiemechanisme van deze epoxidatie te verkrijgen. De eerste onderzoeksinspanning heeft zich gericht op de bereiding van goud/titaan katalysatoren met goed gedefinieerde reaktiesites. **Hoofdstuk 2** gaat over de bereiding, karakterisering, en katalytische activiteit van nieuwe Au/Ti-SBA-15 katalysatoren voor de epoxidatie van propeen met zuurstof en waterstof. Twee verschillende methoden zijn gebruikt voor de bereiding van Ti-SBA-15 dragermaterialen. De resultaten van de karakteriseringen gaven aan dat de bereidingsmethode een essentiële parameter is voor het aantal geïsoleerde tetraedrische sites die worden verkregen in de Au/Ti-SBA-15 materialen. Er werd gevonden dat Au/Ti-SBA-15 materialen bereid met een hechtingsmethode (grafting) van Ti in de SBA-15 structuur een grotere absolute hoeveelheid tetraedrisch Ti bevatten dan Au/Ti-SBA-15 katalysatoren bereid via een hydrothermale synthesemethode. Bovendien bleek dat de depositie van goud beïnvloed werd door de aanwezige hoeveelheid Ti op of in de drager. Goud deeltjes waren groter voor de katalysatoren bereid op een drager met Ti bereid met de grafting methode, vergeleken met hydrothermaal bereide Ti houdende dragers. De katalytische activiteit van de Au/Ti-SBA-15 katalysatoren bleek afhankelijk te zijn van de hoeveelheid en dispersie van Ti op de katalysator en van de goud-deeltjesgrootte. In **Hoofdstuk**

3 hebben we het effect onderzocht van een ammoniumnitraat behandeling van de Au/Ti-SBA-15 katalysatoren om het positieve effect op de katalytische activiteit van de directe propeen epoxidatie met waterstof en zuurstof te kunnen verklaren. Met behulp van ^{29}Si MAS NMR, FT-IR spectroscopie, stikstof adsorptie, UV-Vis DRS en TEM, hebben we dit effect op de morfologie van Au/Ti-SBA-15 materialen onderzocht. TEM foto's gaven aan dat hoog-disperse gouddeeltjes met een diameter van 2 tot 3 nm werden afgezet op ammoniumnitraat behandelde Ti-SBA-15 dragers. Zonder deze behandeling werden voornamelijk grote gouddeeltjes afgezet op het buitenoppervlak van Ti-SBA-15. Met de ^{29}Si MAS NMR en FT-IR resultaten konden we verklaren waarom goud homogeen werd afgezet in de kanalen van ammoniumnitraat behandelde Ti-SBA-15 dragermateriaal. De aanwezigheid van een groot aantal oppervlakte hydroxyl groepen, samen met ammonium groepen op het oppervlakte van de drager hadden een positief effect op de homogene depositie van goud. Geconcludeerd werd dat de superieure activiteit van de behandelde Au/Ti-SBA-15 materialen gecorreleerd kon worden aan een toegenomen aantal adsorptie sites voor goud. De in-situ XAFS studie naar de adsorptie van propeen op goud nanodeeltjes wordt beschreven in **Hoofdstuk 4**. De propeen adsorptie werd onderzocht met behulp van de waterstof oxidatie als testreaktie. Propeen bleek een sterk remmend effect te hebben op de direkte watervormingsreaktie over goud, wat een ongewenste nevenreaktie is tijdens de epoxidatie van propeen met waterstof en zuurstof. De delta-mu XANES analyse resultaten bevestigden dat propeen op goud adsorbeerde door middel van pi-binding. Geconcludeerd kon worden dat de propeenadsorptie op goud een belangrijke stap is in het epoxidatiemechanisme over goud-titaan gebaseerde katalysatoren. In **Hoofdstuk 5** gaan we in op 'Steady State Isotopic Kinetic Analysis' (SSITKA – dynamische isotoopexperimenten bij constante reactiecondities) uitgevoerd op Au/TiO_2 en Au/Ti-SBA-15 katalysatoren om het reactiemechanisme van de propeenepoxidatie met zuurstof en waterstof te onderzoeken. Deze experimenten werden uitgevoerd om te bepalen of zuurstof uit de katalysatordrager een rol speelt bij de productie van propeenoxide. Waargenomen werd dat de isotoop respons voor Au/Ti-SBA-15 veel sneller is dan die over Au/TiO_2 katalysatoren. In beide gevallen was de respons vele malen langzamer dan de isotoopswitch in de gasfase van het niet gereageerde gas. De hoeveelheid intermediairen op het katalysatoroppervlak dat uit deze experimenten berekend kon worden was erg hoog voor zowel de Au/TiO_2 als de Au/Ti-SBA-15 katalysator, hetgeen aangaf dat producten langzaam van het oppervlak van de katalysator desorberen. Gebaseerd op de transiente respons van $C^{16}O_2$, $C^{16}O^{18}O$ en $C^{18}O_2$ geproduceerd op Au/Ti gebaseerde katalysatoren, stelden we voor dat kooldioxide op minimaal twee manieren geproduceerd wordt. Twee partieel geoxideerde species kunnen gevormd worden bij het verbreken van de C-C bonding van de twee benen van de veronderstelde bidentate propoxy

reaktieintermediair. Een verdere oxidatie van deze twee species kan de twee routes naar kooldioxide vorming verklaren. Het was helaas niet mogelijk om te bepalen of zuurstof uit de katalysatordrager daadwerkelijk een rol speelt in de vorming van propeenoxide. We geven een overzicht van alle eigen en gepubliceerde mechanistische studies naar de epoxidatie reaktie met zuurstof en waterstof over goud-titaan gebaseerde katalysatoren in **Hoofdstuk 6**. We bediscussiëren onze resultaten samen met alle relevante theoretische, kinetische, en spectroscopische studies in de literatuur, om zo tot een beter begrip te komen van de actieve reaktiesites, de rol van mogelijke reaktieintermediairen en deactiverende producten, en het mechanisme van de propeenepoxidatie. Ondanks de vele reeds uitgevoerde studies is er op dit moment helaas nog onvoldoende informatie beschikbaar om één enkel gedetailleerd reaktiemechanisme te kunnen voorstellen, hetgeen voldoende ruimte open laat voor verder onderzoek.

List of Publications and Presentations

Publications

E. Sacaliuc, A.M. Beale, B.M. Weckhuysen, T.A. Nijhuis, "Synthesis and characterization of Au/Ti-SBA-15 catalysts for the vapour phase epoxidation of propylene", American Chemical Society, Division of Petroleum Chemistry, Preprints, 52 (2007) 282.

E. Sacaliuc, A.M. Beale, B.M. Weckhuysen, T.A. Nijhuis, "Propene epoxidation over Au-Ti-SBA-15 catalysts", J. Catal., 248 (2007) 235.

T.A. Nijhuis, E. Sacaliuc, A.M. Beale, A.M.J. van der Eerden, J.C. Schouten, B.M. Weckhuysen, "Spectroscopic evidence for the adsorption of propene on gold nanoparticles during the hydro-epoxidation of propene", J. Catal., 258 (2008) 256.

E. Sacaliuc-Parvulescu, H. Friedrich, R. Palkovits, B.M. Weckhuysen, T.A. Nijhuis, "Understanding the effect of post- synthesis ammonium treatment on the catalytic activity of Au/Ti-SBA-15 catalysts for the oxidation of propene", J. Catal., 259 (2008) 43.

T.A. Nijhuis, E. Sacaliuc-Parvulescu, N.S. Govender, J.C. Schouten, B.M. Weckhuysen, "The role of support oxygen in the epoxidation of propene over gold-titania catalysts investigated by isotopic transient kinetics", submitted.

A.M. Beale, S.D.M. Jacques, E. Sacaliuc-Parvulescu, M.G. O'Brien, P. Barnes, B.M. Weckhuysen, "An iron molybdate catalyst for methanol to formaldehyde conversion prepared by a new hydrothermal method and its characterization", Appl. Catal. A: General, submitted.

E. Sacaliuc-Parvulescu, B.M. Weckhuysen, T.A. Nijhuis, "Towards a reaction mechanism for the propene epoxidation with O_2 and H_2 over Au/Ti-based catalysts", in preparation.

Book Chapter

T.A. Nijhuis, E. Sacaliuc, B.M. Weckhuysen, "The epoxidation of propene over gold nanoparticle catalysts", In S.T. Oyama (Ed.), Mechanism in homogeneous and heterogeneous epoxidation catalysis, 2008, Chapter 12. (pp. 339-353) Amsterdam: Elsevier Science.

Oral Presentations

E. Sacaliuc, T.A. Nijhuis, B.M. Weckhuysen, "Novel gold-titania supported catalysts for the epoxidation of propene", VIIth Netherlands Catalysis and Chemistry Conference", Noordwijkerhout, Netherlands, March 2006, oral presentation.

E. Sacaliuc, A.M. Beale, B.M. Weckhuysen, T.A. Nijhuis, "Synthesis and characterization of Au/Ti-SBA-15 catalysts for the vapour phase epoxidation of propylene", 234th ACS National Meeting, Boston, Session on "Mechanism in homogeneous and heterogeneous catalysis", August 2007, oral presentation.

E. Sacaliuc, A.M. Beale, B.M. Weckhuysen, T.A. Nijhuis, "Well dispersed gold nanoparticles on mesoporous Ti/SBA-15 supports as efficient heterogeneous catalysts for selective oxidation of propene", IXth Netherlands Catalysis and Chemistry Conference", Noordwijkerhout, Netherlands, March 2008, oral presentation.

T.A. Nijhuis, E. Sacaliuc, J.C. Schouten, B.M. Weckhuysen, "Direct epoxidation of propene over supported gold catalysts - A study into the reaction mechanism" , 235th ACS National Meeting, New Orleans, April 2008.

T.A. Nijhuis, E. Sacaliuc, B.M. Weckhuysen, J.C. Schouten, "Gold nanoparticle catalysts for the hydro-epoxidation of propene: an in-situ XANES and catalytic study into the adsorption of propene on gold", 14th Int. Congress on Catalysis; Seoul, Korea, July 2008.

T.A. Nijhuis, E. Sacaliuc, B.M. Weckhuysen, J.C. Schouten, "Gold nanoparticle catalysts for the hydro-epoxidation of propene: an in-situ XANES and catalytic study into the adsorption of propene on gold", 20th Int. Symp. on Chemical Reaction Engineering (ISCRE), Kyoto, Japan, September 2008.

Poster Presentations

T.A. Nijhuis, E. Sacaliuc, and B.M. Weckhuysen, "The Epoxidation of Propene over Gold on Titania Catalysts – A Mechanistic Study", 2nd Operando Conference, Toledo, April 2006.

E. Sacaliuc, T.A. Nijhuis, and B.M. Weckhuysen, "Propene epoxidation over Au-Ti-SBA-15 catalysts", Gold, Limerick, September 2006.

E. Sacaliuc, A.M. Beale, B.M. Weckhuysen, T.A. Nijhuis, "Au-Ti-SBA-15 Catalysts for propene epoxidation", VIIIth Netherlands Catalysis and Chemistry Conference, Noordwijkerhout, Netherlands, March 2007.

E. Sacaliuc, A.M. Beale, R. Palkovits, B.M. Weckhuysen, T.A. Nijhuis, "Understanding the effect of post-synthesis ammonium treatment on the catalytic activity of Au/Ti-SBA-15 catalysts for propene selective oxidation", 14th Int. Congress on Catalysis; Seoul, Korea, July 2008.

Acknowledgements

During my time as a PhD-student at the Inorganic Chemistry and Catalysis group at Utrecht University I had the chance to be surrounded by wonderful colleagues and I would like to thank everyone who in one way or another contributed to this thesis. First of all, I would like to express my deep and sincere gratitude to my promoters. Bert, I would like to thank you for accepting me to work in your group and for the thoughtful support, encouragement and fruitful discussions that we had during these years. Your suggestions and guidance gave me the opportunity to always learn many new things. I am extremely grateful to Xander for the careful guidance in these years. I have learned a lot from you. Your encouragement helped me to overcome every difficulty I encountered during this years. The summary in Dutch presented in the last pages of this thesis would not have been possible without your generous help.

I wish to express my gratitude to the committee members for the time spent to carefully read this thesis. Special thanks are given to Andy for his important contribution to my PhD project. You introduced me into the EXAFS world and I was very happy to learn from you. Our discussions always succeeded in making me having new ideas. It has been a real pleasure to collaborate with you. Tom, thank you for your help and suggestions. I would like to thank Regina and Heiner for our valuable collaboration.

I would also like to acknowledge the technical and administrative staff. Dymph and Monique, thank you for being always helpful and friendly. Fouad, thanks for your help and enthusiasm. It is impossible to be near you without smiling. Without the technical support of Ad Mens who was always very helpful and kind, some of the experiments reported in this thesis would not exist. I would like to thank Cor for helping me with the TEM measurements. My gratitude goes to Ad van der Eerden and to all the colleagues who performed my EXAFS measurements.

Many thanks to my friends and colleagues for the wonderful time spent in our group and for the extra-work activities. Nadia, thank you for our conversations, you always gave me hope. I wish you good luck with finishing your PhD. I need to mention Agnieszka, who was very kind and helpful with me. Lukas and Bart, it has been nice to have you as office-mates. I also want to acknowledge to Cristina and Dan for all their help. I wish to thank Leti, Matt, Maria, Ana Iglesia, Philipp, Eli, Ana Mijovilovich for our great time spent together.

It is hard to find my words to express my gratitude to my family, who support me with constant enthusiasm. I will forever be thankful to my mother in law. I remember my time as an

undergraduate student in her lab introducing me into the world of catalyst synthesis. Her enthusiasm and love for catalysis is contagious. I would also like to thank to my father in law for his support.

Multumesc din suflet parintilor mei. A-ti fost intotdeauna alaturi de mine si m-ati sprijinit. Va iubesc si va multumesc ca a-ti avut incredere in mine. Multumiri speciale lui Maria, Aristita si Traian pentru tot sprijinul lor. Buni, este greu sa imi gasesc cuvintele prin care sa iti multumesc, ai fost intotdeuna alaturi de mine. Iti multumesc din toata inima pentru tot ce faci pentru mine si pentru toata energia pozitiva pe care o primesc de la tine.

Teza aceasta iti este dedicata tie Andrei. Am reusit sa trecem peste momente grele in care stateam atat de departe unul de celalalt. Iti multumesc pentru toata dragostea si suportul tau. Fiecare zii alaturi de tine este o sarbatoare. Te iubesc!

Elena

Curriculum Vitae

Elena Parvulescu (born Sacaliuc) was born on 21th of September 1980 in Oltenita, Romania. In June 2003 she obtained a B.Sc. in Chemistry from University of Bucharest. In 2003 she obtained a fellowship at the Laboratory of Inorganic Chemistry, University of Namur, Belgium where she was involved in the synthesis of metal aluminophosphates and their application in liquid phase oxidation of hydrocarbons. Two years later in June 2005 under the coordination of Dr. Viorica Parvulescu, she obtained her M.Sc. in the field of "Catalysis and Catalytic Processes" at the University of Bucharest. In the first year of her master studies she was working as associated assistant researcher at the Romanian Academy Institute of Physical-Chemistry "I.G. Murgulescu", Bucharest. In 2004 she received a fellowship at the Laboratoire de Phisique des Couches Mines Complexe from Institute de Physique de la Matière Complexe, EPFL Switzerland. The research was focused on the deposition/characterisation of thin films of Au, V, Nb on TiO_2 ceramic supports by dc-magnetron sputtering. In January 2005 she started her PhD studies at Utrecht University, Department of Inorganic Chemistry and Catalysis under the supervision of Prof. dr. ir. B. M. Weckhuysen and Dr. ir. T.A. Nijhuis. Her research was financed by STW/NWO and Utrecht University.